MYOSIN-1D EXPRESSION AND DYNAMICS IN POLARIZED CELLS

By

Andrew Eugene Benesh

Dissertation

Submitted to the Faculty of the

Graduate School of Vanderbilt University

In partial fulfillment of the requirements

For the degree of

DOCTOR OF PHILOSOPHY

in

Cell and Developmental Biology

December, 2011

Nashville, Tennessee

Approved:

Professor David M. Miller

Professor Bruce D. Carter

Professor Robert J. Coffey

Professor Matthew J. Tyska

Professor Irina Kaverina

Professor Christopher Janetopoulos

ACKNOWLEDGEMENTS

First, I thank Matt for accepting me into his laboratory as his second graduate student. From him I have learned and appreciated the process that is science. An open-mind and an honest heart are a couple of the basic tools needed to successfully pursue the many avenues that discoveries can lead us down. Importantly, Matt has been extraordinarily patient in teaching me the critical thinking, technical, and soft skills necessary to become a successful scientist, and for this I am grateful.

Likewise, I appreciate the guidance of my committee David Miller, Irina Kaverina, Chris Janetopoulos, Bob Coffey, and Bruce Carter. I am fortunate to have a committee that has been so supportive in allowing me to follow my projects wherever they may lead, but still keep me focused. In addition, I can never forget the moral support and professional guidance they have offered-I could not have matured as I have without their assistance.

One of the greatest opportunities of being in Matt's laboratory was my participation in the Program in Developmental Biology. I was fortunate to have participated in the retreats and journal clubs and I have benefitted from Chris taking an interest in my science. I count these events as some of the most invaluable experiences in developing my presentation skills. Between Matt and Chris I know have matured as a public speaker.

I am fortunate to have worked with great colleagues and friends. Russell, Raj, Suli, Jessi, David, and Scott have helped make the laboratory a fun place to

do science. I thank them for their assistance and camaraderie these past few years.

I would not have made it this far without the support and love of my parents and family. I thank them for instilling in me the values that have gotten me thus far. Their encouragement and pride is inspiring. Plus, I can not forget the cheese my parents would send from WI, nor the pounds of chocolate from my aunt in AZ.

Finally, I thank Emily for standing by me these last couple of years as we finish up our graduate training. Without her friendship and love, I would not be as happy as I am now.

TABLE OF CONTENTS

Page

LIST OF TABLES

Table Page

LIST OF FIGURES

Figure Page

LIST OF ABBREVIATIONS

Cases

CHAPTER I

INTRODUCTION

The myosin superfamily of actin-binding molecular motors is composed of 35 different classes, which are responsible for a range of functions from muscle contraction to protein transport (Odronitz and Kollmar, 2007). Although structurally diverse, these molecules share three domains: an actin-binding, adenosine triphosphate (ATP) hydrolyzing motor domain; a variable repeat IQXXXRKXXXRK (IQ) motif that each bind calmodulin; and a tail domain that binds species specific cargo (Schliwa and Woehlke, 2003). Conventional and some unconventional myosins dimerize, facilitating hand-over-hand processivity along actin filaments (Hartman et al., 2011). However, the unconventional class I myosins have a monomeric motor, and thus are unlikely to be processive. Historically, these motors were hypothesized to facilitate vesicle trafficking (Soldati, 2003) and act as actin-membrane linkers (Cheney and Mooseker, 1992). Exciting new research is uncovering novel roles for this class in membrane-cytoskeletal biology which has important implications for polarized cells (McConnell and Tyska, 2010). Our laboratory studies the function of class I myosins to better understand how certain cell types acquire and maintain polarity. Polarized cells are amenable for studying class I myosins as they possess: 1) a highly organized cytoskeleton; 2) distinct plasma membrane domains for identifying molecular targeting determinants; and 3) cytoskeletal

features that are easily assayed with biochemical or immunofluorescence methods. This dissertation will further explore class I myosin structure, expression, and function; in particular, how those properties relate to polarized cells of the small intestine and nervous system.

Class I myosin structure

Vertebrates express eight class I myosins that are of similar molecular weights (~110 kilo-Daltons (kDa) (Mooseker and Cheney, 1995). These molecules share three structural domains: 1) an N-terminal motor that binds actin and hydrolyzes ATP to produce mechanical force; 2) an internal neck region; and 3) a C-terminal polybasic tail with multiple motifs for specific membrane and cargo interactions (Figure 1) (McConnell and Tyska, 2010). A closer examination is required to appreciate the functional differences between class I myosins.

The motor couples ATPase activity to actin-binding and undergoes conformational changes that result in force generation (Figure 2) (Geeves, 1991; Hackney, 1996). Myosin bound to actin in the nucleotide-free state accepts ATP and then rapidly dissociates from the actin filament. The nucleotide-binding pocket hydrolyzes ATP to form adenosine diphosphate + P_i (ADP•P_i). This myosin-ADP•P_i complex releases P_i and subsequently binds actin. Class I motors undergo a two-step working stroke that results in the release of ADP (Veigel et al., 1999), The rate of ATPase activity determines the amount of time the motor associates with actin, and regulates myosin processivity. Motors that spend a significant amount of time during the ATPase cycle bound to actin have

a high duty ratio (Hartman et al., 2011). However, class I myosins are low duty motors (Spudich, 1994; Lewis et al., 2006; Laakso et al., 2008), and would hypothetically have to act as an ensemble to transport cargo.

Slight conformational changes in the motor domain during the working stroke are amplified in the neck domain resulting in large angular swings ranging from 32° for myosin-1a (Myo1a) (Jontes et al., 1995) and 90° for myosin-1d (Myo1d) (Kohler et al., 2003). The degree of angular swing and length of the neck domain contribute to the myosin step size (Purcell et al., 2002; Kohler et al., 2003). Class I myosin neck domains have a variable number of IQ motifs (1-6) that bind calmodulin (Figure 1) (Cheney and Mooseker, 1992; Coluccio, 1997). Calmodulin associates with IQ motifs in either a Ca^{2+} dependent or independent manner depending on the myosin and IQ motif (Bahler and Rhoads, 2002) and

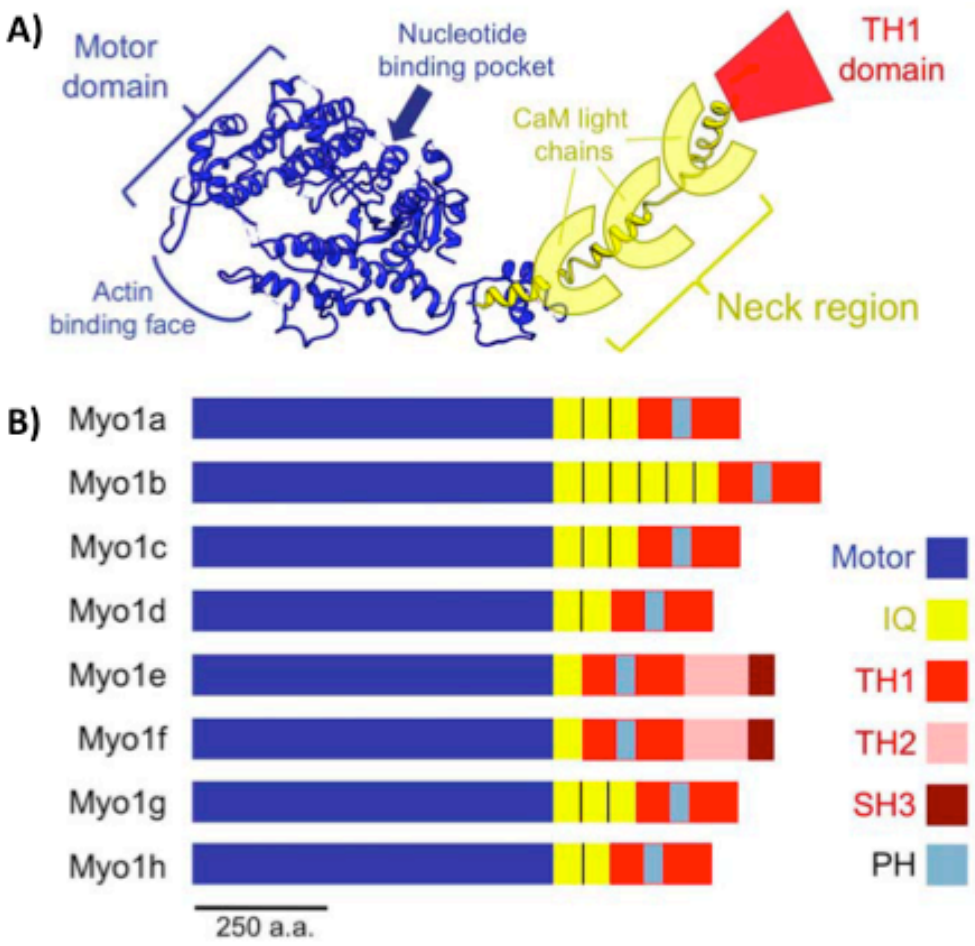

Figure 1 Vertebrates express eight class I myosins.
A) Class I myosins share three structural domains: an N-terminus motor that binds actin and hydrolyzes ATP, a neck region with a variable number of IQ motifs that bind Calmodulin, and a tail domain with several motifs for cargo binding. B) Eight class I myosins are expressed in vertebrates. Figure from (McConnell and Tyska, 2010).

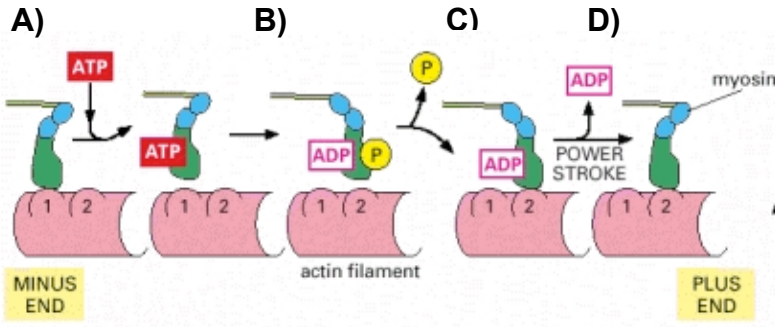

Figure 2 ATPase cycle of myosins.

Myosin hydrolyzes ATP for the generation of force. A) ATP binds the myosin-actin complex causing dissociation from the actin. B) The motor hydrolyzes ATP to form a myosin-ADP•P_i complex, which will release P_i. C) Myosin-ADP binds actin. D) The motor releases ADP causing a conformational change in the motor that tightly binds it to actin, in a process termed the power stroke. Adapted from (Alberts et al., 2002).

accelerates ATPase activity (Swanljung-Collins and Collins, 1991). In addition, calmodulin binding is thought to structurally support the myosin during the power stroke (Spudich, 1994). Recent work suggests that in the absence of calmodulin binding myosin-5 switches from an active to an inactive state where the motor is folded onto the tail domain in a closed conformation (Taylor, 2007). Thus, the neck domain provides multiple levels of regulation that varies both among the individual class I myosins and across classes, segregating each motor to specific tasks based on motor-neck interactions. Finally, the C-terminal tail domain of each class I myosin is unique, with a different binding partner or cargo (Akhmanova and Hammer, 2010).

The many differences in the tail among class I myosins specify the diverse set of functions these molecules participate in the cell (Foth et al., 2006). Class I myosins have a polybasic C-terminal tail domain that binds anionic phospholipids through electrostatic interactions (Adams and Pollard, 1989; Hayden et al., 1990), and have important implications in trafficking and cytoskeletal biology (Huber et al., 2000; Bose et al., 2002; McConnell and Tyska, 2010). The tail domain varies in length and is composed of several binding motifs such as pleckstrin homology (PH) motifs which can bind phosphatidylinositol 4,5-bisphosphate (PIP_2) (Hokanson and Ostap, 2006) and SRC homology 3 (SH3) motifs that putatively bind cytoskeletal regulatory proteins (Figure 1) (Drubin et al., 1990; Geli et al., 2000). All class I myosins have a tail homology 1 (TH1) motif, which contain basic residues, but myosins-1e and -1f (Myo1e and Myo1f) have a tail homology 2 (TH2) motif, which is a putative actin-binding site (Lynch

et al., 1986; Jung and Hammer, 1994). Many tail-cargo interactions have been identified implicating class I myosins in diverse functions. Myo1a binds sucrase isomaltase (SI), (Tyska and Mooseker, 2004) a transmembrane disaccharidase found in the brush border. Myosin-1c (Myo1c) binds cadherin-23 (Siemens et al., 2004), and PHR1 (Etournay et al., 2005), which are both transmembrane proteins in sensory hair cells. In the insulin signaling pathway, Myo1c binds nuclear factor κβ essential modulator (NEMO) (Nakamori et al., 2006) and the G-protein RalA (Chen et al., 2007). Myo1c also binds Neph1, a transmembrane protein containing five extracellular-immunoglobulin repeats in podocytes suggesting a role in kidney filtration (Arif et al., 2011). Lastly, the *Drosophila* homologue for Myo1d binds β-catenin in developing embryos (Speder et al., 2006).

Class I myosin motors bind actin

The physiology of an organism is a well-choreographed interplay among specialized systems, organs, tissues, and at the most basic living unit: cells. Indeed, tissue development and function depend on cell morphology and intracellular organization to orchestrate cell:cell contacts (Miyoshi and Takai, 2008), migration (Gardel et al., 2010), and signaling (Hotulainen and Hoogenraad, 2010). To accomplish these 'directional' processes, cells exhibit polarization in the localization of proteins and lipids to specific cell membrane domains to facilitate the movement of the cell or transfer of a signal in a given direction (Drubin and Nelson, 1996). As a result, each cell surface may have a

unique shape or function that contributes to the overall tissue physiology. Important in these interactions are molecular motors that utilize actin to transport cargo (Hasson and Mooseker, 1995) and provide mechanical forces to coordinate interactions between the cytoskeleton and plasma membrane that contribute to cell polarity and other processes (McConnell and Tyska, 2010).

Class I myosins associate with the actin cytoskeleton, which underlies polarized cell shape and function (Drubin and Nelson, 1996). Morphologically, a polarized cell surface may have microvilli (Tilney and Mooseker, 1971), stereocilia (Flock and Cheung, 1977), filopodia (Edds, 1977), lamella (Abercrombie, 1980), dendrites (Fifkova and Delay, 1982), or junctions (Miettinen et al., 1978) (Figure 3). Each of those cellular structures facilitates a particular function such as absorption (Spiller, 1994), mechanotransduction (Nayak et al., 2007), migration (Lauffenburger and Horwitz, 1996), cell:cell communication (Dent et al., 2011b), or permeability (Steed et al., 2010).

Actin structure and polymerization

Actin polymerization drives membrane rearrangements and formation and maintenance of cellular protrusions such as microvilli (Mooseker, 1985). Actin appears in two forms: a monomeric globular form (G-actin) and a polymer fibrous form (F-actin). G-actin polymerizes to form F-actin, the functional form of actin in the cell. These actin filaments grow from the barbed or plus-ends and depolymerize from the pointed or minus-ends. Class I myosins associate with filopodia, lamellipodia, microvilli, and cortical actin; all structures found among

the polarized cells of the digestive and nervous systems (Skowron et al., 1998; Wang et al., 2003; Komaba and Coluccio, 2010). Below is a review of actin cytoskeletal arrays and regulatory proteins.

Filopodia are linear actin-based bundle protrusions oriented with the plus-ends outward (Faix et al., 2009). Filopodia are important for pushing membrane forward and sensing the environment during migration (Mattila and Lappalainen, 2008). Filopodia formation is activiated by cdc42, a small guanosine triphosphatase (GTPase) (Nobes and Hall, 1995), and nucleation from the filopodial tip is regulated by formins (Mellor, 2010). Filopodial actin bundles are held together with the bundler fascin (Kureishy et al., 2002).

Another polarized actin structure is the lamellipodium which is a broad, thin membranous process supported with branched actin and is important in migration (Mogilner and Keren, 2009). Branched F-actin polymerization is initiated when the arp2/3 complex nucleates a side filament (Insall and Machesky, 2009). Migration requires constant filopodia and lamellipodia

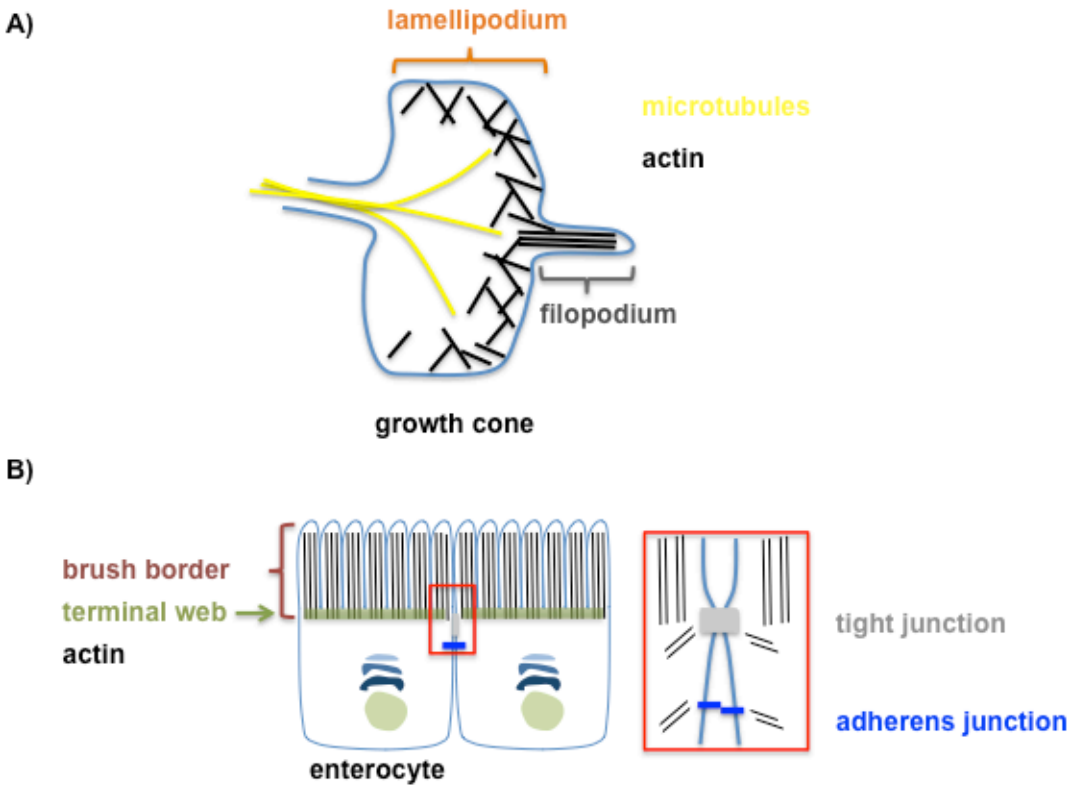

Figure 3 Cartoon representation of polarized cells and cytoskeletal features.

A) Representative growth cone with a filopodial and lamellipodial protrustion. Filopodia are actin-based membrane protrusions important in exploring the extracellular environment. The actin filaments are bundled with the plus-ends oriented towards the filopodial tip. The lamellipodium is also an actin-based membrane protrusion, but consists of a network of branched actin. In addition, microtubules remodeling guides growth cone steering. B) Representative enterocyte with microvilli. These actin-based membrane protrusions define the apical cell surface. Actin is bundled and oriented with plus-ends upward. Junctional complexes help define the apical-basolateral boundary in addition to organizing the cytoskeleton to maintain cell shape.

reorganization through several types of proteins including myosins, but also actin severing proteins like cofilin and gelsolin (Cooper and Schafer, 2000). Together, filopodia and lamellipodia direct forward movement and directionality.

Microvilli are densely packed, actin-based membrane protrusions that define the apical surface. Microvilli increase the surface area for intestinal absorption and release lumenal vesicles (Spiller, 1994; McConnell et al., 2009). In the small intestine brush border actin bundles are composed of 20-30 filaments (Mooseker, 1985) and are bound to together with fimbrin (Bretscher, 1981). The protein villin has dual roles: in the presence of low Ca^{2+} it will bundle actin (Mooseker et al., 1980), but at high Ca^{2+} concentrations villin severs actin bundles (Walsh et al., 1984). However, the mechanism of microvillar actin nucleation is not well established.

Finally, actin stabilizes cell:cell junctions that are important for cell signaling (Maruthamuthu et al., 2010). F-actin interacts with α-actinin, which associates with the α-catenin, β-catenin, and the cadherin complex at the junction (Sanger et al., 1983; Miyoshi and Takai, 2008). In addition, many cytoskeletal regulatory proteins associate with the junctions including arp2/3 and cofilin (Miyoshi and Takai, 2008). In the polarized epithelial cell, actin forms a cortical network that contributes to cell contractility, facilitating polarization and tissue development (Owaribe et al., 1981; Zhang et al., 2005).

Class I myosins in polarized cells of the digestive and nervous systems

Polarized cells are present in every tissue throughout the body, but the digestive and nervous systems exquisitely demonstrate the functional importance of asymmetric cells. The small intestine epithelia or 'enterocyte' is important for nutrient absorption and blocking pathogen entry (Catalioto et al., 2011). Disruptions to enterocyte polarity contribute to malabsorption diseases (Khubchandani et al., 2011), and the rest of the body becomes susceptible to pathogens (Catalioto et al., 2011). In the nervous system, neurons and glia must be polarized to propagate input stimuli from cell to cell. In fact, failure to fully polarize the neurons or glia may lead to various mental retardations and diseases such as autism, Alzheimer's, and schizophrenia (Lin and Koleske, 2010).

Class I myosins and the small intestine epithelium

The epithelium lining the small intestine lumen serves as a selective barrier for the body to regulate the passage of nutrients and protect against invasion of pathogens (Catalioto et al., 2011). The enterocyte exhibits distinct apical-basolateral polarity, and class I myosins target to each of these compartments. First, the apical domain is a well-ordered array of tightly packed microvilli (~1,000) that forms the brush border of each enterocyte (Holmes and Lobley, 1989). Each microvillus is an actin-based plasma membrane protrusion supported by 20-30 filaments with the plus-ends oriented distally (Tilney and Mooseker, 1971). Electron microscopy revealed the presence of a membrane-

actin cross linker, that was later identified as the first class I vertebrate motor (Mooseker and Cheney, 1995). Microvilli are also enriched in enzymes such as SI, intestinal alkaline phosphatase (IAP), aminopeptidases, and phospholipases (McConnell et al., 2011).

The minus-ends of microvillar actin protrude into the terminal web at the base of the brush border. The terminal web is an actin-spectrin meshwork that is enriched in myosin-2 and is an important site for trafficking (Mooseker, 1985). On the apical-lateral surface, just below the plane of microvilli are the tight and adherens junctions, which are two centers for cell-cell contact important for cell communication and structure. The actin cytoskeleton plays an important part in organizing and maintaining these structures during development (Ivanov, 2008). Tight junctions regulate epithelial permeability with claudins and ZO-1 and provide an important barrier between apical and lateral membrane (Balda and Matter, 2008). The cytoskeleton and β-catenin contribute to lateral polarity by orchestrating the organization of the cadherin complex (Chen et al., 1999), which regulate cell:cell contacts (Baum and Georgiou, 2011).

In addition to the cell structures detailed above, epithelial polarity is maintained by sorting of proteins and lipids to the appropriate membrane (Bryant and Mostov, 2008), and relies in part on myosins and the actin and microtubule cytoskeleton network (Weisz and Rodriguez-Boulan, 2009). Class I myosins may be able to target to specific compartments (apical versus lateral membrane) themselves based on affinity for particular phospholipids (Hayden et al., 1990; Hokanson et al., 2006). Indeed, mature epithelia have polarized membrane

composition. The apical surface is enriched in glycolipids and cholesterol (Christiansen and Carlsen, 1981), while the basolateral membrane is enriched in phospholipids (Kawai et al., 1974) such as phosphatidylinositol 3,4,5-trisphosphate (PIP_3), (Gassama-Diagne et al., 2006). Properly polarized membrane facilitate sorting of specific proteins to the appropriate surface, for example glycophosphatidylinositol (GPI) anchored proteins are trafficked apically (Levental et al., 2010). Misregulation sorting of polarity factors not only impedes cell polarization, but also lumen formation (Martin-Belmonte et al., 2008).

Microvilli have been the focus of intense research to better understand how these polar extensions contribute to brush border physiology (Mooseker, 1985). In particular, the class I myosin, Myo1a was identified as the cross-linker in electron microscopy images and characterized biochemically to have ATPase activity and calmodulin binding domains (Mooseker and Tilney, 1975b; Howe and Mooseker, 1983). The motor at first was hypothesized to be an actin-membrane linker or help modulate brush border Ca^{2+} levels (Mooseker, 1985). Lipid binding analysis demonstrated the molecule preferred anionic phospholipids, hypothetically through the polybasic tail domain (Hayden et al., 1990). The role of Myo1a became more apparent with the generation of a Myo1a dominant negative construct, the Myo1a TH1 domain. These experiments revealed that Myo1a binds sucrase-isomaltase and helps retain the disaccharidase in detergent resistant membranes in the brush border (Tyska and Mooseker, 2004). Moreover, the TH1 domain was sufficient for brush border localization, and the tail governs membrane interactions (Tyska and Mooseker, 2002).

However, with the generation of a Myo1a knockout (KO) mouse, in depth *in vivo* functional analysis was possible. While the animals appeared normal at the whole level, brush border composition was compromised (Tyska et al., 2005). Initial studies showed an increase in Myo1c in the brush border, decreased SI, myosin-6, and cytokeratins. Surprisingly, given the high levels of Myo1a normally present in wildtype (WT) animals (Mooseker and Tilney, 1975b), microvilli still formed in the absence of Myo1a. Morphologically, the brush border exhibited slight membrane herniations and intermicrovillar spacing defects (Tyska et al., 2005).

Further studies comparing WT and MYO1A KO brush borders revealed that in the presence of ATP, isolated WT brush borders exhibited apical membrane translation along the microvillar actin bundles (McConnell and Tyska, 2007). Close examination revealed that vesicles were shed from the microvillar tips, an activity that was dramatically reduced in KO brush borders (McConnell and Tyska, 2007). This result is consistent with Myo1a being responsible for powering membrane translation along the actin bundles. Indeed, *in vivo* studies revealed that WT animals shed IAP-enriched vesicles of uniform size (McConnell et al., 2009). However, KO vesicles varied in size and were not enriched in IAP (McConnell et al., 2009). In addition, biophysical studies comparing isolated WT and KO brush borders revealed Myo1a contributes to membrane tension (Nambiar et al., 2009). Despite the observed defects in KO brush border morphology, and reduced vesicle shedding, the fact that these structures and activities were still present suggested there might be a compensatory

mechanism. Indeed, brush border proteome analysis suggested that another class I myosin might be upregulated in the absence of Myo1a (Benesh et al., 2010). Studies in polarized epithelia have revealed class I myosins target cytoskeletal features other than microvilli (Skowron et al., 1998; Tyska et al., 2005; Speder et al., 2006; Goldblum et al., 2011).

Class I myosins have been observed at tight and adherens junctions in polarized epithelia. For example, Myo1c has been shown to interact with tight junction ZO-1 (Skowron et al., 1998; Goldblum et al., 2011). Myo1c localization is not exclusive to the tight junctions; in fact, immunofluorescence data reveals this molecule is along the entire lateral membrane (Tyska et al., 2005). Interestingly, the *Drosophila* Myo1d homologue has been shown to interact with β-catenin at the adherens junction (Speder et al., 2006). These myosins might be involved in targeting other complex members to these sites or may have a more general role in orchestrating trafficking events along the membrane (Soldati, 2003; Speder and Noselli, 2007). The work presented in Chapter II details myosin-1d expression and dynamics in the enterocyte. However, Myo1d also has high expression in the nervous system (Bahler et al., 1994), which includes the polarized cell types neurons and glia.

Class I myosins and the nervous system

Responsible for sensing the stimuli of the world around and within us, the nervous system propagates input signals from every region of the body towards the brain where the electrical signals are processed. There are two main cell

types in the nervous system responsible for facilitating neural activity: neurons and glia. These polarized cells rely on the actin and microtubule cytoskeleton to maintain their polarity and modulate synaptic plasticity (Fifkova and Delay, 1982; Gardiner et al., 2011) and class I myosins have active roles in several processes important in these cytoskeletal-driven events (Lin et al., 1996; Lund et al., 2005).

The polarized morphology and function of a mature neuron is supported by the underlying cytoskeleton. Input signals or neurotransmitters are received at dendritic spines, which are actin-supported mushroom-cup shaped processes enriched in proteins important for intracellular and cell:cell signaling including postsynaptic density-95 (PSD-95) a multi-PDZ scaffolding protein, N-methyl-D-aspartate (NMDA) and α-amino-3-hydroxy-5-methyl-4-isoxazole propionic-acid (AMPA) receptors (Li and Sheng, 2003). Actin in the dendritic spines is arranged as a densely branched network with barbed-ends oriented towards the membrane (Fifkova and Delay, 1982). Also, the cytoskeleton plays an important role during spinogenesis: filopodia protrude from the dendrite to search for a synaptic partner, and develop into the mature dendrite shaped mushroom cap described above (Yoshihara et al., 2009). Likewise, the microtubule cytoskeletal network organizes synapse formation through remodeling and acting as a track for cargo transport (Conde and Caceres, 2009)

The dendritic processes converge onto the cell body, which contains the nucleus. From the cell body protrudes a single axon, the main route along which electrical signals are transmitted within the neuron (Debanne et al., 2011). Microtubules in the axon are oriented with their plus-ends towards the axonal tips

(Heidemann et al., 1981; Baas et al., 1988) and act as a track for cargo transport. Microtubule stability along the axon is also polarized in nature, where more stable, posttranslationally detyrosinated and acetylated α-tubulin is found at the minus-ends compared to the more dynamic tyrosinated α-tubulin at the plus-ends (Baas and Black, 1990). Recent work suggests that axon maturation depends on microtubule stability (Witte et al., 2008).

Finally, neurotransmitters such as glutamate are exocytosed from the distal axonal synapses (presynapse) to be taken up by neighboring dendrite postsynaptic receptors such as NMDA or AMPA. The presynapse is densely packed with vesicles that fuse with the synaptic membrane. This fusion is regulated with soluble N-ethylmaleimide-sensitive-factor attachment-protein receptor (SNARE) machinery, vesicle-associated membrane protein (VAMP), and scaffolding proteins Bassoon and Piccolo (Rizo and Rosenmund, 2008; Zanazzi and Matthews, 2009). The actin is found in two populations: a membrane and a dense non-membrane associated actin (Landis et al., 1988; Hirokawa et al., 1989). Functional studies have shown that disruption of the actin cytoskeleton with latrunculin A increases neurotransmitter release (Morales et al., 2000), suggesting that the non-membrane actin population may act as an obstacle for vesicle movement (Dillon and Goda, 2005). Actin at the membrane facilitates synapse structure and remodeling (Li and Sheng, 2003).

The cytoskeleton also plays an important role in neuronal migration. The leading tip of a migrating neuron, or growth cone, is necessary for axonal pathfinding (Dent et al., 2011a). The growth cone is a fan shaped protrusion that

consists of both filopodia and lamellipodia that explore the extracellular landscape (Dent and Gertler, 2003). Actin and microtubule remodeling are necessary for growth cone steering and involves the coordination between cytoskeletal proteins (Marsh and Letourneau, 1984; Dent and Kalil, 2001; Dent et al., 2011a).

Glia are important to neuronal migration, synapse formation, and myelination (a process discussed below) (Eroglu and Barres, 2010). In fact, glia are the most populous cell type in the nervous system outnumbering neurons 10 to 1 and include microglia, astrocytes, Schwann cells, and oligodendrocytes. Schwann cells and oligodendrocytes are members of the peripheral and central nervous systems (PNS and CNS), respectively, and are capable of ensheathing neurons in myelin, an insulating membrane that facilitates the propagation of the action potential (Hudson, 2001).

Oligodendrocytes and Schwann cells in principal follow a similar myelination program, such that they both extend multiple processes from the cell body that myelinate by wrapping around an axon. The main difference is that an oligodendrocyte myelinates multiple axons while a Schwann cell targets a single axon (Simons and Trotter, 2007). The oligodendrocyte will wrap the axon in multiple layers of myelin that appears under electron microscopy as a dense, compact ensheathment (Wang et al., 2008). Myelination is a multistep process that requires the coordination of the cytoskeleton to wrap axons (Bauer et al., 2009). First, oligodendrocyte processes must send filopodial processes in search of an axonal partner (Simpson and Armstrong, 1999; Bacon et al., 2007).

Once an axon has been selected, the oligodendrocyte process begins to wrap around the axon. Although the mechanism remains unknown, the cytoskeleton is assumed to have an instrumental role in the wrapping process. Proposed models revolve around constant remodeling of the actin cytoskeleton (Bauer et al., 2009) and research has even suggested myosins have a role in the process (Sloane and Vartanian, 2007; Wang et al., 2008). Thus, in neurons and glia branched actin networks and the microtubule cytoskeleton are important for synapse remodeling, migration and axonal ensheathment. Similar to the enterocyte, the actin cytoskeleton forms connections with junctional proteins in neurons and glia (Schnadelbach et al., 2001; Kwiatkowski et al., 2007).

Cadherins localize to synapses and are thought to facilitate synaptogenesis (Togashi et al., 2002; Jontes et al., 2004). β-catenin also localizes to dendrites and synapses (Murase et al., 2002; Togashi et al., 2002), and organizes presynaptic vesicles at the membrane (Bamji et al., 2003). In postsynapses, β-catenin regulates formation of the mushroom-cup shaped dendrite (Togashi et al., 2002). Finally, in Schwann cells, β-catenin orchestrates polarity and the timing of myelination (Lewallen et al., 2011).

As described above, cytoskeletal dynamics regulate synapse formation, plasticity and migration. Interestingly, class I myosins have been directly implicated in neuronal migration. Myo1c appears to have a role in growth cone protrusion and lamellipodial retrograde flow (Diefenbach et al., 2002). Given the number of membrane-cytoskeletal remodeling events in synapse formation, class

I myosins are ideal candidates for involvement in this process. For example, Myo1d is also highly expressed in the nervous system (Bahler et al., 1994).

Similar to enterocytes, neurons and glia exhibit distinct membrane compartments defined by lipid composition. Studies in hippocampal neurons revealed that hemagglutinin viral factors and GPI anchored proteins were trafficked to axons, while glycoprotein viral factors were transported to dendrites (de Hoop and Dotti, 1993). Similar differential transport is seen in polarized epithelia, where hemagglutinin and GPI anchored proteins are trafficked to the apical surface, and glycoproteins accumulate at the basolateral membrane (de Hoop and Dotti, 1993). Oligodendrocyte myelin is enriched in glycosphingolipids and cholesterol similar to the apical membrane of an enterocyte, but the plasma membrane of the cell body is the target of apical-like transport in epithelia (de Vries et al., 1998; de Vries and Hoekstra, 2000). Moreover, viral glycoproteins accumulate in the myelin; further suggesting trafficking to the sheath mirrors basolateral transport in epithelia cells (Klunder et al., 2008).

Myo1d expression and function

Myo1d is expressed in multiple vertebrate tissue types including lung, kidney, and brain, but until recently had not been observed in the small intestine (Bahler et al., 1994; Benesh et al., 2010). Intriguingly, Myo1d expression is the highest in the CNS (Bahler et al., 1994). Examination of the rat cerebrum cortex and thalamus revealed Myo1d is expressed in neurons where the motor exhibited punctate cytosolic localization (Bahler et al., 1994). Similarly,

immunofluoresence of the glioma cell line, C6, revealed Myo1d punctate staining (Bahler et al., 1994). Western blot analysis demonstrated that Myo1d expression is developmentally regulated, with a steady increase in forebrain levels during maturity to adulthood (Bahler et al., 1994). Interestingly, microarray data analysis of purified cells from mouse brain revealed that Myo1d transcripts increase more than 60-fold during oligodendrocyte maturation (Cahoy et al., 2008). In addition, the motor was identified in the myelin proteome suggesting that Myo1d is at high levels in the white matter of the CNS (Ishii et al., 2009; Jahn et al., 2009).

Although Myo1d is expressed in most tissue types, the vertebrate function of the motor is not well understood. Studies with Madin-Darby Canine Kidney (MDCK) cells, which are polarized kidney epithelia, suggest that the motor is important in the early endocytic recycling pathway (Huber et al., 2000). Immunofluoresence staining of MDCK cells reveal that Myo1d subcellular localization is punctate (Huber et al., 2000). Furthermore, treating live MDCK cells with antibody targeting Myo1d inhibited progression of vesicles through the early endocytic pathway (Huber et al., 2000).

However, studies in the Drosophila embryo identified a novel role for Myo1d during left-right body patterning (Hozumi et al., 2006; Speder et al., 2006). Mutations within the motor domain resulted in *situs-inversus* of the *Drosophila* gut and gonads (Hozumi et al., 2006; Speder et al., 2006). While the mechanism underlying how Myo1d contributes to left-right patterning remains unknown, it was shown that the tail domain interacts with Armadillo (the *Drosophila* β-catenin

homologue (Speder et al., 2006). Hypothetically, Myo1d targets β-catenin to the adherens junctions affecting cellular polarity through either the cytoskeletal network or downstream nuclear targets (Speder et al., 2006). Whether Myo1d contributes to left-right patterning in the developing vertebrate is not known.

While vertebrate Myo1d function during development is mostly unexplored, the motor has been associated with the developmental disorder autism. Single nucleotide polymorphism studies of patients with autism compared to controls revealed an association with MYO1D (Stone et al., 2007). However, the mechanism of how mutations to MYO1D contribute to autism etiology has not been studied.

Summary

The work in this dissertation began with an interest in how class I myosins contribute to the apical microvillar actin array. To this aim, I validated expression of a novel class I myosin, Myo1d, in the small intestine, and characterized Myo1d localization in the enterocyte. Myo1d localizes to three subcellular regions in the small intestine enterocyte. First, Myo1d localizes along the lateral membrane from the tight junctions towards the basal membrane. Myo1d also targets to the terminal web, which is an actin-spectrin meshwork at the base of the brush border. Lastly, Myo1d localizes to microvillar tips and is to our knowledge the first vertebrate protein identified to target this structure.

Given that Myo1a is known to be at high density in the brush border, we were interested in how the structurally similar motor, Myo1d, is capable of

sharing the same cytoskeletal array. Immunofluorescence of the small intestine revealed Myo1a localizes along the microvillar axis, while Myo1d localizes at the microvillar tips and terminal web. However, in the MYO1A KO brush border, Myo1d redistributes along the entire length of the microvillar axis. Biochemical analysis and live imaging suggest Myo1d is outcompeted along the actin bundle and the membrane, and is more dynamic in the brush border compared to Myo1a (Benesh et al., 2010). Taken together, this suggests that Myo1a and Myo1d compete for the brush border cytoskeletal array.

While Myo1d seems capable of compensating for the loss of Myo1a in the brush border, we were interested in identifying a unique role for the protein. Performing a yeast 2-hybrid screen, we identified aspartoacylase, a protein implicated in fatty acid synthesis and expressed in polarized cells of the kidney, small intestine, and brain (Hershfield et al., 2006; Surendran et al., 2006). Aspartoacylase catabolizes N-acetyl-L-aspartate (NAA), and the resulting products are hypothesized to regulate neuronal osmolarity and contribute to oligodendrocyte myelination (Namboodiri et al., 2006). Interestingly, aspartoacylase has relatively high expression in the brain compared to protein levels in other tissues, (Bhakoo et al., 2001) similar to Myo1d (Bahler et al., 1994). Recent studies suggest Myo1d is present in isolated myelin (Yamaguchi et al., 2008; Ishii et al., 2009; Jahn et al., 2009) and is greatly upregulated during oligodendrocyte maturation (Cahoy et al., 2008). Moreover, single polymorphism nucleotides in MYO1D are associated with autism (Stone et al., 2007), suggesting an important role for the motor during neurodevelopment.

Intriguingly, autism patients exhibit altered NAA levels across brain regions (Kleinhans et al., 2007). Taken together, we hypothesized that Myo1d may interact with aspartoacylase to modulate NAA levels. We were therefore interested in determining if Myo1d and aspartoacylase are coexpressed in similar cell types. First, we were interested in fully characterizing Myo1d expression in neuronal and myelinating cells to expand upon the screens mentioned above.

While Myo1d is expressed in neuronal cells, expression in myelinating cells has not been fully established. In light of similar expression for Myo1d and aspartoacylase in the brain, we were interested in determining what neural cell types express Myo1d by investigating the polarized cells of the PNS and CNS. Intriguingly, in teased sciatic nerve bundles, Myo1d associates with both myelinating Schwann cells and axons. However, in the mouse cerebellum, Myo1d is predominantly expressed in neurons. Immunofluorescence data demonstrates Myo1d expression is developmentally regulated, and is present in the Purkinje and granule cell layers. Similar to Myo1d localization in the cortex, the motor exhibits cytosolic, punctate subcellular localization in cell bodies, along axons, and in dendrites. In addition, biochemical and immunofluorescence data suggest that Myo1d and aspartoacylase interact. Binding assays determined Myo1d interacts with the aspartoacylase C-terminus, which is hypothesized to sterically hinder catalytic activity (Bitto et al., 2007). Given the proposed roles for aspartoacylase, myosin-1d may regulate neuronal osmolarity or fatty acid synthesis. From these studies, Myo1d exhibits unique subcellular localization between cell types, high mobility, and an interaction with aspartoacylase.

The goal of this dissertation is multifold: 1) characterize Myo1d expression in the small intestine (Chapter II); 2) explore how similar class I myosins occupy the same cytoskeletal array (Chapter II); 3) characterize Myo1d expression in the nervous system (Chapter III); and 4) detail an interaction between Myo1d and aspartoacylase, a protein implicated in fatty acid synthesis (Chapter III).

CHAPTER II

DIFFERENTIAL LOCALIZATION AND DYNAMICS OF CLASS I MYOSINS IN THE ENTEROCYTE MICROVILLUS

This chapter was published under this title in *Molecular Biology of the Cell*, March 15, 2010, (Benesh et al).

Intestinal epithelial cells lining the small intestine exhibit a remarkably well-organized apical brush border composed of a tightly packed array of microvilli. Integral to the stability of each microvillus is the core actin bundle and associated actin-binding proteins. Early electron micrographs of microvilli revealed the presence of lateral bridges that connect the microvillar membrane to the underlying actin bundle (Mooseker and Tilney, 1975a; Matsudaira and Burgess, 1979). These bridges were later identified as the actin-based motor protein, Myo1a (Mooseker and Tilney, 1975a; Matsudaira and Burgess, 1979; Howe and Mooseker, 1983; Collins and Borysenko, 1984). Since the initial visualization of Myo1a, the list of myosins known to reside in the brush border has continued to grow; we now know that representatives from classes I, II, V, VI, and VII target to this actin-rich domain (Heintzelman et al., 1994; Chen et al., 2001). The diversity of myosins in the brush border highlights the complexity of this cytoskeletal environment and underscores the need to understand how these myosins interact and function together to contribute to epithelial physiology.

An example of the complex interactions between myosins in the brush border was recently provided by cell biological studies of Myo1a, which has been implicated in a wide variety of enterocyte functions ranging from the organization of apical membrane domains (Tyska and Mooseker, 2004), to the control of apical membrane tension (Nambiar et al., 2009), and the shedding of vesicles from the tips of microvilli (McConnell et al., 2009). Indeed, analysis of a Myo1a KO mouse revealed defects in brush border membrane composition and the presence of apical membrane herniations in a subset of enterocyte brush borders (Tyska et al., 2005). Despite these defects, Myo1a KO mice demonstrate no overt physiological symptoms, giving rise to the possibility that other myosins may be able to partially compensate for the absence of Myo1a function in these animals. This idea is supported by more recent studies in isolated brush borders, which show that membrane shedding from microvillar tips is significantly reduced, but not abolished in the absence of Myo1a (McConnell and Tyska, 2007). Moreover, immunofluorescence studies do indicate that another short-tailed class I motor, Myo1c redistributes from basolateral membranes to the brush border in the absence of Myo1a (Tyska et al., 2005). However, Myo1c is only one of seven vertebrate class I myosins that hold the potential to function in place of Myo1a. While the limited availability of high quality antibodies restricted the scope of these initial studies, a probe-independent approach, such as proteomic analysis, may provide more comprehensive information on how the absence of myosin-a impacts the complement of motor proteins that reside in the brush border.

Here we describe a proteomic approach that led us to identify Myo1d as another short-tailed class I myosin in the microvillus. Within WT enterocytes, Myo1d localizes to the basolateral membrane and brush border terminal web; Myo1d is also enriched in striking puncta at the distal tips of microvilli. In Myo1a KO mice, Myo1d levels in the brush border are increased approximately two-fold; this increase is accompanied by a marked redistribution of Myo1d along the length of the microvillus. We also found that in contrast to Myo1a, the microvillar targeting of Myo1d requires both IQ and TH1 domains. Finally, FRAP studies show that although Myo1d and Myo1a exhibit comparable turnover kinetics in the brush border, Myo1a has a significantly larger immobile fraction. In addition to establishing Myo1d as a component of the brush border cytoskeleton, these results suggest that dynamics may govern the localization and function of different, yet closely related myosins that target common actin-rich structures. They also highlight the utility of proteomic methods in defining the resident motor proteins that populate specific actin arrays.

Materials and methods

Proteomic analysis

Brush borders were isolated from adult mice, sacrificed in accordance with Vanderbilt IACUC protocols. A total of five paired preparations (one preparation included 25 WT and 25 Myo1a KO) were completed for mass spectrometry analysis. Once brush borders were collected (described below), total protein

concentration was determined using a BCA protein assay kit (Pierce). brush borders were resuspended in Lamelli loading buffer and separated on a 10% NuPage gel (Invitrogen). After samples were run into the gel ~2.0 cm, the gel was stained with Coomassie Blue G-250 (Bio-Rad), and then destained with sterile milliQ water. The protein-containing region was excised from the gel and minced with a razor blade (Supplemental Fig. 1). Gel fragments were then submitted to Vanderbilt University Mass Spectrometry Core for tryptic digest and subsequent proteomic analysis. Tandem mass spectra were matched to peptide sequences via the MyriMatch algorithm (September, 2007 build) (Tabb et al., 2007; Cao et al., 2008). The IPI Mouse 3.33 database provided protein sequences, with each sequence present in both forward and reverse orientations. Variable modifications included oxidation of methionine and loss of ammonia from N-terminal glutamines; all cysteines were considered to be alkylated. IDPicker (Zhang et al., 2007) filtered the raw identifications to a 1% FDR and required proteins to feature at least two distinct sequences to be included in the reports. The software also applied a parsimony filter to remove subset and subsumed proteins.

Immunofluorescence

Intestine tissues were dissected and flushed with 37° C Hank's Balanced Salt Solution (Invitrogen). 3 mm fragments of intestine were fixed with 4% paraformaldehyde in PBS (50 mM EGTA, 137 mM NaCl, 7 mM Na2HPO4, and 3 mM NaH2PO4, pH 7.2) for 30 minutes at 4° C and then cryoprotected overnight

at 4° C in 1M Sucrose in TBS. Samples were embedded into OCT and 10 μm sections were cut using a Leica CM 1900 cryostat. Sections were permeabilized for one second with –20° acetone, and washed with PBS. Next, sections were blocked in 10% BSA/PBS for 20 minutes, and washed. Sections were then incubated with primary antibody targeting Myo1a (4P1, 1:200) and Myo1d (C13, K18, or H60; Santa Cruz, 1:50), or IAP (Sigma Aldrich, 1:200) diluted in PBS for one hour and then washed. Secondary antibodies donkey anti-goat (Molecular Probes, 1:200) and Alexa-conjugated Phalloidin (Molecular Probes/Invitrogen, 1:200) were diluted in PBS and applied to sections for twenty minutes in darkness. Finally, sections were washed three times and prepared for coverslips using ProLong Anti-fade (Molecular Probes/Invitrogen). Samples were viewed on an Olympus FV-1000 with a 100x objective lens. All images were contrast enhanced, pseudo-colored, and cropped with ImageJ v. 1.42h (NIH). brush borders were straightened using the ImageJ Straighten Curved Objects plug-in (Eva Kocsis, NIH). After straightening, pixel intensities for red, green, and blue channels were averaged along the axis perpendicular to the microvillar axis using a LabView program developed in house. Average pixel intensities were then plotted relative to position along the microvillar axis.

Preparation of whole cell homogenates

Intestinal tissues were collected from WT and Myo1a KO mice and placed in ice-cold sucrose dissociation solution (200 mM sucrose, 0.02% Na-Azide, 12 mM EDTA-K, 18.9 mM KH2PO4, and 78 mM Na2HPO4, pH 7.2) for two hours.

Mucosa was scraped from the intestine with a blunt straight-edge and then resuspended in homogenization buffer (10 mM imidazole, 4 mM EDTA-K, 1 mM EGTA-K, 0.02% Na-Azide, 1 mM DTT, and 1 mM Pefabloc, pH 7.2).

Brush border isolation and fractionation

Brush borders were isolated from mouse small intestinal tissues as previously described (Tyska et al., 2005). For biochemical extraction, isolated brush border pellets were first treated with 1% NP-40 in buffer A' (75 mM KCl, 20 mM imidazole, 1 mM EGTA, 2.5 mM MgCl2, 0.02% Na-Azide, 1 mM DTT, and 1 mM Pefabloc pH 7.2) for five minutes on ice. Samples were then centrifuged at 5,000 x g for 10 min. The resulting pellet was washed twice in A' with 10 min spins at 5,000 x g. Detergent extracted brush borders were then treated with 2 mM ATP in A' and quickly sedimented at 10,000 x g for 10 min at 4° C. The resulting supernatant was collected and then centrifuged at 100k x g for 1 hr at 4° C (Beckman, TL-100 ultracentrifuge). The 100k x g pellet was resuspended in a volume of A' equivalent to the supernatant.

Immunoblotting

Primary antibodies used for immunoblotting were diluted to 1:1000, including Myo1a (4P1, developed by our laboratory), EGFP (Molecular Probes, A11122) and non-muscle Myo2 (Biomedical Technologies). H60 (Santa Cruz Biotechnology) and antibody #482 which targets amino acids 991-1006 of Myo1d were both used at 1:500 (a gift from Martin Bahler, Westfälische Wilhelms-

Universität Münster, Münster, Germany)(Huber et al., 2000). Secondary antibodies included fluorescent IRDye800 conjugated donkey anti-rabbit IgG (Licor) and fluorescent conjugated Alexa680 donkey anti-goat IgG (Molecular Probes). Blots were processed according to manufacturers recommendations and scanned on an Odyssey Imager (Licor). For some biochemical experiments, the secondary antibody was HRP-conjugated goat anti-rabbit IgG, in these cases, immunogens were imaged with ECL reagents according to the manufacturers recommendations (GE Healthcare).

Molecular cloning

A full length Rattus norvegicus Myo1d clone (IMAGE I.D. 7106587) was obtained from the Mammalian Gene Collection (http://mgc.nci.nih.gov/). Conventional PCR cloning was used to insert the Myo1d coding sequence into pEGFP-C1 (Clontech) with a forward primer containing a Sac1 site (AATTGAGCTCGCGCCATGGCGGAGCAGGAGAG) and a reverse primer with a BamH1 site (TGTTGGATCCTCAATTCCCGGGCACACTGA). Myo1d-1d Motor (nucleotides 1-2109) was cloned into the pmCherry-N3 vector with the same forward primer as above and a reverse primer with a BamH1 site (TGGTGGATCCGAGGACAACCCTGACGAGCATC). Myo1d-MotorIQ (nucleotides 1-2217) was cloned into the pmCherry-N3 vector with the same forward primer as above and a reverse primer containing a BamH1 site (GGTTGGATCCGTACGACTTCACTTTATAGC). Myo1d IQ-TH1 (nucleotides 1708-3018) was inserted into the EGFP-C1 vector using the EcoR1 and Sac1

sites. The Myo1d TH1 domain (nucleotides 2242-3018) was cloned into the EGFP-C1 vector using a forward primer containing a Sac1 site (GCGAGCTCACGGGGTCAAGA) and the same reverse primer as above. The Myo1d IQ domain (nucleotides 2082-2241) was cloned into the EGFP-C1 vector using a forward primer containing an EcoR1 site (CGGCGGATCCGAATCGCCTGGCTACCTCGTG) and a reverse primer containing a BamH1 site (CTACGAATTCCATCGCGCCCAGATGCTCGTCAGG).

Cell culture

LLC-PK1-CL4 cells were cultured in Alpha Minimum Essential Media (Invitrogen), 10% defined fetal bovine serum (Hyclone), and 2 mM L-Glutamine (Invitrogen). Cells were incubated at 37° C and 5% CO2. LLC-PK1-CL4 cells were transfected using Lipofectamine 2000 (Invitrogen) according to the manufacturer's protocols.

Fluorescence recovery after photobleaching

FRAP was performed as previously described (Tyska and Mooseker, 2002). Briefly, LLC-PK1-CL4 cells stably expressing EGFP-Myo1d or EGFP-Myo1a were grown to confluency on Matek 35 mm glass bottomed dishes. Prior to imaging, complete media was exchanged for 25 mM HEPES buffered DMEM lacking phenol red and mineral oil was layered on top to prevent media evaporation. Cells were incubated in a WeatherStation (Precision Control) at 37˚C and imaged using an Olympus FV-1000 laser scanning confocal

microscope. A field of 105.6 x 105.6 μm was scanned every three seconds and a ROI for photobleaching was set at 5 μm2. Bleaching was performed with three scans at 100% transmission. Immediately after bleaching, the entire field was scanned at three second intervals. ImageJ was used to extract the ROI integrated pixel intensities from raw data files; intensity data was then exported to a Microsoft Excel where background and t = 0 intensity values were subtracted from each time point. Intensity data was normalized so that the scan immediately prior to photobleaching was equal to 1. Using SigmaPlot v.10, recovery data was fit to the following kinetic model: IROI(t ≥ 0) = α - A1exp-k1t - A2exp-k2t where IROI is the ROI intensity at time t ≥ 0, α is the mobile fraction, Ax is the amplitude of the exponential process with rate kx.

Results

Four class I myosins reside in the mouse enterocyte brush border

To identify class I myosin proteins that may be compensating for the loss of Myo1a in KO brush borders, we submitted five paired preparations of brush borders isolated from adult WT and KO mice for proteomic analysis with two-dimensional liquid chromatography tandem mass spectrometry (2D-LC-MS/MS). Resulting mass spectra were assigned to peptides with MyriMatch, a database search algorithm employing multivariate hypergeometric analysis (Tabb et al., 2007). Peptides were then assigned to proteins using IDPicker, a parsimony-based protein assembly tool (Zhang et al., 2007). The peptide counts reported

here represent the total number of peptides assigned to a given myosin from all five brush border preparations (Table 1). While this shotgun proteomic approach does not allow for a rigorous quantification of protein levels in our samples, relative comparisons between genotypes are possible as equal amounts of total protein were subject to 2D-LC-MS/MS. Indeed, the number of peptides obtained for non-muscle myosin-2 (nm Myo2c), a protein not expected to change in KO brush borders (Tyska et al., 2005), was nearly identical between genotypes. In contrast, the number of detectable calmodulin peptides decreased in KO samples, consistent with earlier findings (Tyska et al., 2005).

Proteomic analysis of the brush border detected four class I myosins: Myo1a, Myo1c, Myo1d, and Myo1e. Three of these four identifications have been reported in previous studies (Tyska et al., 2005). Consistent with immuno-fluorescence observations showing the redistribution of Myo1c into the brush border in the absence of Myo1a (Tyska et al., 2005), we observed a ~30% increase in the number of Myo1c peptides detected in Myo1a KO samples. However, the presence of high levels of Myo1d in WT brush borders was an unexpected result. In addition, Myo1d peptide counts increased ~130% in the absence of Myo1a. These data show that Myo1d is a constituent of the brush border under normal circumstances and the principal class I myosin in brush borders lacking Myo1a.

Table 1 Proteomic analysis of class I myosins in the enterocyte brush border

Protein	IPI identifier	WT total*	KO total*	% change
Myo1a	IPI00465712.5	1068	3	-99.7
Myo1c	IPI00620222.2	19	25	31.6
Myo1d	IPI00408207.2	171	395	131.0
Myo1e	IPI00330649.4	6	11	83.3
Calmodulin	IPI00467841.6	8	3	-62.5
Nm Myo2c	IPI00453996.1	1796	1801	0.3

*Total spectra obtained in the analysis of five, paired WT and Myo1a KO brush border preparations; see Supplemental Methods for details.

Myo1d localizes to the brush border terminal web and microvillar tips

Given that Myo1d has not been previously observed in the vertebrate brush border, we sought to validate our proteomics data with conventional cell biological methods. To examine Myo1d localization in the enterocyte, we stained sections of mouse small intestine with a commercially available antibody (C13; Santa Cruz Biotechnologies). This anti-Myo1d probe targeted the enterocyte basolateral membrane as well as the terminal web of the brush border (Figure 4A), a cytoskeletal meshwork at the base of microvilli that consists of the actin bundle rootlets, spectrin, nm Myo2, interwoven with an array of intermediate filaments (Mooseker, 1985). The observed C13 terminal web staining was a consistent feature along the full length of villi throughout the small intestine. Strikingly, the C13 probe also labeled a population of discrete Myo1d puncta at the distal ends of microvilli (Figure 4B). Phalloidin labeling revealed that Myo1d puncta appear at the distal tips of core actin bundles (Figure 4B, inset). Close examination of frozen sections revealed that C13 labeled microvillar tips mostly along the distal half of the villus.

Interestingly, when two other commercially available Myo1d antibodies (K18 and H60) were applied to sections of small intestine, these antibodies each targeted a distinct subcellular Myo1d population. The K18 antibody targeted Myo1d at microvillar tips, while the H60 antibody targeted the terminal web and basolateral membrane (Figure 5). Thus, the C13 staining described above (Figure 4) represents a composite of the labeling patterns produced by these two

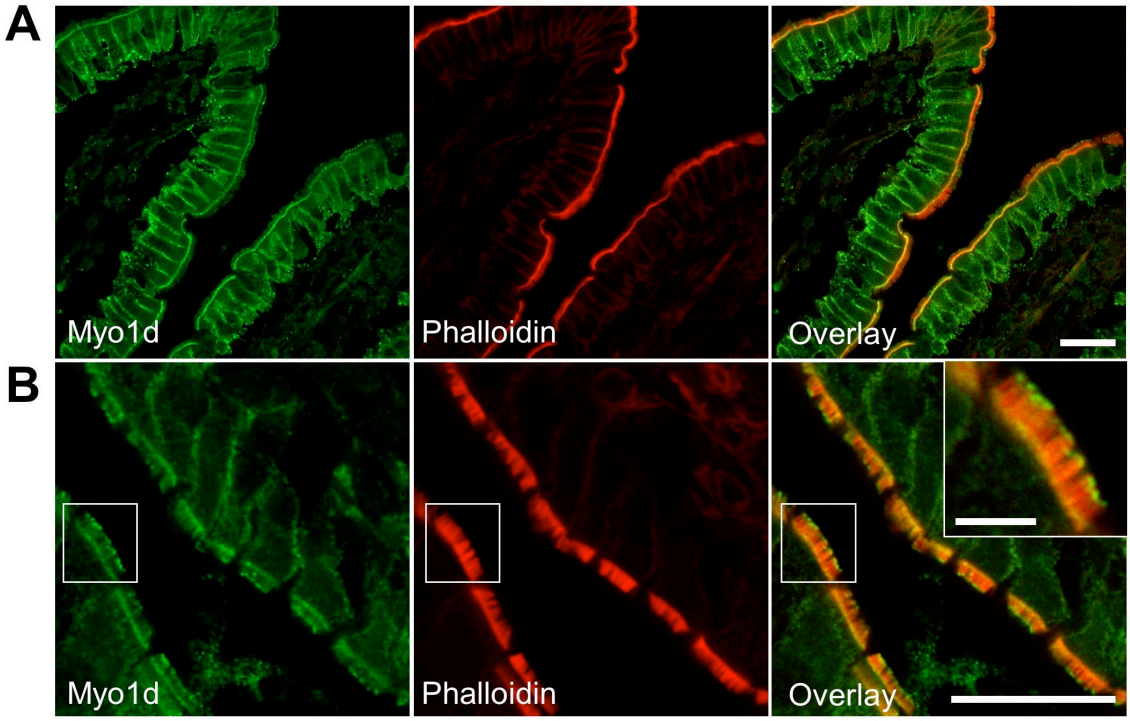

Figure 4 Myo1d localizes to the enterocyte basolateral membrane, terminal web, and microvillar tips.

Representative frozen sections of mouse small intestine stained with antibodies targeting Myo1d (green) and Alexa488 (or 633)-conjugated phalloidin (red). (A and B) Myo1d C13 antibody targets the basolateral membrane, terminal web, and microvillar tips of enterocytes. Bar is 20 μm. Inset bar is 5 μm.

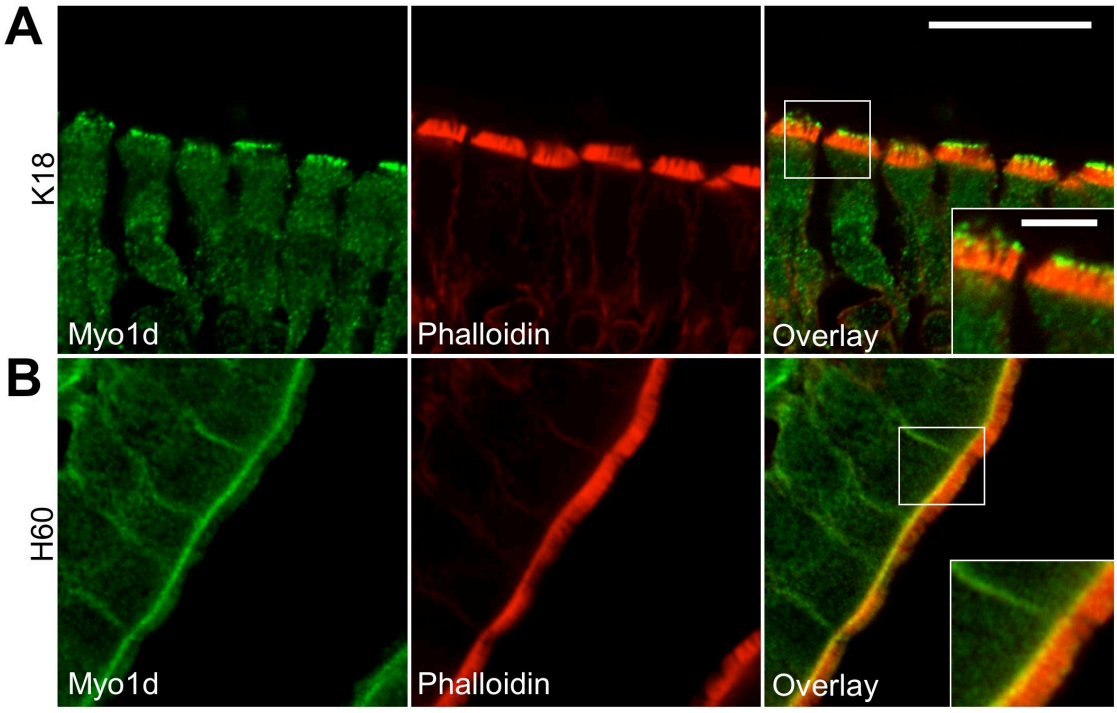

Figure 5 Myo1d localizes to the basolateral membrane, terminal web, and tips of microvilli.

Two additional commercially available antibodies (K18 and H60) each target a unique Myo1d subcellular population. Together, these two antibodies produce a composite pattern of the C13 antibody labeling. (A) The Myo1d K18 antibody targets microvillar tips. (B) The Myo1d H60 antibody labels the basolateral membrane and terminal web. Bar is 20 µm; inset bar is 5 µm.

probes. The different patterns observed here are likely related to the fact that these probes target distinct C-terminal epitopes of Myo1d, which may be differentially masked or exposed in different regions of the enterocyte.

Myo1d partially colocalizes with IAP at microvillar tips

Recent studies have revealed that enterocyte microvilli release small vesicles enriched in IAP from their distal tips (McConnell et al., 2009). These previous experiments also showed that IAP is enriched in discrete puncta at microvillar tips, presumably intermediates in the vesicle formation and release pathway. To determine if Myo1d is present in these puncta, we double-stained intestinal frozen sections for Myo1d and IAP. Confocal imaging revealed bright regions of IAP staining at microvillar tips as previously reported (Figure 6). While Myo1d tip labeling was readily observed, only a subset of the Myo1d signal at microvillar tips colocalized with IAP-enriched puncta. In some regions, IAP enriched puncta were observed at more distal positions than Myo1d (arrowheads, Figure 6B inset), giving rise to the possibility that vesicles released into the lumen may not be enriched in this motor. This is consistent with our previous proteomic analysis of microvillus-derived vesicles (McConnell et al., 2009), which identified a total of three Myo1d peptides in two out of three preparations (unpublished data). Together these data suggest that Myo1d may play a role in the early stages of vesicle formation at microvillar tips, but is not included as “cargo” in vesicles that are ultimately released into the intestinal lumen.

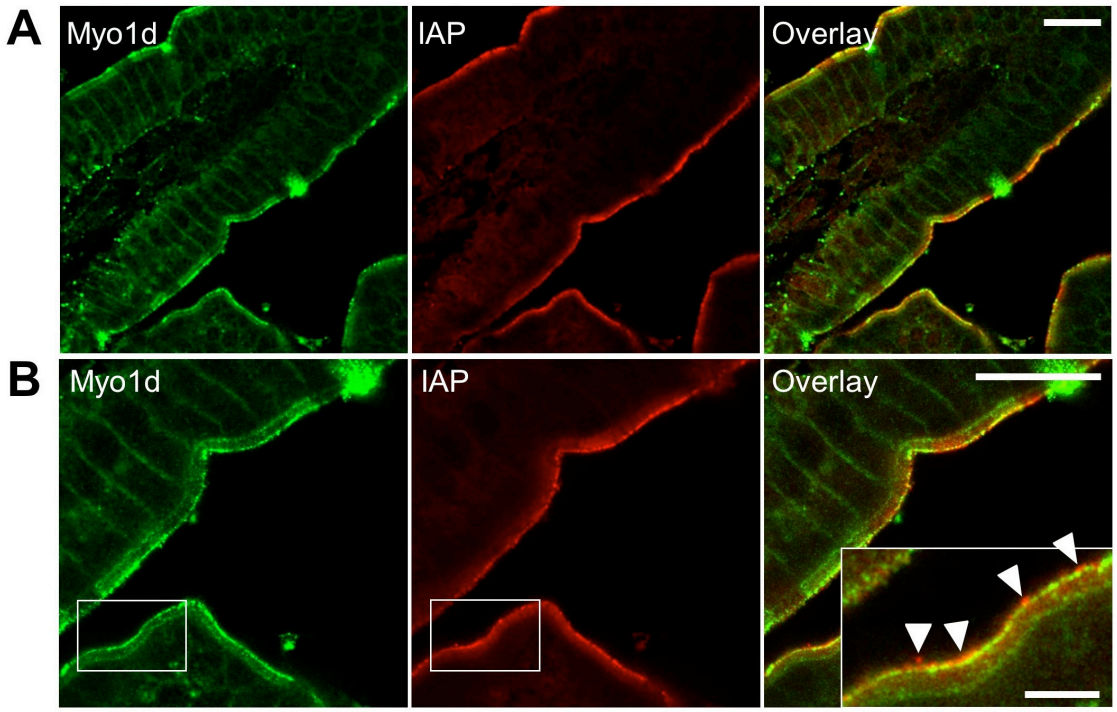

Figure 6 Myo1d and IAP partially colocalize at tips of microvilli.

Frozen sections of mouse small intestine labeled with antibodies targeting Myo1d (green) and IAP (red). (A) Confocal image of a villus demonstrating both Myo1d and IAP localize to microvillar tips. (B) Representative view of partial colocalization between Myo1d and IAP at microvillar tips. Myo1d at microvillar tips appears in two populations: alone in distinct puncta, and colocalized with IAP. Arrowheads mark IAP enriched puncta that lack Myo1d at the extreme distal tips of microvilli. Bars are 20 μm in A and B, 5 μm in B inset.

Subcellular fractionation of Myo1d is altered in the absence of Myo1a

As a first step toward understanding how Myo1d responds to the absence of Myo1a, we examined whole cell levels of Myo1d in WT and Myo1a KO enterocytes. Western blots of mucosal scrapings show that total cellular levels of Myo1d are unaltered in KO animals (Figure 7A). This suggests that the increase in peptide counts observed in our proteomic analysis is likely the result of a redistribution of the Myo1d population normally expressed in enterocytes. To further investigate this possibility, isolated brush borders were biochemically extracted using detergent and ATP. Brush borders were first exposed to 1% NP-40 to release detergent soluble membranes (DSMs). As expected, neither Myo1a nor Myo1d were released from the brush border by detergent treatment (Figure 7B). Next, the NP-40 insoluble fraction was treated with 2 mM ATP to release myosin motors and bound cargoes such as detergent resistant membranes (DRMs, +ATP, S in Figure 7B), from core actin bundles (+ATP, P in Figure 7B). In WT brush borders, almost all of the Myo1d solublized with ATP treatment, while Myo1a distributed equally between ATP soluble and insoluble fractions. Thus, in the presence of ATP, Myo1a may have a greater affinity for actin compared to Myo1d. This finding may help explain why Myo1a effectively prevents Myo1d from targeting along the length of microvillar actin bundles in WT brush borders. In Myo1a KO brush borders, the amount of Myo1d associated with core actin bundles following ATP treatment increased dramatically (+ATP, P in Figure 7B).

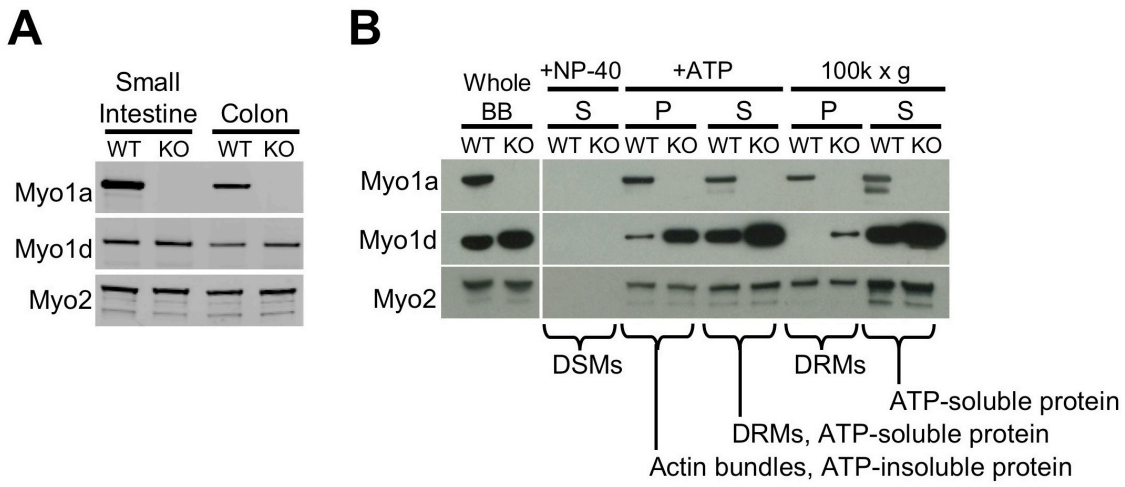

Figure 7 Myo1d redistributes within the enterocyte in the absence of Myo1a

(A) Whole cell lysates were created from WT and KO small intestine and colon mucosal scrapings and then blotted for Myo1a and Myo1d. (B) Compartmentalization of Myo1d within the brush border is Myo1a-dependent. Myo1d protein levels are slightly higher in KO brush borders compared to WT brush borders. Neither Myo1d nor Myo1a are found with detergent solublized membranes (DSMs) from whole brush borders following treatment with 1% NP-40 (+NP-40, S). Upon treatment with mM ATP, Myo1a distributes equally between soluble (+ATP, S) and insoluble (+ATP, P) fractions. Most Myo1d is found in the supernatant, with low levels remaining in the pellet. In the absence of Myo1a, the amount of Myo1d associated with actin bundles increases dramatically. Centrifugation of the ATP supernatant (+ATP, S) at 100k x g enables the separation of DRMs (100k x g, P) from purely soluble proteins (100k x g, S). In WT samples, Myo1a partitions equally between the DRM and soluble fractions, while Myo1d does not sediment with DRMs. However, Myo1d signal appears in the DRM-enriched 100k x g pellet in Myo1a KO samples. The 100k x g gel samples were concentrated 2.5-fold relative to all other samples. As Myo2 is a brush border component that is not expected to change in the absence of Myo1a (see Table I), blots for Myo2 are shown as a loading control.

The supernatant created following ATP treatment (+ATP, S in Figure 7B) contains soluble myosins, such as Myo1a, and Myo1a-associated cargoes including DRMs (Tyska and Mooseker, 2004). To determine if Myo1d also interacts with DRMs, these membranes were sedimented from the ATP soluble fraction using ultra-speed sedimentation (100k x g, 1 hr). In WT samples, Myo1a was found in both the DRM (100k x g, P in Figure 7B) and soluble protein (100k x g, S in Figure 7B) fractions, while Myo1d was strictly soluble. In Myo1a KO samples, however, Myo1d was detectable in the DRM-containing 100k x g pellet (100k x g, P in Figure 7B). Together these fractionation studies suggest that in KO enterocytes, the brush border population of Myo1d reorganizes to occupy compartments that are normally only occupied my Myo1a (e.g. actin bundles and DRMs).

Myo1d redistributes along the length of microvilli in the absence of Myo1a

To further explore the nature of Myo1d redistribution throughout the brush border in the absence of Myo1a, we stained frozen sections of WT and Myo1a KO small intestine with antibodies directed against both motors. Similar to previous reports (Heintzelman et al., 1994; Skowron and Mooseker, 1999; Tyska et al., 2005), Myo1a demonstrated uniform signal along the length of the microvillus (Figure 8A). However, the populations of Myo1d at the terminal web and tips of microvilli did not exhibit observable overlap with Myo1a. Indeed, high-resolution confocal micrographs revealed that Myo1a was actually excluded from the distal tip compartment occupied by Myo1d (Figure 8A, inset). Quantification

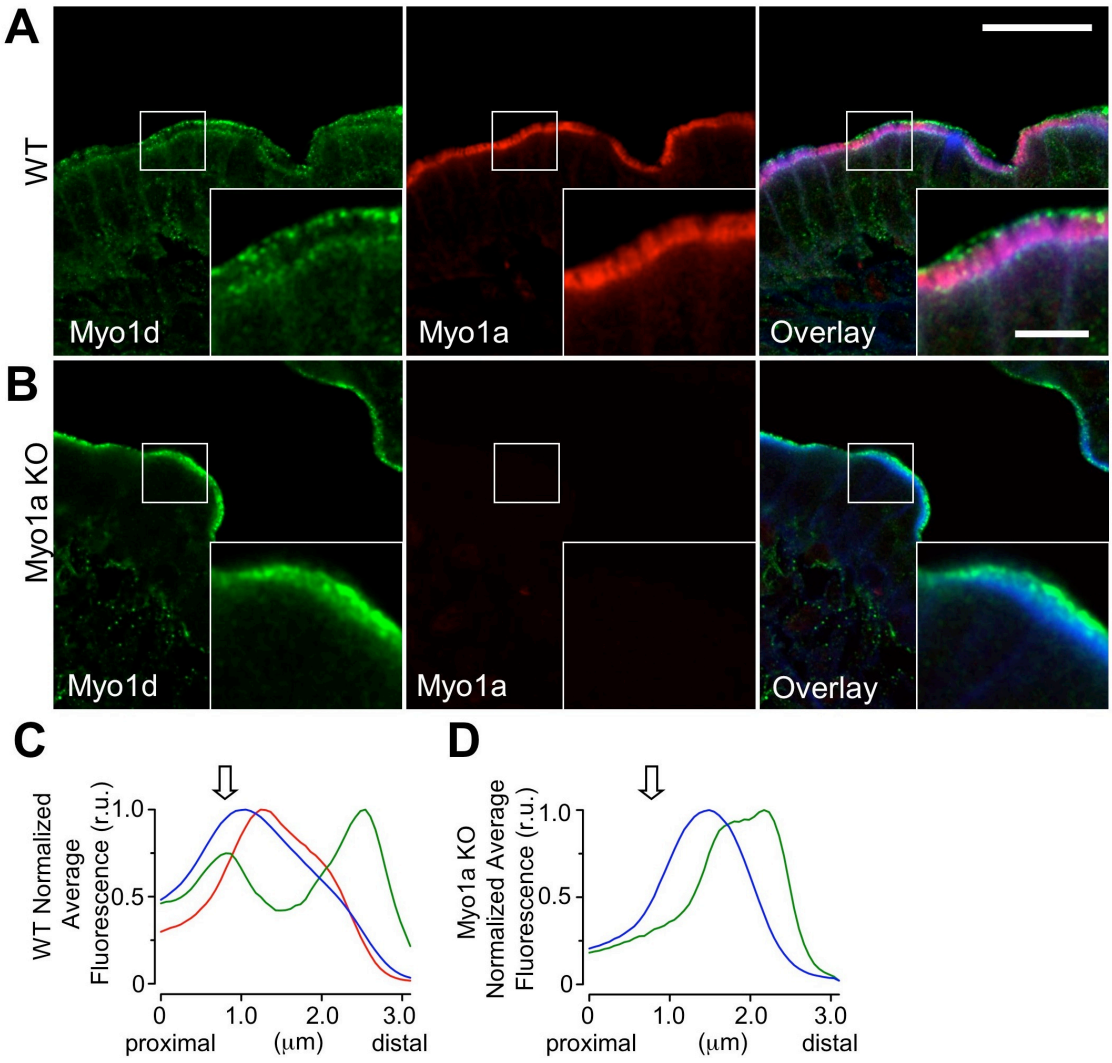

Figure 8 Myo1a and Myo1d exhibit differential localization within the brush border.

(A) Confocal images of adult WT mouse small intestine frozen sections stained for Myo1d (green, C13 antibody), Myo1a (red), and F-actin (blue). In the brush border, Myo1d occupies microvillar tips and the terminal web, while Myo1a localizes along the length of microvilli. (B) KO mouse sections stained in an identical manner reveal that Myo1d is found along the length of microvilli in the absence of Myo1a. Myo1d still occupies microvillar tips, but redistributes from lateral plasma membrane and the terminal web. (C, D) Plots show the average pixel intensity along the microvillar axis from proximal (base) to distal (tip) for Myo1d (green), Myo1a (red), and phalloidin (blue) fluorescence signals. The arrow indicates the position of the terminal web. Representative micrographs of "straightened" brush borders used to create these plots are shown in Supplemental Fig. 3. Bar is 20 μm. Inset bar is 5 μm.

of fluorescence (Figure 8C & D) revealed that the Myo1a signal begins just distal to the terminal web and parallels the phalloidin signal along the microvillar axis (red line, Figure 8C). However, the Myo1d signal peaks in two regions that flank the phalloidin signal, corresponding to the terminal web and microvillar tips, respectively (green line, Figure 8C). The distinct distributions observed here suggest that even closely related short-tailed class I myosins may be responsible for distinct functions within the microvillus.

Intriguingly, in the absence of Myo1a, Myo1d demonstrated prominent staining along the length of microvilli (Figure 8B and D), a result consistent with the biochemical fractionation data presented above (Figure 8B). Both terminal web and basolateral membrane labeling in the KO enterocytes were significantly reduced relative to WT samples (Figure 8B, Figure 9), suggesting that Myo1d signal along the length of microvilli in KO brush borders appears at the expense of these two populations. In contrast to the terminal web and basolateral populations, distinct microvillar tip labeling was still observed, indicating that Myo1d targets to this compartment independent of Myo1a levels in the brush border (Figure 8B and D).

In combination, these data reveal that outside of the microvillar tip compartment, the subcellular localization of Myo1d depends on the level of Myo1a present in the brush border. Moreover, by showing that Myo1d redistributes along the length of microvilli in the absence of Myo1a, these results also demonstrate that Myo1d is well positioned to compensate for lost Myo1a function in the KO brush borders.

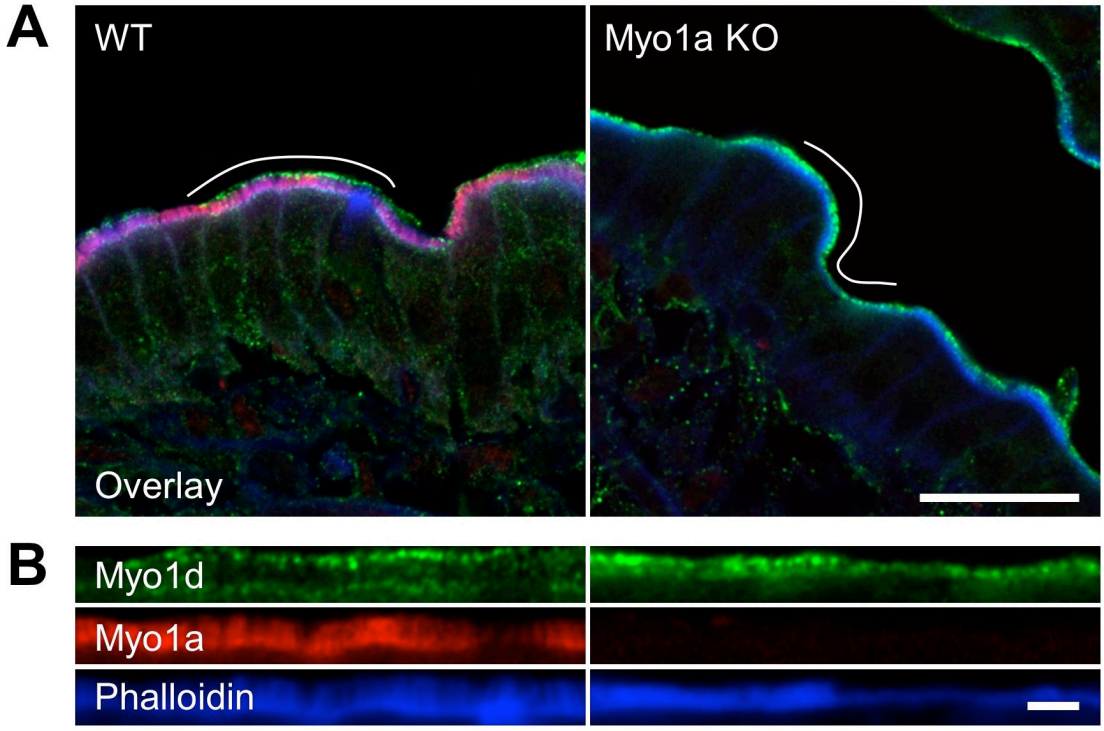

Figure 9 Myo1d brush border localization is altered in KO.

(A) Images from Figure 8 shown with the curved white line marking the region selected for "straightening" and analysis in ImageJ. (B) Straightened brush border segments marked by the curved line in A. Bar is 20 μm; inset bar is 3 μm.

Myo1d targeting to the brush border requires both IQ and TH1 domains

In order for Myo1d to fulfill functions normally carried out by Myo1a, one would expect this motor to target to the apical membrane using a mechanism similar to Myo1a. Previous work has shown that the TH1 domain alone is sufficient for Myo1a localization to microvilli (Tyska and Mooseker, 2002). To investigate which domains are required for Myo1d localization, we expressed truncated EGFP-tagged forms of Myo1d and analyzed their subcellular distribution. Constructs consisting of EGFP fused to different portions of Myo1d (Myo1d, a.a. 1-1006; Myo1d-IQTH1, a.a. 570-1006; Myo1d-TH1, a.a. 748-1006 (Figure 10A,B); Myo1d-Motor, a.a. 1-703; Myo1d-MotorIQ, a.a. 1-739, and Myo1d-IQ, a.a. 694-747 (Figure 11A) were expressed in LLC-PK1-CL4 (CL4) cells and their ability to localize to the plasma membrane and specifically, apical microvilli were examined using confocal microscopy. Consistent with endogenous staining (Figure 4), full-length Myo1d localized to both microvilli and the basolateral membrane (Figure 10D). Myo1d-IQTH1 also localized to microvilli and the basolateral membrane, similar to the full-length construct (Figure 10E). However, the Myo1d-TH1 domain alone appeared mostly cytosolic with weak targeting to microvilli (Figure 10F). Finally, Myo1d-Motor, Myo1d-MotorIQ and Myo1d-IQ domains failed to exhibit proper targeting (Figure 11). These experiments show that while both IQ and TH1 domains appear to be necessary, neither is sufficient for the proper targeting of Myo1d.

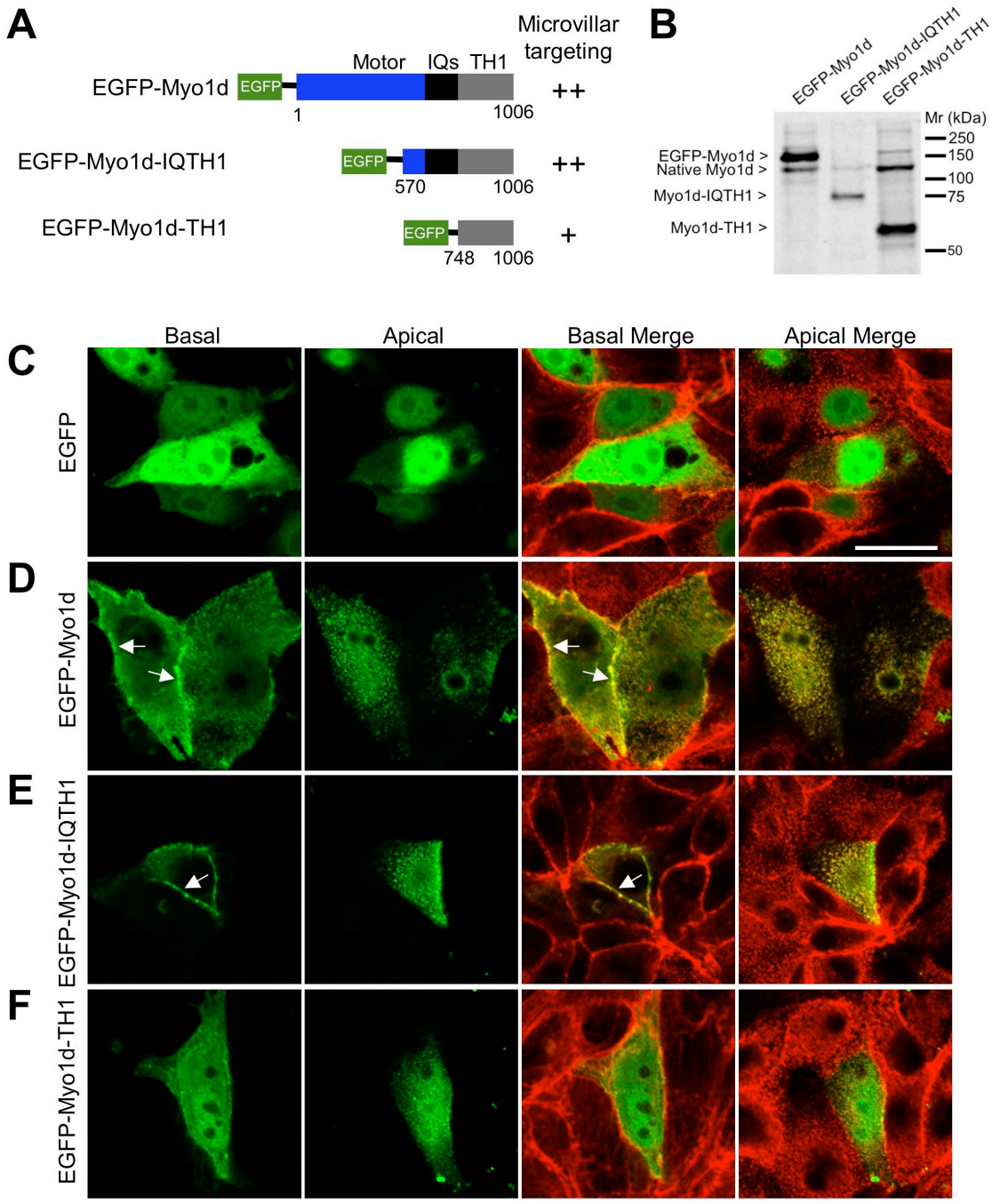

Figure 10 Truncation analysis reveals that both IQ and TH1 domains are needed for proper localization of Myo1d.
(A) Cartoon depiction of constructs that were generated for studying Myo1d localization determinants. EGFP was fused to the N-terminus of the full-length molecule, Myo1d-IQTH1, or Myo1d-TH1. An indication of the ability of each (**Figure 10 continued**)

Figure 10 continued

construct to target to microvilli is provided to the right of the cartoon. (B) Western blots with the H60 anti-Myo1d antibody confirm that fragments of the expected size are produced in CL4 cells. (C-F) Confocal micrographs of CL4 cells expressing one of three EGFP-tagged Myo1d constructs or EGFP alone (green) and counter-stained with Alexa488 or Alexa 633-conjugated phalloidin (red). Merges of green and red channels are shown at both apical and basal planes. (C) EGFP alone demonstrates diffuse localization throughout the cytosol and nucleus. (D) EGFP-Myo1d is enriched in microvilli and also targets the lateral plasma membrane, in a manner similar to that previously reported for EGFP-Myo1a (Tyska and Mooseker, 2002). (E) EGFP-Myo1d-IQTH1 localizes to microvilli and lateral membranes in a manner similar to full-length Myo1d. (F) EGFP-Myo1d-TH1 demonstrates low level targeting to microvilli and plasma membrane. Bar in A is 20 μm and serves as a calibration for all panels.

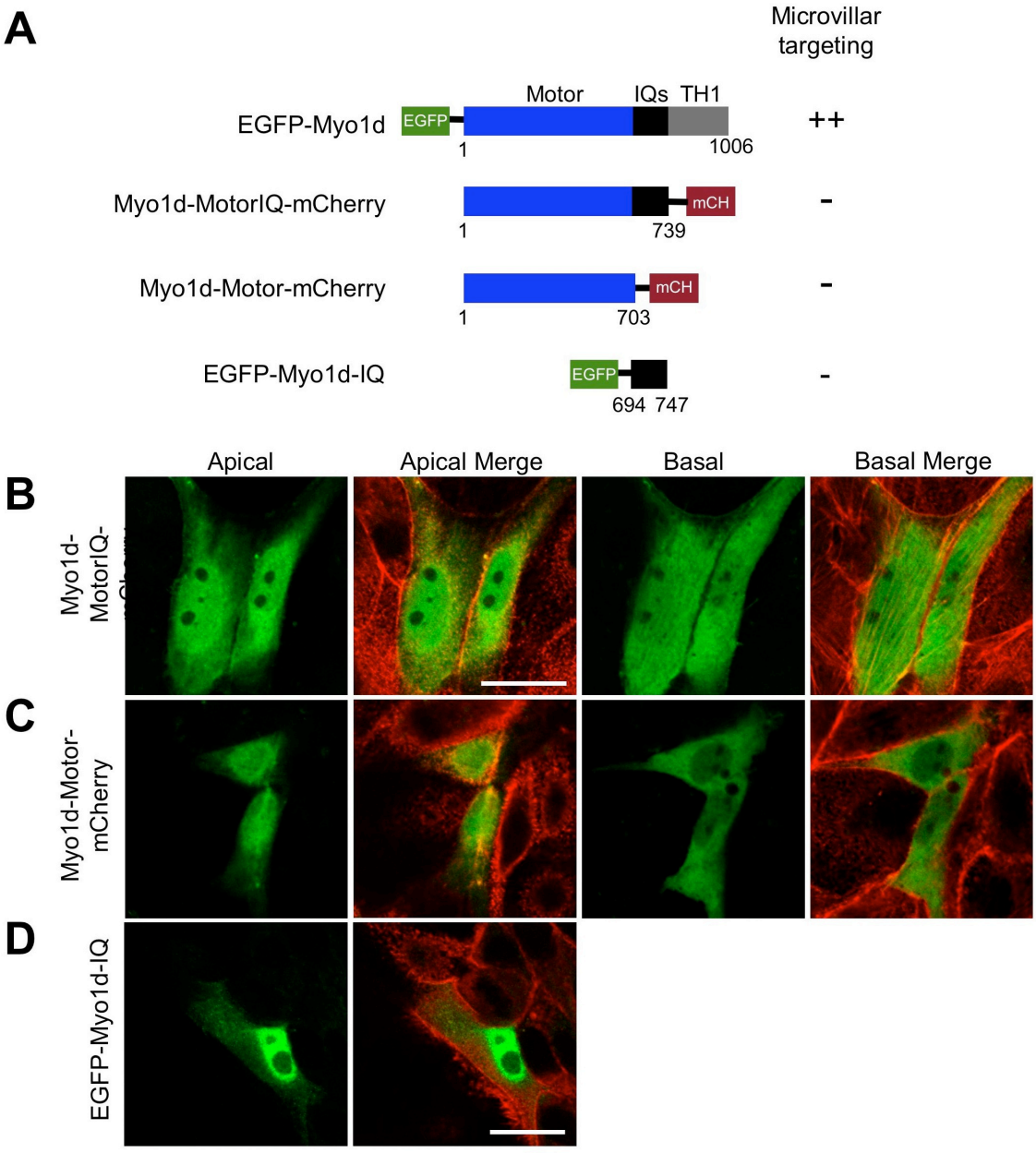

Figure 11 Cartoon depiction of constructs that were generated for studying Myo1d localization determinants.

(A) mCherry was fused to the C-terminus of Myo1d-Motor or Myo1d-MotorIQ. The amino acid numbers included in each construct are shown; an indication of the ability of each construct to target to microvilli is provided to the right of the cartoon. (B, C, D) EGFP-Myo1d-MotorIQ, EGFP-Myo1d-Motor, EGFP-Myo1dIQ domain constructs do not localize to microvilli or the plasma membrane. Bar in (B) is 20 μm.

FRAP reveals that Myo1a is less dynamic than Myo1d

The altered Myo1d distribution in Myo1a KO brush borders suggests that these two class I myosins may compete for shared binding sites (e.g. membrane receptors) within the microvillus. From this perspective, the non-overlapping distributions of Myo1d and Myo1a observed in WT enterocytes could be explained by differential dynamics within the brush border. For example, Myo1a may exhibit slower turnover rates or a larger immobile fraction relative to Myo1d, making it difficult for the latter to occupy common binding sites along the length of the microvillus. To test this model, we performed FRAP analysis on CL4 cells expressing EGFP-Myo1d or EGFP-Myo1a to measure turnover kinetics in this brush border model system (Tyska and Mooseker, 2002). CL4 cells express very low levels of both Myo1a and Myo1d (only detectable via western blot), and thus provide a convenient opportunity to examine the dynamics of these two motors independent of one another, but in the same cellular background. For these experiments, we used a laser scanning confocal microscope to photobleach a region (5 μm2) in the focal plane of microvilli (Figure 12A and B). FRAP recovery data were fit to a general kinetic model which assumes that the mobile population consists of two components: a fast population that represents freely diffusing protein, and a second slower population that represents protein interacting with brush border components (Figure 12C) (Tyska and Mooseker, 2002). Interestingly, the fast mobile components measured for Myo1a and Myo1d were nearly identical at ~0.34 s-1; recovery rates for the slow mobile components were also similar at ~0.06 s-1 (Figure 12E).

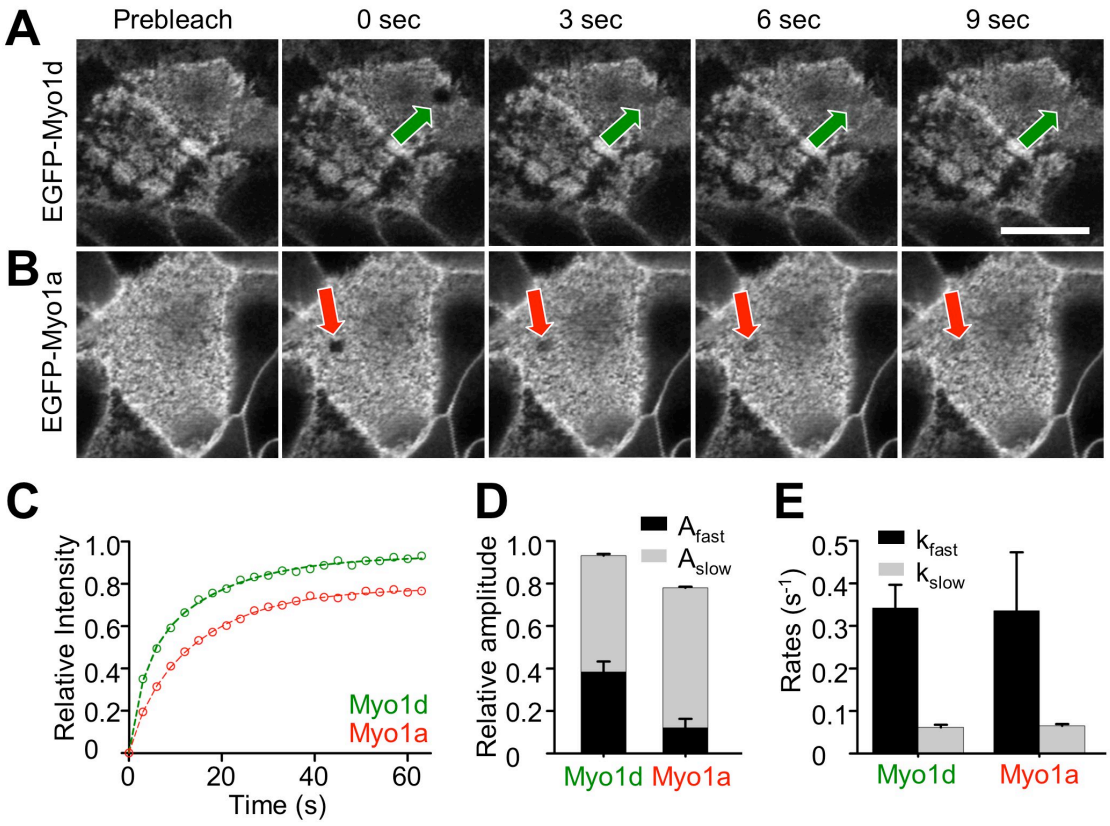

Figure 12 Myo1a and Myo1d demonstrate differential dynamics in the brush border.

(A) EGFP-Myo1d and (B) EGFP-Myo1a were expressed in CL4 cells and grown on filters for FRAP studies. Micrographs show representative examples of photobleaching; ROIs are marked with an arrow. (C) Averaged datasets (n = 14 for EGFP-Myo1a, n = 22 for EGFP-Myo1d) of the relative fluorescence recovery in photobleached regions were fit to a general kinetic model as outlined in Methods. Myo1d (green) demonstrates more complete recovery (i.e. a higher mobile fraction) when compared to Myo1a (red). (D) Stacked bar graphs of the amplitudes for Myo1d and Myo1a (Fast phase, black; Slow phase, gray). (E) Bar graphs of the rate constants for Myo1d and Myo1a (Fast phase, black; Slow phase, gray). Bar in A is 20 μm and serves as a calibration for all images.

Table 2 Summary of FRAP kinetic data

Construct	*n*	A_{fast}	k_{fast} (s^{-1})	A_{slow}	k_{slow} (s^{-1})	A_{fast}/A_{slow}	Mobile Fraction (α)
EGFP-Myo1a	14	0.12 ±0.04	0.34 ±0.14	0.66 ±0.04	0.06 ±0.01	0.18	0.78 ± 0.01
EGFP-Myo1d	22	0.38 ±0.05	0.34 ±0.05	0.55 ±0.04	0.06 ±0.01	0.69	0.93 ± 0.01

Photobleaching recovery curves were fit to a kinetic model as described in Methods. Values listed here represent fit parameters ± standard error of the fit; A_x= amplitude for process x, k_x = rate for process x, and *n* = number of brush borders sampled.

However, significant differences were observed in the total mobile fractions for Myo1a and Myo1d, 0.78 vs. 0.93, respectively (Figure 12C,D; Table 2 Summary of FRAP kinetic data). Fits to the data indicate that the differences in mobile fraction are accompanied by different amplitudes for the fast and slow mobile components. Myo1a demonstrated a very low ratio of fast to slow amplitudes (Afast/Aslow = 0.18), whereas Myo1d demonstrated a much higher ratio (Afast/Aslow = 0.69; Figure 12D, Table 2). Thus, while Myo1a and Myo1d demonstrate comparable turnover kinetics in the brush border, Myo1a appears to have a significantly larger immobile fraction (i.e. a lower mobile fraction) on the timescale of these FRAP measurements (~1 minute). These results suggest that differences in dynamics may help explain how similar motor molecules can display distinct subcellular localizations within the same organelle.

Discussion

Multiple class I myosins in the microvillus

In this study, we exploit an unbiased shotgun proteomic approach to examine the complement of class I myosins that reside in the vertebrate brush border; we also explore how this complement changes in the absence of the major brush border component, Myo1a. Four class I myosins were identified in our analysis: Myo1a, Myo1d, Myo1c, and Myo1e (listed in order of decreasing peptide counts). In addition to Myo1a, previous studies have reported the presence of Myo1c and Myo1e in the apical domain of the enterocyte (Skowron

et al., 1998; Tyska et al., 2005). Although early studies demonstrated the presence of Myo1d transcripts in vertebrate small intestine (Bahler et al., 1994), the high levels of Myo1d in the brush border and its unique localization at the tips of microvilli were unexpected. While Myo1d was abundant in WT brush borders, peptide counts increased ~2.3-fold in Myo1a KO samples, the most robust change observed for any of the myosins-I detected in this analysis. These data suggest that Myo1d is a component of the microvillus under normal conditions and is the motor most likely to recover functions that are compromised in the absence of Myo1a.

Myo1a dependent targeting of Myo1d in the microvillus

Studies presented here show that Myo1d localization in the brush border and its distribution along the microvillus are strongly influenced by the high levels of Myo1a that are normally expressed in the enterocyte. We propose that the differential localization and dynamics observed for Myo1a and Myo1d are the result of differences in the binding affinities that these motors exhibit for microvillar components. For example, when brush border fractions are exposed to millimolar levels of ATP, almost all of the Myo1d is released, whereas only ~50% of the Myo1a is solublized (Figure 7B). This indicates that Myo1a has a higher affinity for actin in the presence of ATP. In addition, the amount of Myo1d found in actin bundle-containing fractions increases markedly in the absence of Myo1a (+ATP, P; Figure 7B). Higher affinities for actin would enable Myo1a to out-compete Myo1d for binding sites along the microvillus length. This model

becomes even more attractive if one turns to the proteomics data to gain insight on the relative abundance of these motors in the microvillus. Based on the number of peptides detected in each case, Myo1a is ~5-fold more abundant than Myo1d. Thus, the total number of Myo1d molecules in the brush border demonstrate ~1:1 stoichiometry with the "immobile" population of Myo1a molecules (~20% of the total).

Function of Myo1d in WT brush borders

The unique punctate localization pattern of Myo1d at microvillar tips and prominent banding at the terminal web implies that this motor may be carrying out distinct functions at these locations. Myo1d located in the terminal web may play a role in the short-range transport, docking and/or fusion of apically directed vesicles derived from the Golgi complex (Fath and Burgess, 1993). Indeed, previous Myo1d studies have shown that this motor associates with vesicle populations in neurons (Bahler et al., 1994), and early endosomal vesicles in MDCK cells (Huber et al., 2000), supporting a role in trafficking. More recently, Myo1d was implicated in left-right asymmetrical gut patterning during Drosophila development (Hozumi et al., 2006; Speder et al., 2006), although the implications for Myo1d function in the vertebrate gut have not been explored.

One of the most striking findings of the current study was the punctate Myo1d staining observed at the tips of microvilli. Early electron micrographs of brush border microvilli revealed a dense tip complex at the distal end of core actin bundles (Mooseker and Tilney, 1975a), yet the composition of this complex

remains poorly characterized. Although Eps8 has been localized to microvillar tips in *C. elegans* (Croce et al., 2004), to our knowledge, Myo1d is the first motor protein shown to target to the distal tip compartment in these structures. While myosin-7b localizes to the distal half of microvilli (Chen et al., 2001), and myosin-5 exhibits distal microvillar localization (Heintzelman et al., 1994), neither myosin clearly exhibits the punctate localization at microvillar tips displayed by Myo1d. The tip localization described here is reminiscent of myosin-10 accumulation at filopodia tips, where it regulates the formation of these dynamic protrusions (Berg and Cheney, 2002). In the stereocilium, another parallel actin bundle supported protrusion, Myosin-3a localizes espin to the stereocilia tip where it plays a critical role in regulating stereocilia length (Les Erickson et al., 2003; Schneider et al., 2006; Salles et al., 2009). Myosin-15a also localizes to stereocilia tips (Belyantseva et al., 2003) and has been implicated in the tip-ward transport of whirlin (Belyantseva et al., 2005). Thus, Myo1d at the tips of microvilli may function in the control of actin bundle dynamics or perhaps the transport of components along the microvillar axis. Alternatively, Myo1d could play a role in the formation and/or release of vesicles from microvillar tips (McConnell and Tyska, 2007) as suggested by the partial colocalization with IAP at the distal ends of microvilli.

Myo1d function in the absence of Myo1a

While the TH1 domains of Myo1d and Myo1a only share 22.2% identity, they are both enriched in basic residues that are required to properly target both Myo1a

(Tyska and Mooseker, 2002) and Myo1d to microvilli. This shared feature may allow these two molecules to bind similar protein and/or lipid targets and engage in similar functions. In the vertebrate brush border, Myo1a forms bridges that link the actin core bundle and plasma membrane, suggesting that this molecule may play a role in maintaining the structural integrity of this complex cytoskeletal domain. Indeed, recent biophysical studies of isolated brush borders and cultured epithelial cells demonstrate that Myo1a controls membrane tension by contributing adhesion to the cytoskeleton (Nambiar et al., 2009). Myo1d redistribution along microvilli may rescue membrane tension in KO brush borders, but any rescue is expected to be partial due to the lower levels of Myo1d in this structure. Indeed, while a subset of enterocytes in Myo1a KO small intestine exhibit large herniations of brush border membrane (Tyska et al., 2005), many cells also demonstrate near normal apical membrane morphology. This mixed population suggests that some enterocytes are able to compensate for the loss of Myo1a. Other recent studies have established that Myo1a plays a critical role in regulating the formation and release of vesicles from microvillar tips (McConnell and Tyska, 2007; McConnell et al., 2009). These studies revealed that Myo1a KO animals produce fewer vesicles that are larger than normal and perturbed in their composition. Thus, microvillar membrane shedding may be a second aspect of Myo1a function that is partially compensated by Myo1d.

Conclusion

In this study, we present data establishing Myo1d as a component of the enterocyte brush border; these data also suggest that Myo1d may play a role in compensating functions that would otherwise be lost in Myo1a KO mice. The differential localization of these two closely related myosins within individual microvilli and the striking localization of Myo1d to the microvillus tip are likely the result of distinct dynamics and possibly differences in actin bundle binding affinity. Future studies will investigate the functional role of Myo1d populations in the terminal web and at microvillar tips, and explore the detailed mechanism(s) underlying compensation in the Myo1a KO mouse.

Acknowledgements

The authors would like to thank Chin Chiang (VUMC) and his laboratory for use of his cryostat, Martin Bahler (Westfälische Wilhelms-Universität Münster, Münster, Germany) for kindly providing a Myo1d antibody, the VUMC Cell Imaging Shared Resource, the VUMC Mass Spectrometry Research Center, and members of the Tyska laboratory for their advice and support. This work was supported by grants from the National Institutes of Health (R01 DK-075555, MJT; R01 CA-126218, DLT; P30 DK-058404, VUMC Digestive Diseases Research

Center) and the American Heart Association (09GRNT2310188, MJT; Pre-doctoral Fellowship, AEB).

CHAPTER III

EXPRESSION AND LOCALIZATION OF MYO1D IN THE DEVELOPING NERVOUS SYSTEM

This title is in the peer review process and will be resubmitted in the near future. Contributors to this work include: Andrew E. Benesh, Jonathan T. Fleming, Chin Chiang, Bruce D. Carter, and Matthew J. Tyska.

The myosin superfamily is a diverse collection of actin-binding, ATP-hydrolyzing molecular motors that sort into at least 35 different structural classes (Odronitz and Kollmar, 2007). Class I myosins comprise one of the largest subfamilies (eight genes in vertebrates) and are defined by a monomeric heavy chain and the potential to bind directly to acidic phospholipids (McConnell and Tyska, 2010). These molecules are also expressed in a variety of cells including Myo1a in epithelia of the small intestine (Cheney and Mooseker, 1992), Myo1f in kidney (Krendel et al., 2007), Myo1c in cochlea (Hasson et al., 1997), as well as Myosin-1g (Myo1g) in lymphocytes (Patino-Lopez et al., 2010) and Myo1d in neurons (Bahler et al., 1994) where they have been implicated in a wide range of functions at the actin/membrane interface (McConnell and Tyska, 2010).

Myo1d, previously named myr4 and myosin Iγ, was first identified in the rat cerebral cortex, spinal cord, brainstem, and cerebellum, in addition to a number of other tissues (Bahler et al., 1994). As a short-tailed class I myosin,

Myo1d contains a conserved motor domain, two IQ motifs that bind calmodulin, and a basic C-terminal tail homology-1 (TH1) domain (Bahler et al., 1994). Functional studies suggest that Myo1d plays a role in membrane trafficking (Huber et al., 2000), the control of membrane tension (Nambiar et al., 2009), and the establishment of left-right asymmetry during *Drosophila* development (Hozumi et al., 2006; Speder et al., 2006). Aside from these initial reports, our understanding of Myo1d function in the context of vertebrate physiology remains largely unexplored.

Three recent lines of evidence suggest that Myo1d plays an important role in nervous system tissues. First, linkage analysis of autistic individuals revealed a potential association with MYO1D (Stone et al., 2007). Second, mass spectrometry studies have identified Myo1d as a component of the myelin proteome (Yamaguchi et al., 2008; Ishii et al., 2009; Jahn et al., 2009). Third, Myo1d is a significantly upregulated transcript during oligodendrocyte maturation, along with other classical myelin-associated components (Nielsen et al., 2006; Cahoy et al., 2008). All of these investigations implicate Myo1d in neurodevelopment and further suggest that this motor plays a role in the process of myelination. However, there is currently no cell biological data to validate or extend the results derived from these broad screening studies.

The goal of this study was to investigate the expression, localization, and function of Myo1d during neurodevelopment. Here, we show that Myo1d is present in both the PNS and CNS. In the CNS, our analysis focused on the cerebellum, where Myo1d expression is limited to neurons, exhibiting a punctate

distribution along axons and in cell bodies. This motor was not found in glial cells as expected based on previous studies (Nielsen et al., 2006; Cahoy et al., 2008). We also identified aspartoacylase as a putative binding partner for Myo1d in Purkinje cells. Aspartoacylase functions in fatty acid synthesis and mutations in this protein lead to leukodystrophy (Namboodiri et al., 2006). Together, these findings hold implications for understanding the contribution of Myo1d to neurodevelopment and neurological disorders such as autism or Canavan disease.

Materials and methods

Sciatic nerve tissue preparation

Following a published protocol (Spiegel et al., 2007), sciatic nerve was dissected from adult mouse, and then fixed in 4% paraformaldehyde/PBS for 30 min at 4° C. The nerve was washed in 1 M sucrose/Tris buffered saline (TBS) and then placed in glycerol until the tissue was teased apart under a dissecting microscope. After individual fibers were separated, isolated material was placed on Superfrost®/Plus microscope slides (Fisher Scientific) and washed 3 times with PBS to remove residual glycerol.

Brain preparation

Mice 14 days old and younger were sacrificed according to Vanderbilt IACUC guidelines. Briefly, whole brains were removed and placed in 4%

paraformaldehyde/Phosphate buffered saline (PBS; 50 mM EGTA, 137 mM NaCl, 7 mM Na_2HPO_4, and 3 mM NaH_2PO_4, pH 7.2) and allowed to rotate at 4° C for 4, 6, or 8 hours for mice that were 3, 7, and 14 days old, respectively. Next, tissue was cryoprotected overnight in 1 M sucrose/TBS (50 mM Tris, 150 mM NaCl) at 4° C. The following day, sucrose was washed out with OCT (Sakura Finetek) and then frozen in OCT. Samples were sectioned at 15 µm thickness with a Leica CM 1900 cryostat and applied to Superfrost®/Plus microscope slides for further analysis. For generation of the $L7^{cre}$;$YFP^{membrane}$ reporter mouse, Rosa-$YFP^{membrane}$ mice (Jackson Laboratories,) were crossed with $L7^{cre}$ (Jackson Laboratories), and genotyped. Tissue was processed similarly as wildtype.

Immunofluorescence

Sciatic nerves were permeabilized with 0.1% or 1% Triton® X-100 (Sigma-Aldrich) for 30 min, and rinsed three times in PBS. Next, fibers were blocked with 5% bovine serum albumin, fraction V (BSA; Research Products International Corp.) in PBS. Antibodies targeting Myo1d (H60, polyclonal, 1:50, Santa Cruz Biotechnology, Inc.), myelin basic protein (SMI-94, monoclonal, 1:100, Covance), and light-neurofilament (DA2, monoclonal, 1:100, Cell Signaling) were applied to the samples overnight at 4° C. We previously have shown that the Myo1d H60 antibody is specific (Benesh et al., 2010), and consistently provides the best signal to noise results for immunofluoresence and Western blots. The next day, unbound primary antibodies were removed with three 5-min washes of PBS. Secondary antibody was added to each sample for 45 min (Alexa Fluor® 488 or

568 goat anti-mouse [IgG] or goat anti-rabbit, Invitrogen Molecular Probes). Samples were washed with PBS three times and adhered to glass slides with Prolong® Gold antifade (Invitrogen).

Brain slices were thawed to room temperature and a Super HT Pap Pen (Research Products International Corp.) was used to draw a hydrophobic boundary around tissue sections. Samples were washed briefly in PBS to remove residual OCT, and then permeabilized with 0.1% Triton® X-100 (Sigma-Aldrich) for 30 min at RT. When staining for myelin basic protein, samples were permeabilized with acetone for 30 min at 4° C. After three 5-min washes with PBS, samples were blocked with 5% BSA/PBS for 30 min at RT. Primary antibodies used in study: anti-Myo1d, anti-myelin basic protein, anti-neurofilament-L, anti-neurofilament-H (RMdO 20, monoclonal, 1:200, Cell Signaling), anti-calbindin (C26D12, polyclonal, 1:200, Cell Signaling), anti-O4 (MAB1326, monoclonal, 1:200, Research and Development Systems), anti-neun (MAB377, monoclonal, 1:200, Millipore), anti-aspartoacylase (sc-109208, goat, 1:50, Santa Cruz). Samples were incubated overnight at 4° C. Tissue was then washed in three 5-min washes with PBS before adding the appropriate secondary antibody species (Alexa Fluor® 488 or 568 goat anti-mouse (IgG or IgM) or goat anti-rabbit, Invitrogen Molecular Probes) for 45 min at RT in darkness. The secondary antibody was washed out in three 5-min washes before sealing a coverslip over the sample with Prolong® Gold antifade. Brain slices were imaged on a Leica TCS-SP5 confocal microscope (Leica Microsystems) with 10x and 63x objectives. Brain slices seen in Figures 2 and 3

were imaged on an Ariol® SL-50 platform (Genetix) with the assistance of Joseph Roland in the Epithelial Biology Center, Vanderbilt University Medical Center. All images were pseudo-colored, contrast enhanced, and cropped in ImageJ 1.44j (National Institutes of Health, http:/imagej.hig.gov/ij). 10x images were stitched together in Photoshop CS5 using the 'Automerge' feature.

Yeast 2-hybrid assay

A human kidney Matchmaker cDNA library was screened according to the manufacturer's instructions (Clontech). Briefly, Myo1d tail was subcloned (nucleotides 2230-3021) into the pGBKT-7 vector with a forward primer containing an EcoR1 site (AGCAGAATTCAAAGCCAGGCGATTCCACGGGGTC) and a reverse primer containing a BamH1 site (ATCGGGATCCATTCCCGGGCACACTGAGGAT). Myo1d tail pGBKT-7 transformed AH109 yeast tested negative for leaky HIS3 expression and auto-transcriptional activation. The bait-containing AH109 strain was mated with the Y187 yeast pre-transformed library in liquid culture overnight. Mating mixtures were streaked onto synthetic dropout plates (without Histidine, Leucine, and Tryptophan) and incubated for a week at 30° C. Colonies were replica plated on quadruple synthetic dropout plates (without Histidine, Leucine, Tryptophan, Adenine). DNA was extracted from clones picked from quadruple synthetic dropout plates, amplified by PCR, and sequenced according to manufacturer's instructions.

In vitro pull-down

BL21-Gold(DE3)pLysS (Stratagene, #230134) bacterial cells were transformed with pQE-32 vector (Qiagen, #32915) containing *H*s aspartoacylase cDNA or not transformed, and were streaked on plates to enable single colony selection. Colonies were picked and grown in 5 ml LB broth (FisherScientific, BP1426-2) overnight to test expression levels. 50 μl of a high expressing clone was used to inoculate a 50 ml starter culture that was grown overnight. The following day, 25 ml of starter culture was added to 500 ml LB broth and grown until the OD_{600} reached 0.6. To induce over-expression, isopropyl ß-D-1-thiogalactopyranoside (IPTG) (500 μm, Sigma-Aldrich, 15502) was added to cultures, which were then allowed to grow for an additional 3-4 hours. Bacteria were then pelleted in a Beckman X-15R at 5,000 x *g* for 20 minutes, 4° C. The pellet was snap-frozen in liquid N_2 and stored at -80° C. To begin lysis, pellets were thawed and resuspended in 20 ml of Lysis buffer (100 mM KCl, 10% glycerol, 20 mM Tris-HCl, 10 mM Imidazole, fresh 10 mM ß-mercaptoethanol, 0.2 ml fresh chicken lysozyme/gram of pellet, 1 mM Pefabloc, pH 8.5). Resuspended bacteria were agitated for 15 min at room temperature, and then sonicated with a Branson Sonicator 250 at 300W, 50% duty cycle five times for 10 sec. After bacterial lysis, the supernatant was clarified by centrifugation at 20,000 x *g* (Sorvall, SS-34 rotor). To bind the 6x-His tag aspartoacylase constructs to Ni-NTA resin (Qiagen), 2.5 ml of resin was equilibrated with Lysis buffer; the bacterial lysate was then added to resin and rotated for 1 hr at 4° C. The supernatant flow-through was removed by centrifugation (5 min at 500 x *g*).

Resin was washed three times in Wash Buffer (300 mM KCl, 20 mM Tris-HCl, 20 mM Imidazole, pH 8.5). His-tagged aspartoacylase was then incubated with LLC-PK1-CL4 (CL4) cell lysates containing either EGFP or EGFP-Myo1d. CL4 homogenates were prepared as previously described (Tyska and Mooseker, 2004). Briefly, confluent CL4 cells in a T-75 flask were washed three times with 37° C TBS, scraped, and then pelleted (500 x *g*, 10 min). Next, CL4 cells were resuspended in nine pellet volumes of Homogenization Buffer (2 mM EGTA, 150 mM KCl, 5 mM $MgCl_2$, 1 mM Dtt, 1 mM Pefabloc, 40 mM imidazole, 1 mM ATP, 1% Triton X-100, pH 7.2) and homogenized in a dounce. The homogenate was then centrifuged at 15,000 x *g* for 20 min at 4° C. The CL4 supernatant was incubated with the His-tagged aspartoacylase bound Ni-NTA resin overnight at 4° C. The following day, the resin was washed three times with Wash Buffer and then treated with boiling Laemmli sample buffer to prepare associated proteins for SDS-PAGE.

Immunoblotting

Protein samples were separated using SDS-PAGE. After electrophoresis, gels were transferred to a nitrocellulose membrane overnight (35V, 4° C). Membranes were rinsed three times with deionized water, blocked with nonfat dry milk in PBS, and then incubated with primary antibodies anti-GFP (1:500, Molecular Probes, A11122) or anti-His (1:1,000, Cell Signaling, 27E8) for 1 hr at RT. Blots were then washed with PBS-Tween 0.1% three times before adding secondary antibody (1:1000,IRDye® 680 goat anti-mouse, 827-11080, IRDye®

800 goat anti-rabbit, 827-08365, LI-COR) for 30 min. After washing three more times with PBS-Tween 0.1%, blots were imaged with an Odyssey LI-COR Imaging System.

Results

Myo1d is present in myelinating and non-myelinating cells of the PNS

Myo1d was originally identified in the rat cerebrum, spinal cord (Bahler et al., 1994), and sciatic nerve (Lund et al., 2005). Recently, microarray studies demonstrated that Myo1d transcripts are present in oligodendrocytes (Cahoy et al., 2008), and proteomic studies suggest that this motor is also associated with myelin (Yamaguchi et al., 2008; Ishii et al., 2009; Jahn et al., 2009). To further develop our understanding Myo1d function in myelinating cells and neurons, we used high-resolution confocal imaging to characterize the distribution of this motor in the PNS and CNS. To this end, we first dissected mouse sciatic nerve bundles for immuno-fluorescence labeling and confocal imaging. To visualize the distribution of Myo1d in sciatic nerve, the nerve bundle was teased into constituent fibers (a single axon wrapped by Schwann cells), which were then stained with antibodies targeting Myo1d, myelin basic protein (MBP) to label Schwann cells (Mirsky et al., 1980), or neurofilament light chain to label axons (Fabrizi et al., 1997; Sotelo-Silveira et al., 2000). Interestingly, Myo1d exhibited

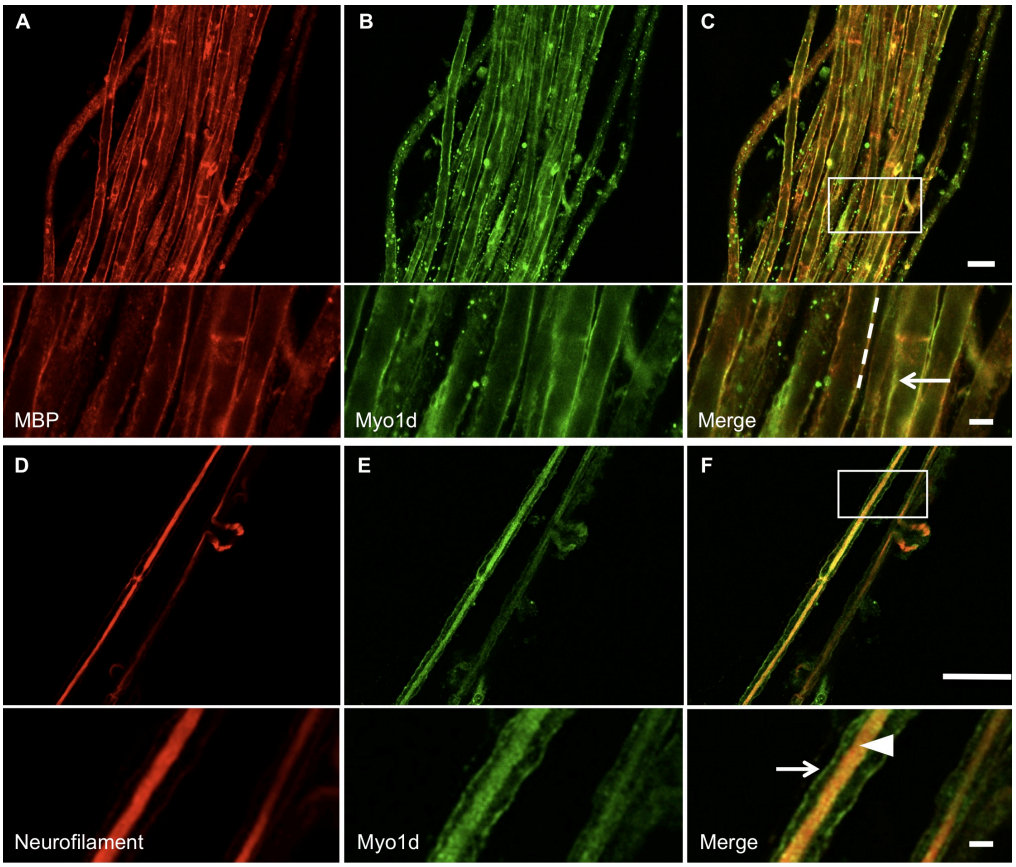

Figure 13 Myo1d colocalizes with MBP in Schwann cells.

Teased mouse sciatic nerve bundles were treated with 0.1% Triton X-100 and antibodies targeting MBP (red) and Myo1d (green). A) MBP localizes along the axonal ensheathment and colocalizes with Myo1d (B). C) Both proteins target to ensheathment around the axon, arrow. D-F) Teased sciatic nerve fibers were treated with 1% Triton X-100 and antibodies specific for neurofilament (red) (D), and Myo1d (E). F) Myo1d and neurofilament colocalize along the axon (arrowhead) while Myo1d maintains localization on the axon ensheathment (arrow). A-C) Bar, 20 mm; inset bar is 5 mm. D-F) 50 mm, inset bar is 5 mm.

robust co-localization with MBP along the myelin sheath enveloping neurons (Figure 13A-C). In teased fibers that were exposed to higher levels of Triton X-100 (1%) to increase permeabilization, the motor maintained localization along the myelin sheath, but also co-localized with neurofilament labeling along the length of axons (**Error! Reference source not found.**D-F). These high-resolution confocal images indicate that Myo1d is present in both neurons and myelinating cells in the PNS. These data are also consistent with Western blots of sciatic nerve samples (Figure 14), brightfield studies demonstrating Myo1d is in the sciatic nerve (McQuarrie and Lund, 2009), and proteomic studies suggesting that Myo1d is present in myelinating cells (Yamaguchi et al., 2008; Ishii et al., 2009; Jahn et al., 2009).

Myo1d exhibits a developmentally regulated distribution in the cerebellum

To explore the cellular distribution and sub-cellular localization of Myo1d in the CNS, we applied a similar staining strategy to frozen sections of the developing mouse brain. At postnatal day 7 (P7), Myo1d exhibits broad expression throughout the whole brain, with enrichment in select regions, including the hippocampal formation and cerebellar Purkinje cell layer (Figure 15). We noticed prominent axonal tract staining in the cerebellum and pontine region in agreement with previous biochemical analyses (Bahler et al., 1994). The choroid plexus nonspecifically bound secondary and is an artifact (data not shown). We chose to focus further studies on the cerebellum as this region

undergoes dramatic maturation of both neuronal and myelinating cell populations to form highly organized cell layers during early

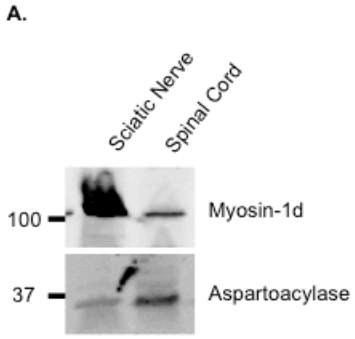

Figure 14 Myosin-1d is present in sciatic nerve and spinal cord.

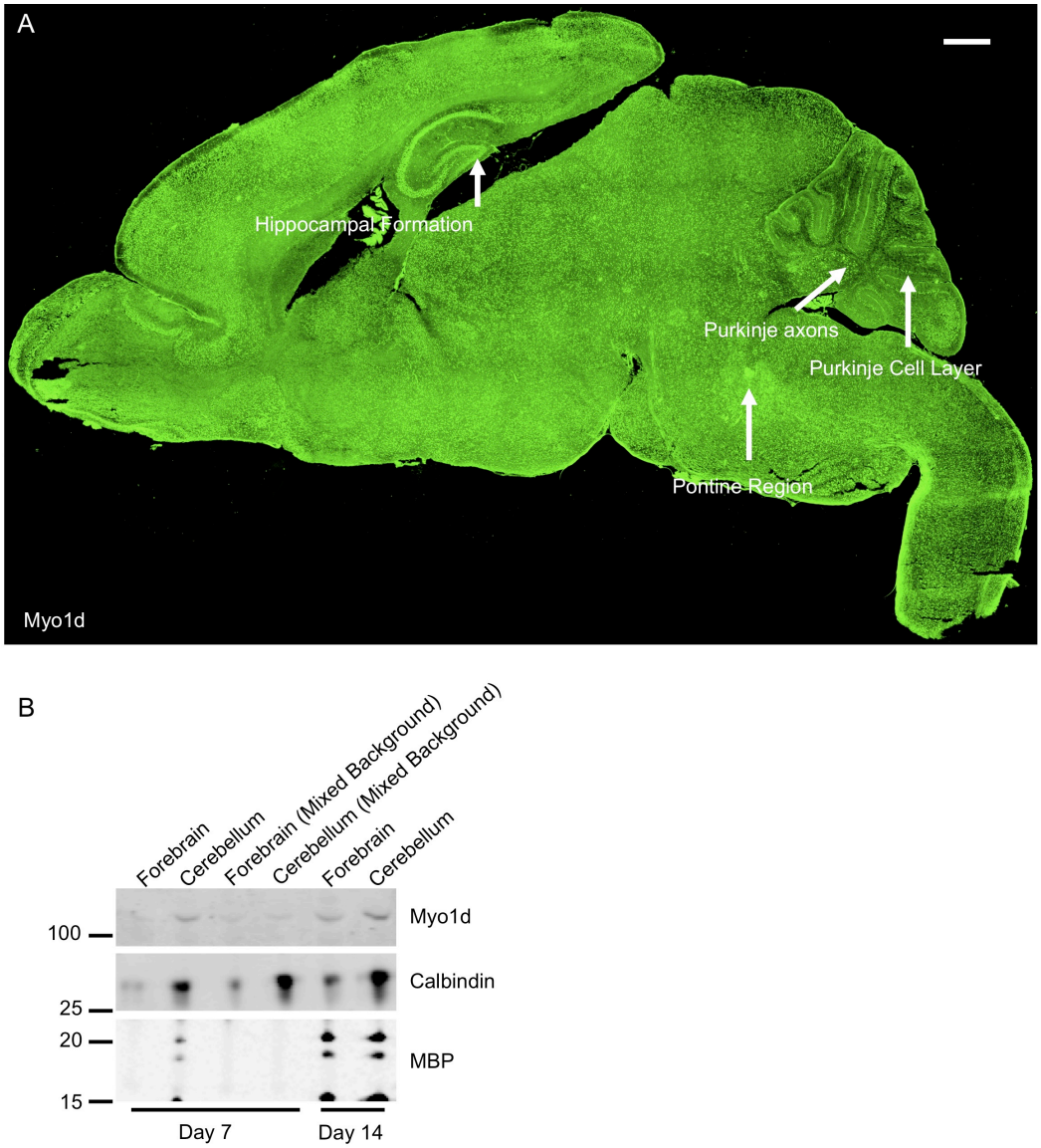

Figure 15 Myo1d is expressed throughout the mouse brain.

A) P7 mouse brain was stained with antibody targeting Myo1d. Myo1d expression is seen throughout the brain with enrichment in select regions including the hippocampal formation and Purkinje cell layer. Interestingly, axonal tract labeling is evident in the pontine region and cerebellum. Bar, 500 μm. B) Western blot analysis of P7 and P14 forebrain and cerebellum Myo1d levels.

mouse postnatal development, and had higher Myo1d levels by Western blot compared to mouse forebrain (Figure 15).

Beginning with P3 prior to myelination (Skoff et al., 1976), Myo1d expression is present throughout the cerebellum in the Purkinje and granule cell layers, and in the region of the deep nuclei (Figure 16A-A''). However, expression is largely absent from the molecular cell layer demonstrating that Myo1d expression is not present in all neural cell types (Figure 16A'). At P7, after the onset of myelination (Skoff et al., 1976), Myo1d expression expands along tracts that co-label with MBP, a marker for myelin (Kornguth and Anderson, 1965) (Figure 16B-B''). At this time point, Myo1d expression is maintained in the Purkinje cell layer, but in the granule cell layer, expression has shifted to the apex of the cerebellar lobules (Figure 16B''). Myo1d exhibits a similar expression pattern at P13, with pronounced expression in Purkinje cells and a subset of granule cells (Figure 16C-C''). These data indicate that Myo1d expression patterns are developmentally regulated, as suggested by previous biochemical studies (Bahler et al., 1994). In particular, Myo1d enrichment along axons increases concomitantly with maturation and expression in granule cells becomes restricted to the apex of cerebellar lobules.

Myo1d is mostly absent from oligodendrocyte precursors and oligodendrocytes

Upon the onset of myelination at P7, Myo1d expression expands along axonal tracts suggesting that this motor is found in Purkinje cell axons or in

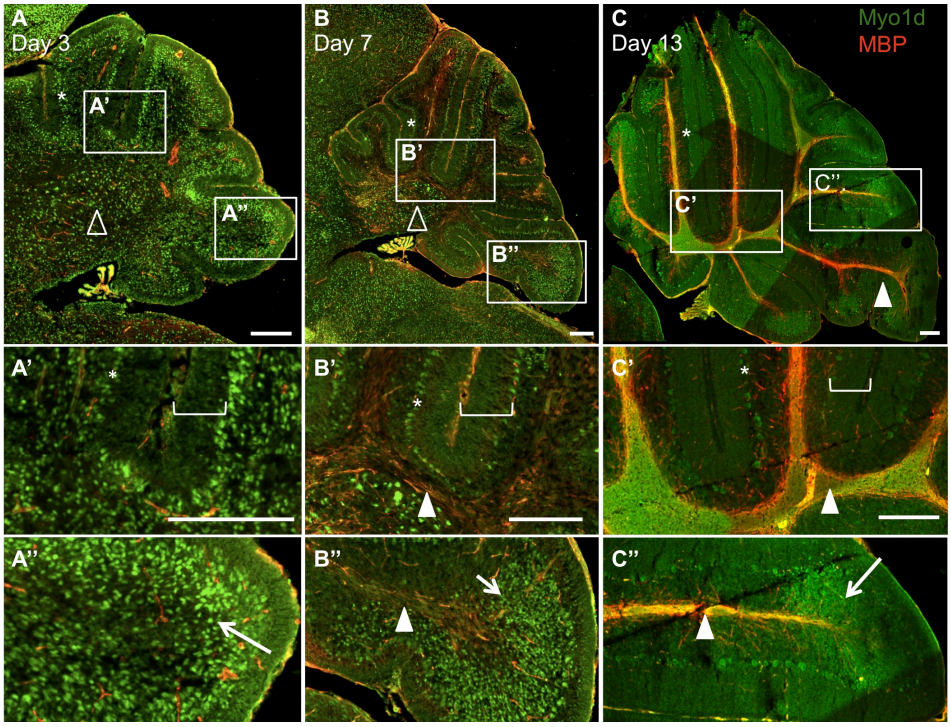

Figure 16 Myo1d distribution in the cerebellum is developmentally regulated.

Mouse cerebella were stained with Myo1d (green) and MBP (red) at P3, P7, and P13. A) Myo1d is expressed throughout the cerebellum in the Purkinje (asterisk) and, region of deep nuclei (open triangle). A') The motor is absent from the molecular cell layer (bracket). A'') Myo1d is also present throughout the granule cell layer (arrow). B-B'') Upon the onset of myelination at day 7, myoisn-1d expression has expanded along axonal tracts (arrowhead). B'-B'') Myo1d is present in the Purkinje cell layer and has a restricted expression pattern in the granule cell layer. C-C'') At day 13, Myo1d expression is maintained in the Purkinje and granule cell layers, and is distinctly present along axonal tracts. Bar, 200 μm.

oligodendrocyte processes that myelinate these axons (or both). To distinguish among these possibilities, we performed high-resolution confocal microscopy on labeled P3 and P14 mouse brains with an antibody targeting O4, the earliest marker known for mature oligodendrocytes (Schachner et al., 1981; Sommer and Schachner, 1981). At P3, O4 appears in an arc at the base of the cerebellum in the region of the deep nuclei and there is minimal expression overlap with Myo1d (Figure 17A-C). In fact, O4-positive and Myo1d-positive cells appear interspersed in a mutually exclusive pattern. We also analyzed O4 and Myo1d labeling in P14 mice cerebella (Figure 18). Interestingly, Myo1d was present along axons, whereas O4 labeled cellular processes clearly enveloped axons in these sections. As a control, we stained mouse cerebella with an antibody targeting calbindin, a Purkinje specific marker (Jande et al., 1981; Roth et al., 1981; Baimbridge and Miller, 1982), and O4. This data shows O4-positive processes interwoven among Purkinje axons (Figure 18G-I), in the same manner observed in Myo1d-labeled sections. Taken together, our high-resolution imaging data indicate that at early and intermediate time points in cerebellar development, Myo1d is either not present or is expressed at very low levels in oligodendrocytes.

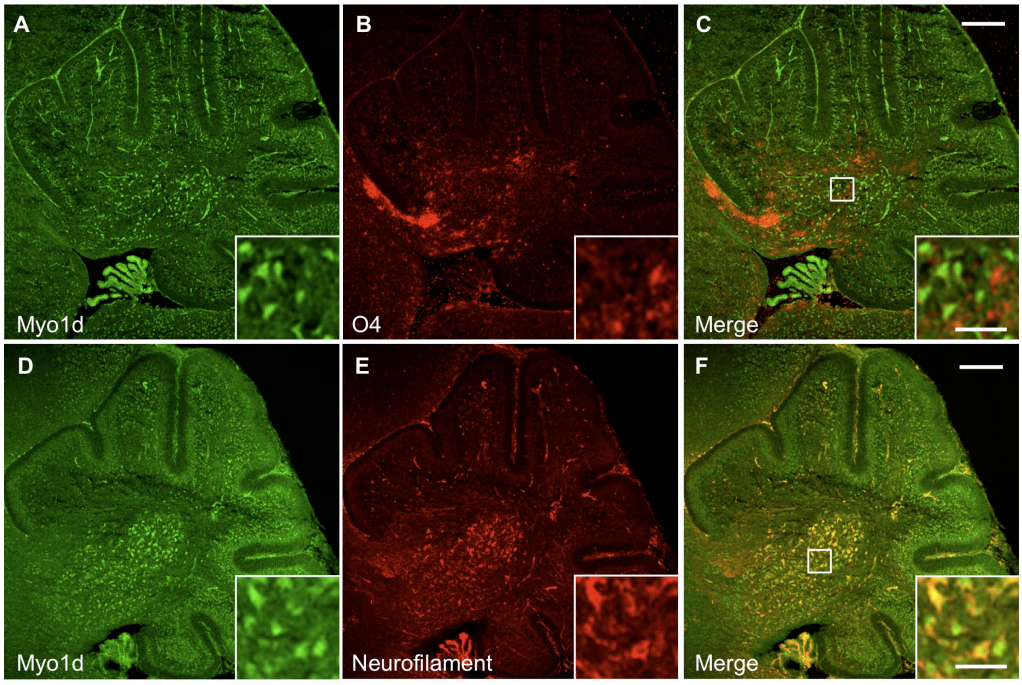

Figure 17 Myo1d is predominantly expressed in neurons at P3.

Mouse cerebella were labeled with antibodies specific for Myo1d (A) and oligodendrocyte progenitor marker, O4 (B). C) Myo1d expression does not overlap with O4. However, when cerebella were stained with antibodies for Myo1d (D) or neurofilament (E), there was greater overlap between both proteins (F). Bar, 200 μm; inset, 50 μm.

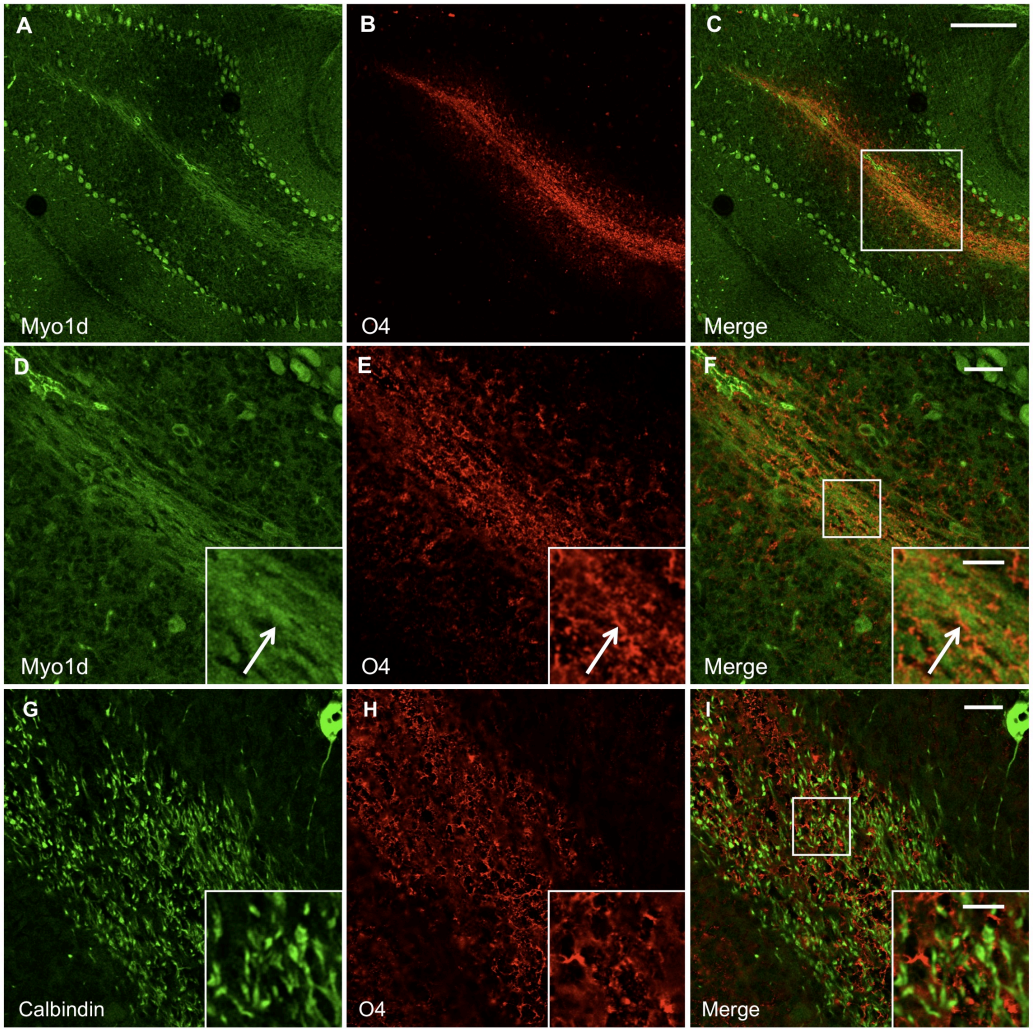

Figure 18 Myo1d is mostly absent from O4-labeled myelin tracts.

To determine if Myo1d is present in myelin tracts, P14 mouse cerebellum was costained with antibodies for Myo1d (A & D) (green) and O4 (B&E) (red). Confocal image magnified along a white matter tract. Myo1d appears to be specific for axonal tracts (arrow) and Purkinje cells, while O4 is in a separate cell population that wraps around the axons (F). G) Antibodies targeting Calbindin (green) clearly target Purkinje cells, dendrites and axons. H) O4 myelin positive processes form a web-like pattern. I) O4 processes wrap around Calbindin-labeled axons. A-C) Bar, 150 μm; D-I) Bar, 25 μm; inset, 10 μm.

Myo1d localizes to neuronal cell bodies, processes, and axons

To validate that Myo1d is expressed predominantly in neurons, mouse cerebella at P3 and P7 were costained for this motor and heavy neurofilament. At P3, Myo1d exhibits clear colocalization with neurofilament in the cerebellar nuclei and granule cell layer (Figure 17D-F). However, at P7, Myo1d and neurofilament exhibit overlapping expression in the Purkijne cell layer, Purkinje axonal tracts, and in the cerebellar nuclei (Figure 19A-C). High magnification images in the region of the cerebellar nuclei reveal that Myo1d is cytosolic in cell bodies, localizes along processes (Figure 19D-F), and along axon tracts (Figure 19G-I). Staining with heavy neurofilament antibodies also revealed Myo1d localization along Purkinje dendrites (Figure 20). In Purkinje cell bodies, we observed cytosolic Myo1d with punctate labeling distributed throughout the soma as well as regions of enrichment around the cell cortex. We confirmed Myo1d expression in Purkinje cells and axons using a Purkinje specific $L7^{cre}$;$YFP^{membrane}$ reporter mouse (Zhang et al., 2001) (Figure 20D-E). To validate Myo1d expression in the granule cell layer, we stained the mouse cerebella for NeuN, a neuronal specific nuclear protein that is an established marker for this cell population. While the NeuN staining pattern was evident throughout the entire granule cell layer, Myo1d expression is only evident in a subpopulation of granule cells at the apex of the cerebellar lobules (Figure 21). Together, these results lead us to conclude that, in the context of the cerebellum, Myo1d is expressed in neurons (Bahler et al., 1994), but is unlikely to be present in myelinating cells (Yamaguchi et al., 2008; Ishii et al., 2009; Jahn et al., 2009).

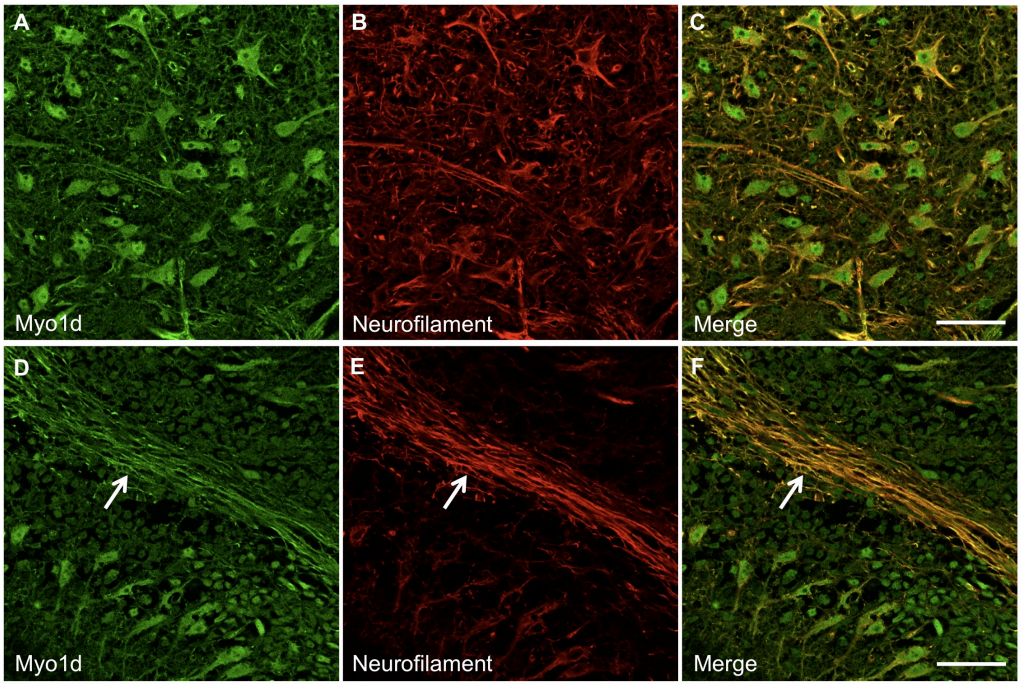

Figure 19 Myo1d exhibits localization along neuronal processes and axons.

P7 cerebella were labeled with antibodies targeting Myo1d (A) (green) and neurofilament (B) (red). Myo1d and neurofilament colocalize along axonal tracts and in the region of the deep nuclei (C). D-F) Myo1d has a cytosolic subcellular distribution and is present along neuronal processes. G-I) Myo1d is expressed along axonal tracts (arrow). A-C) Bar, 500 μm; D-I) Bar, 50 μm.

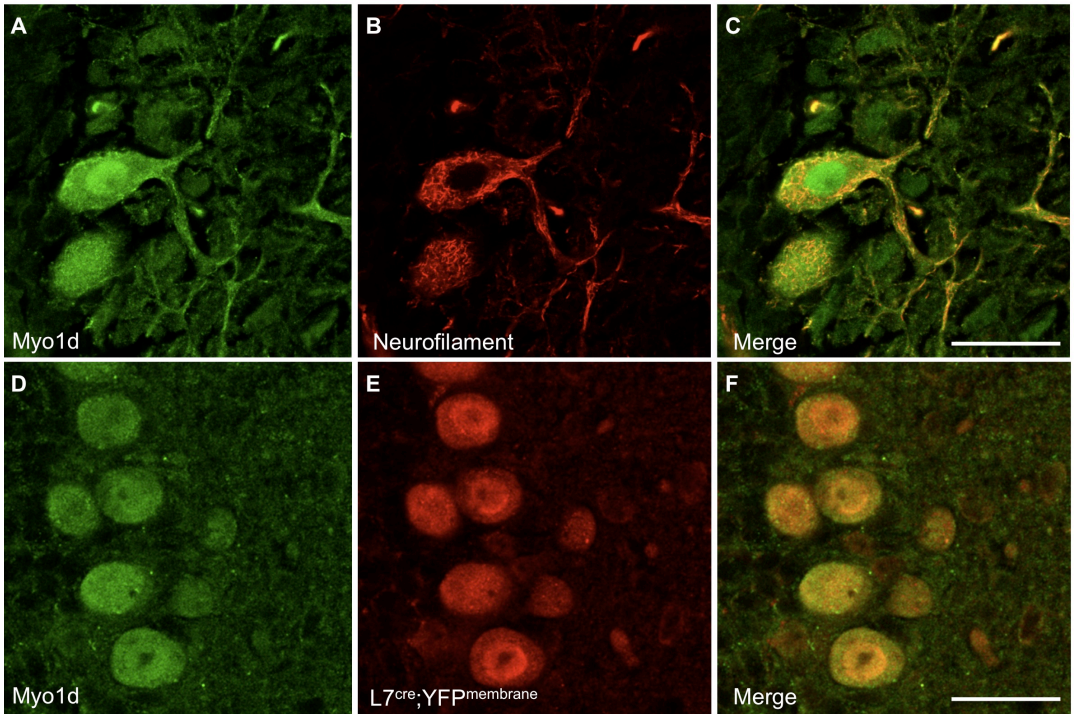

Figure 20 Myo1d exhibits cytosolic and dendritic subcellular localization in Purkinje cells.

We colabeled sagittal cross sections of P14 tissue with antibodies for Myo1d (A) and neurofilament (B). A) Myo1d has punctate cytosolic localization pattern and appears along dendrites. The motor appears more densely along the cell cortex. (D-F) Antibodies targeting Myo1d and GFP were applied to coronal cross sections of $L7^{cre}$;$YFP^{membrane}$ mouse cerebella. (D) Myo1d is present in Purkinje cells with L7, a specific Purkinje cell marker. Bar, 25 μm.

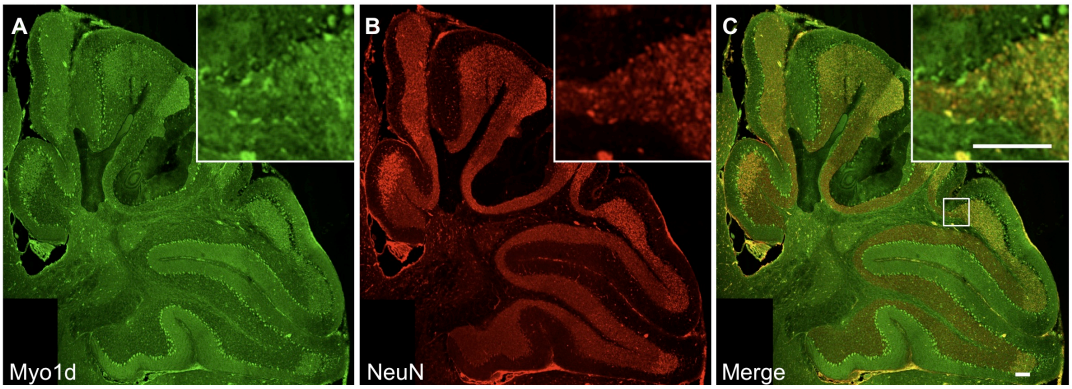

Figure 21 Myo1d is expressed in a distinct subpopulation of granule cells.

To confirm Myo1d is in the granule cell layer, we stained day 14 cerebella with Myo1d (A) and NeuN (B) specific antibodies. C) Myo1d expression in the granule cell layer is restricted to the apex of the lobules in the granule cell layer. All bars, 100 μm.

Myo1d interacts and partially co-localizes with aspartoacylase, an enzyme critical for fatty acid metabolism in the central nervous system

Performing a yeast 2-hybrid screen with the Myo1d TH1 (i.e. tail) domain as bait, we identified aspartoacylase (Figure 22), a 313 amino acid protein that catabolizes NAA and is expressed in kidney, small intestine, and brain (Kaul et al., 1993; Surendran et al., 2006). To confirm that neither bait nor prey caused auto-activation, we expressed the Myo1d TH1 or aspartoacylase alone in AH109 yeast. Neither construct was capable of initiating auto-activation. The interaction between these two proteins was confirmed with a biochemical pull-down approach; we over-expressed EGFP or EGFP-Myo1d in pig kidney epithelial cells and lysates were incubated with His-tagged aspartoacylase that was purified from BL21 *E. coli* and captured on a Ni-NTA resin. Aspartoacylase interacted with Myo1d and was detected in pull-down samples (Figure 22D). EGFP-Myo1d did not bind Ni-NTA resin, supporting that the interaction between aspartoacylase and Myo1d was specific.

Based on structural studies, aspartoacylase has two domains, an N-terminal 212 a.a. domain and a C-terminal 100 a.a. domain (Bitto et al., 2007), which could potentially interact with the Myo1d TH1. Using the same yeast-2-hybrid approach, we determined that Myo1d TH1 interacts with the C-terminus of aspartoacylase (Figure 22C). Based on the solved aspartoacylase structure and other carboxypeptidase family members the carboxyl-terminus is hypothesized to sterically block catalytic activity (Bitto et al., 2007). Given our results, this suggests that Myo1d binding may modulate aspartoacylase activity.

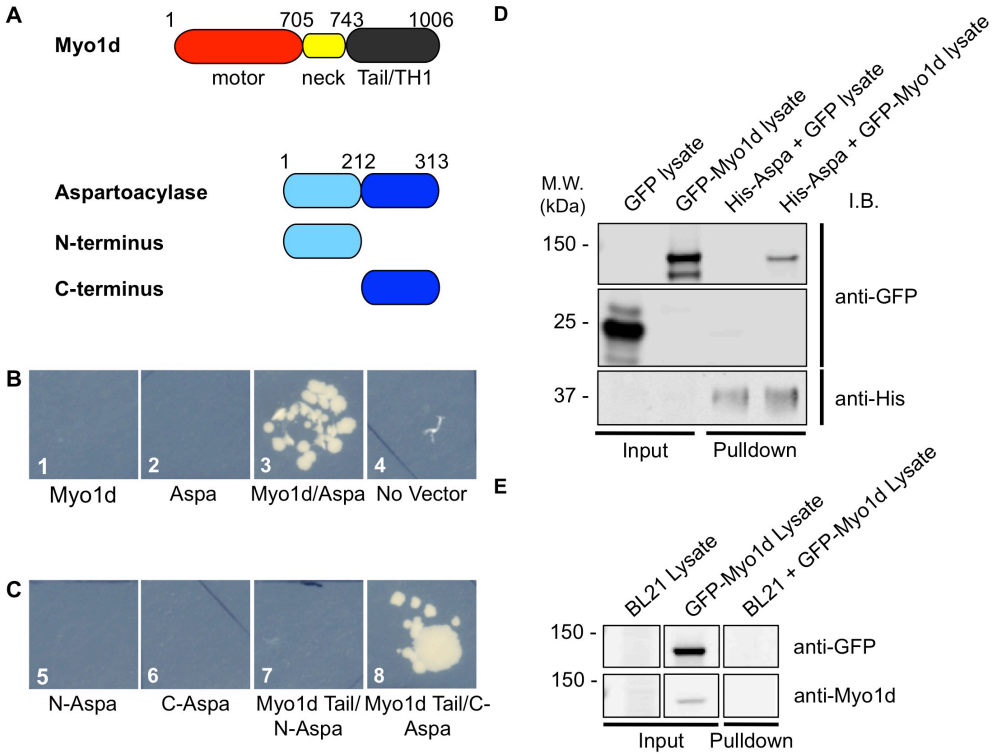

Figure 22 Myo1d interacts with aspartoacylase.

To identify potential binding partners for Myo1d, we performed a yeast 2-hybrid screen. A) The tail domain (amino acids 743-1006) was used as bait in a screen of a human cDNA kidney library. A) Aspartoacylase has two domains: the N-terminus (amino acids 1-212) and C-terminus (213-313). B) Yeast were streaked out onto triple nutrient dropout plates. *1:* AH109 yeast expressing Myo1d tail alone, *2:* AH109 yeast expressing aspartoacylase alone, *3:* Myo1d tail interacts with aspartoacylase, *4:* AH109 without any vector. (**Figure 21 continued**)

Figure 21 continued

C) *5:* AH109 yeast expressing aspartoacylase N-terminus (N-Aspa), *6:* AH109 yeast expressing aspartoacylase C-terminus (C-Aspa), *7:* AH109 yeast with both Myo1d tail and aspartoacylase N-terminus, *8:* Myo1d and aspartoacylase C-terminus together. D) Myo1d interacts with aspartoacylase in an *in vitro* pull-down. His-tagged aspartoacylase was expressed in BL21 bacteria, and EGFP or EGFP-Myo1d containing lysates were collected for an *in vitro* pull-down experiment. His-tagged aspartoacylase interacts with EGFP-Myo1d, while not interacting with EGFP controls. E) EGFP-Myo1d does not nonspecifically bind Ni-NTA resin in the presence of BL21 lysate.

We also performed immuno-fluorescence labeling and confocal imaging of mouse cerebellum to determine if Myo1d and aspartoacylase colocalize in the CNS, which would provide evidence in support an *in vivo* interaction. Staining mouse frozen sections with antibodies targeting Myo1d and aspartoacylase revealed that these proteins share expression in Purkinje cells and a subpopulation of granule cells (Figure 23A-C). Aspartoacylase staining was not observed in oligodendrocytes, but the Purkinje cell labeling described here is similar to that reported by the Human Protein Atlas (http://www.proteinatlas.org). Magnification of the Purkinje cell layer revealed that aspartoacylase staining was cytosolic similar to previous work (Madhavarao et al., 2004) (Figure 23D-F). Moreover, Myo1d and aspartoacylase are present in cell bodies and along dendrites, which suggests a subpopulation of these two proteins are positioned to physically interact *in vivo.* Taken together, these *in vitro* and *in vivo* data provide evidence in support of a transient interaction between Myo1d and aspartoacylase in neurons of the cerebellum.

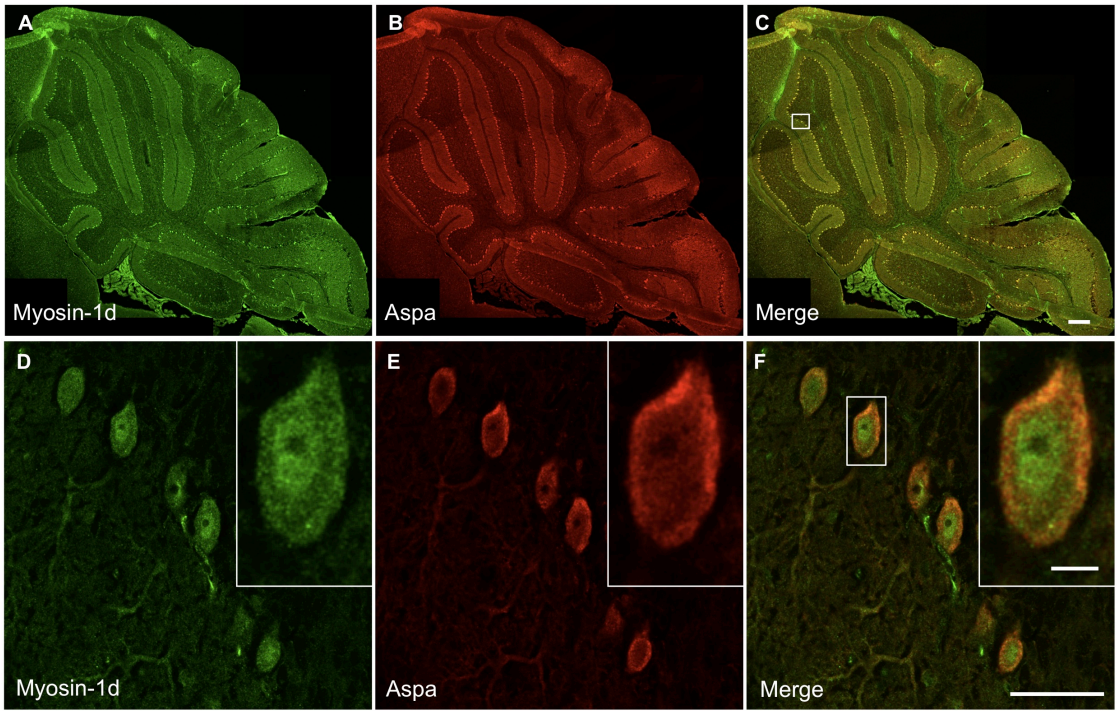

Figure 23 Myo1d and aspartoacylase localize around the Purkinje cell cortex

P14 mouse cerebella were colabeled with antibodies for Myo1d (A & D) (green) and aspartoacylase (B & E) (red). A-C) Myo1d and aspartoayclase expression overlaps in the Purkinje and granule cell layer. D-F) Magnification of the Purkinje cell layer reveals Myo1d and aspartoacylase partially co-localize at the cell cortex of Purkinje cells. Both proteins exhibit a diffuse cytosolic labeling and localization along dendrites. A-C) Bar, 200 μm; D-E) Bar, 10 μm; inset 5μm.

Discussion

These studies extend prior immuno-fluorescence analyses that were limited to the sciatic nerve and cerebrum (Bahler et al., 1994; Lund et al., 2005), and more recent microarray and proteomic studies that suggest Myo1d is expressed in myelinating cells (Cahoy et al., 2008; Yamaguchi et al., 2008; Ishii et al., 2009; Jahn et al., 2009). Our high-resolution confocal data indicate that Myo1d is expressed in both myelinating cells and neurons. However, expression in myelinating cells was only detectable in the PNS. In the context of the CNS, our studies are the first to describe the developmental expression and localization of Myo1d in the mouse cerebellum. Here, Myo1d is most highly expressed in neurons, where it localizes throughout cell bodies, axons and other processes. Importantly, Myo1d expression appears as early as P3 in the internal granule layer, becoming detectable at P7 in Purkinje cell axons, and expanding along axon tracts throughout later stages of neurodevelopment. We also report Myo1d binds to aspartoacylase, a protein linked to fatty acid synthesis and Canvan disease (Moffett et al., 2007).

Myo1d is expressed in myelinating cells of the PNS, but not the cerebellum

Recent proteomic investigations identified Myo1d as a component of mouse and human myelin, suggesting that this motor is present in myelinating cells (Yamaguchi et al., 2008; Ishii et al., 2009; Jahn et al., 2009). Indeed, we observed that Schwann cells clearly express Myo1d, which co-localizes with

MBP. However, our studies of the cerebellum demonstrate that Myo1d is not detectable in precursor or mature oligodendrocytes, at least at the level of resolution afforded by confocal microscopy. This difference may reflect a distinct functional requirement for the motor in Schwann cells that may not exist in oligodendrocytes. In fact, studies with myosin-2 have highlighted disparate roles for this motor in oligodendrocyte and Schwann cell myelination (Wang et al., 2008). In oligodendrocytes, decreasing myosin-2 levels facilitates myelination, whereas in Schwann cells myosin-2 deficiency leads to perturbations in cytoskeletal polarity and reduced myelinating activity (Wang et al., 2008). Myo1d may also have disparate roles in oligodendrocytes and Schwann cells, which would be supported by the data described here.

Roles for Myo1d in myelinating cells of the PNS

What is the role of Myo1d in Schwann cells? Dominant negative studies with another unconventional myosin, myosin-5a, implicate this motor in myelination possibly through a role in transporting VAMP2 along oligodendrocyte processes (Sloane and Vartanian, 2007). Because Myo1d is monomeric, the motor is unlikely to perform processive cargo transport along actin filaments. However, Myo1d does target to distinct membrane compartments (Huber et al., 2000; Benesh et al., 2010) and is able to contribute to membrane-cytoskeleton adhesion (Nambiar et al., 2009). Thus, an alternative possibility is that this motor may facilitate the deformation of membrane relative to F-actin during the extension of myelin-rich processes in Schwann cells. Actin polymerization drives

the filopodial and lamellopodial extension of myelin-rich processes in search of axonal targets (Bauer et al., 2009) and Myo1d may help remodel membrane protrusions during these events.

Possible functions for Myo1d in neurons

In the context of neurons, myosin superfamily members have proposed roles ranging from organelle transport to orchestrating actin rearrangements with consequences for migration and synaptic function (Hirokawa et al., 2010). Myo1d was identified in pyramidal neurons of the cerebral cortex and thalamus (Bahler et al., 1994), and was also shown to be upregulated at lesions in sciatic nerve (Lund et al., 2005). However, the expression pattern of Myo1d in the cerebellum has not been described. Our studies demonstrate Myo1d is found in cerebellar neurons including Purkinje and granule cells. Intriguingly, Myo1d is only expressed in a subpopulation of granule cells at the apex of the cerebellar lobules, which receive inputs from the pontocerebellar fibers (Voogd and Glickstein, 1998).

Previous studies revealed that Myo1d exhibits cytosolic and punctate sub-cellular localization in cell bodies, and also localizes along axons and dendrites in the cortex (Bahler et al., 1994; Lund et al., 2005). We report similar sub-cellular localization in cerebellar Purkinje neurons. While the motor is expressed in neurons of the cortex and cerebellum, the function(s) for Myo1d in these cells remains uncharacterized. Observed Myo1d puncta might represent vesicles or other small membranous organelles, as described for other class I myosins

(Bose et al., 2002). Myo1d does exhibit punctate staining in the C6 glial cell line (Bahler et al., 1994) and MDCK cells, where it may facilitate early endosomal trafficking (Huber et al., 2000). However, punctate staining has also been linked to functions other than vesicle transport in neurons. For example, myosins-1b exhibits a punctate distribution in growth cones where it may control retrograde flow (Lewis and Bridgman, 1996). It has also been proposed that Myo1d might associate with larger organelles such as the smooth endoplasmic reticulum, to enable the 'ratcheting' of F-actin through sciatic nerve (McQuarrie and Lund, 2009). Additional studies will be needed to fully understand the nature and functional implications of the punctate staining observed in the current work.

Our data indicate that Myo1d becomes enriched along axons at the onset of myelination, which may reflect a developmental stage-dependent function for this motor. Indeed, myelination coincides with neuronal maturation, and includes clustering of lipids and ion channels to axonal subdomains, which facilitates conductance (Barres and Raff, 1999; Simons and Trajkovic, 2006). Since class I myosins interact with specific lipid species (Hokanson et al., 2006) and retain transmembrane proteins within lipid rafts (Tyska and Mooseker, 2004), one possibility is that Myo1d may help orchestrate lipid or protein clustering along axons. Interestingly, studies in *Drosophila* reveal that Myo31DF (a MYO1D homolog) co-localizes with β-catenin at adherens junctions of enterocytes (Speder et al., 2006). This interaction is proposed to regulate cell-cell contacts because mutations in Myo31DF give rise to left-right asymmetry defects during development (Hozumi et al., 2006; Speder et al., 2006). Neurons also depend

on the β-catenin/cadherin complex for cell adhesion and synaptic plasticity (Murase et al., 2002; Togashi et al., 2002), and therefore might rely on Myo1d in a similar manner, to facilitate these processes during neuronal maturation.

Myo1d interacts with aspartoacylase in vitro

Our data suggests that Myo1d interacts with aspartoacylase, which catabolizes NAA. Myo1d binds to the C-terminus of aspartoacylase (a.a. 212-313), which may sterically hinder the active site as suggested by structural studies of aspartoacylase function (Bitto et al., 2007). Our data also demonstrate that Myo1d and aspartoacylase are co-expressed in Purkinje neurons. While aspartoacylase NAA catalytic activity is found predominantly in oligodendrocytes (Baslow et al., 1999), aspartoacylase protein is also expressed in large neurons (Madhavarao et al., 2004; Moffett et al., 2011). Although published studies have not observed Purkinje cell aspartoacylase expression (Madhavarao et al., 2004), staining catalogued in the Human Protein Atlas corroborates our findings.

In addition to contributing acetic acid for fatty acid synthesis (Chakraborty et al., 2001; Madhavarao et al., 2005), NAA is also hypothesized to have roles important in maintaining viable neuronal populations. Indeed, many neuropathies such as schizophrenia, multiple sclerosis, and epilepsy are associated with altered CNS NAA levels (Moffett et al., 2007). Proposed functions for neuronal NAA include regulating osmolarity (Baslow and Yamada, 1997; Baslow, 1998), neuron-glia interactions (Baslow, 2000), and energy metabolism (Miller et al., 1996). Most notably, mutations in aspartoacylase can

lead to higher NAA levels and the lethal leukodystrophy, Canavan disease (Namboodiri et al., 2006). Given the number of neuropathies associated with altered NAA levels, maintaining the proper concentration of NAA in neurons and oligodendrocytes appears to be essential for normal CNS function.

Most studies of aspartoacylase activity have focused on oligodendrocytes or myelin, and therefore a neuronal role for the protein has not been reported to date. Since several studies including our own demonstrate aspartoacylase expression in neurons (Madhavarao et al., 2004; Moffett et al., 2011), it is possible that the neuronal aspartoacylase may provide a mechanism for buffering NAA concentrations, which would contribute to replenishing acetate and aspartate levels. In addition, we propose that Myo1d modulates aspartoacylase activity, either through sequestering the protein to discrete locations or directly interfering with activity at the aspartoacylase catalytic site. Indeed, our immuno-fluorescence data demonstrates that Myo1d exhibits a punctate cytosolic distribution and localizes with aspartoacylase around Purkinje cell soma.

Recent genetic studies of autistic individuals revealed multiple SNP variants with strong association to MYO1D (Stone et al., 2007). Other work has shown that autistic individuals have decreased NAA levels throughout the brain (Friedman et al., 2003; Levitt et al., 2003). While autism etiology is unknown, the disease is considered a developmental neurological disorder influenced by multiple genetic and environmental factors (DSM-IV, 2000). Given that Myo1d exhibits expression throughout the brain (cortex, brain stem, and cerebellum),

which coincides with axonal maturation, this motor is well-suited to make wide-ranging contributions to CNS development and function.

In conclusion, Myo1d is is present in myelinating cells of the PNS, but not CNS suggesting distinct roles for this motor in these different tissues. However, Myo1d expression is present in both sciatic and cerebellar neurons. We also demonstrate that the cerebellar distribution of Myo1d is developmentally regulated in both Purkinje and granule cells. Specifically, during early postnatal development Myo1d expression becomes restricted to cerebellar lobule apexes. Moreover, Myo1d subcellular enrichment increases along Purkinje cell axons during early postnatal maturation. Finally, we identified aspartoacylase, an enzyme critical for maintaining proper levels of NAA in the brain, as a potential Myo1d binding partner. The data presented here provide the foundation for functional assays, which will be required for fully understanding the role of Myo1d during neurodevelopment, and its potential link to neurological disorders such as autism and Canavan disease.

Acknowledgements

The authors would like to thank all members of the Tyska laboratory for their advice and support, and the VUMC Cell Imaging Shared Resource. We also thank the Wente and Coffey laboratories for their technical advice. This work was supported by grants from the National Institutes of Health (R01-DK075555,

MJT) and the American Heart Association (pre-doctoral fellowship, AEB; 09GRNT2310188, MJT).

CHAPTER VI

CONCLUSIONS AND FUTURE DIRECTIONS

Conclusions

This dissertation details several new findings regarding Myo1d expression and function in polarized cells such as enterocytes, glia, and neurons. This work is the first to visualize Myo1d distribution in the small intestine. In enterocytes, Myo1d localizes to three subcellular compartments including the lateral membranes, terminal web, and microvillar tips. Intriguingly, Myo1d subcellular localization and function appear to be regulated by the presence of Myo1a along the microvillar actin bundles. Prior to our studies, understanding of Myo1d expression in myelinating cells was limited to microarray data (Cahoy et al., 2008) and mass spectrometry analysis of isolated myelin from the brain (Yamaguchi et al., 2008; Ishii et al., 2009; Jahn et al., 2009). However, we were able to observe by immunofluorescence Myo1d expression only in the myelinating cells of sciatic tissue compared to the cerebellum. Our studies also revealed that Myo1d is mostly found in neuronal cells of the mouse cerebellum during early postnatal development and interacts with aspartoacylase, a protein in the fatty acid synthesis pathway.

Myo1d localizes within the enterocyte to distinct cellular domains, which suggests the motor is primed for several different functions. Myo1d is the first vertebrate protein shown to target to the microvillar tips (Benesh et al., 2010),

where the protein may orchestrate brush border assembly or maintain actin bundle length (Sokac et al., 2006). The motor also targets to the brush border terminal web and lateral membrane, suggesting the protein may be involved in trafficking pathways or localizing cargo to these sites. Myo1d localization to the lateral membrane of vertebrate cells is reminiscent of similar sub-cellular localization in *Drosophila* embryos (Speder and Noselli, 2007), and suggests that Myo1d targets the adherens junctions (Figure 24).

Myo1d exhibits differential localization and dynamics with Myo1a (Benesh et al., 2010). We hypothesize that the class I motors do segregate based on different functions and targeting determinants, such as affinity for different lipids. Indeed, differences between Myo1a and Myo1d were seen in our biochemical and live-cell imaging experiments. First, Myo1d exhibits a smaller immobile population compared to Myo1a (Benesh et al., 2010). Plus, Myo1d is more sensitive to ATP compared to Myo1a (Benesh et al., 2010). Lastly, Myo1d is only detectable in DRMs in the absence of Myo1a (Benesh et al., 2010). Myo1d redistributes along the microvillar axis in the absence of Myo1a (Benesh et al., 2010), which supports the notion that these molecules do have a propensity to compensate for each other. Closely related genes are an important evolutionary mechanism for coping with disease states. When mutations arise in one gene, the closely related gene is able to partially overlap (Sartorius et al., 1998).

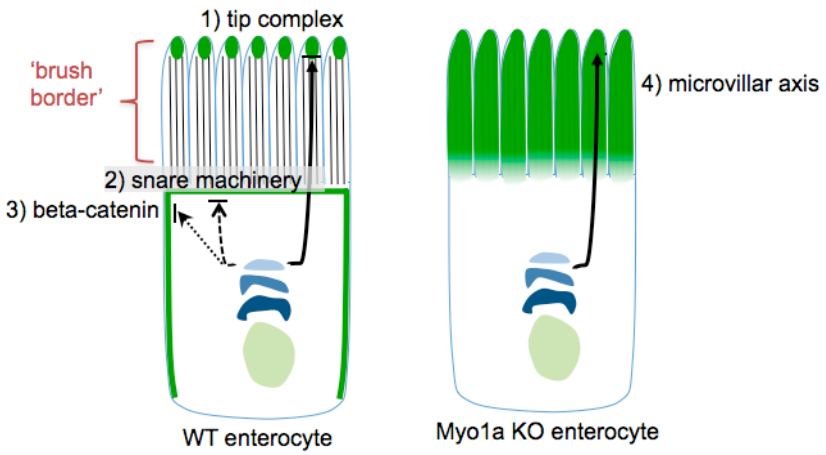

Figure 24 Model representing possible functions for Myo1d in WT and KO enterocytes.

1) Myo1d localizes to microvillar tips where the molecule partially overlaps with IAP. Intriguingly, Myo1d remains associated with microvillar tips, while IAP is sorted onto vesicles as cargo. We hypothesize that Myo1d may orchestrate lipid or protein sorting to create a niche at the tip primed for vesicle release. 2) Myo1d localizes to the terminal web at the base of the brush border. This site is enriched in vesicle trafficking machinery important for docking. 3) Myo1d localizes along the enterocyte lateral membrane. Myo1d may also be involved in trafficking events at this membrane. In addition, it is known Myo1d interacts with β-catenin at the adherens junctions. The significance of this interaction still needs to be explored. 4) Myo1d redistributes along the microvillar axis in the Myo1a KO brush border. Myo1d may contribute to cytoskeletal-membrane tension in the KO animal.

Chapter III is the first observation that Myo1d is expressed in Purkinje and granule cells of the cerebellum. Subcellular localization is punctate and cytosolic in the cell body, axons, and dendrites. This is consistent with prior studies that have shown Myo1d to exhibit cytosolic punctate localization in neurons of the cortex and thalamus (Bahler et al., 1994). This punctate staining may be indicative of association with vesicles. Indeed, Myo1d and other class I myosins have been observed in the trafficking pathways (Hasson and Mooseker, 1995).

Myo1d expression in the cerebellum is developmentally regulated in neurons. Upon myelination, Myo1d expands along axons of the white matter tracts in mouse cerebellum. As development proceeds, Myo1d expression becomes restricted to a subpopulation of granule cells at the apex of the cerebellar lobules (Figure 25).

Myo1d interacts with aspartoacylase, a protein involved in catabolizing NAA. Immunofluorescence of the mouse cerebellum demonstrates the two proteins are coexpressed in Purkinje cells. We hypothesize that Myo1d modulates aspartoacylase activity in Purkinje cells, acting to buffer NAA levels in the brain (Figure 26). Intriguingly, aspartoacylase and Myo1d are both expressed in neurons and kidney cells (Bahler et al., 1994; Hershfield et al., 2006), suggesting the two proteins may have a conserved role across cell types.

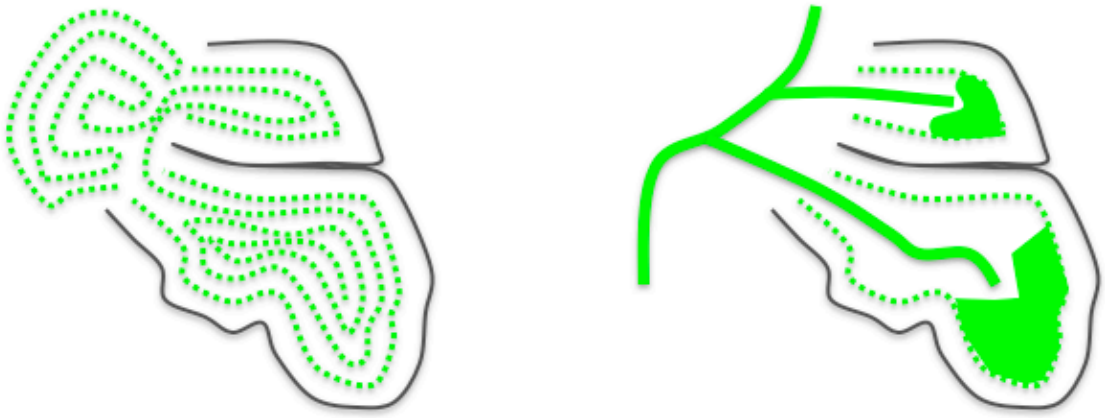

Figure 25 Myo1d expression pattern changes upon onset of myelination.

Prior to myelination, Myo1d expression is found throughout the cerebellum including the granule and Purkinje cell layers. After myelination, Myo1d expression expands along Purkinje cell axons and becomes restricted within the granule cell layer to the apex of the lobules.

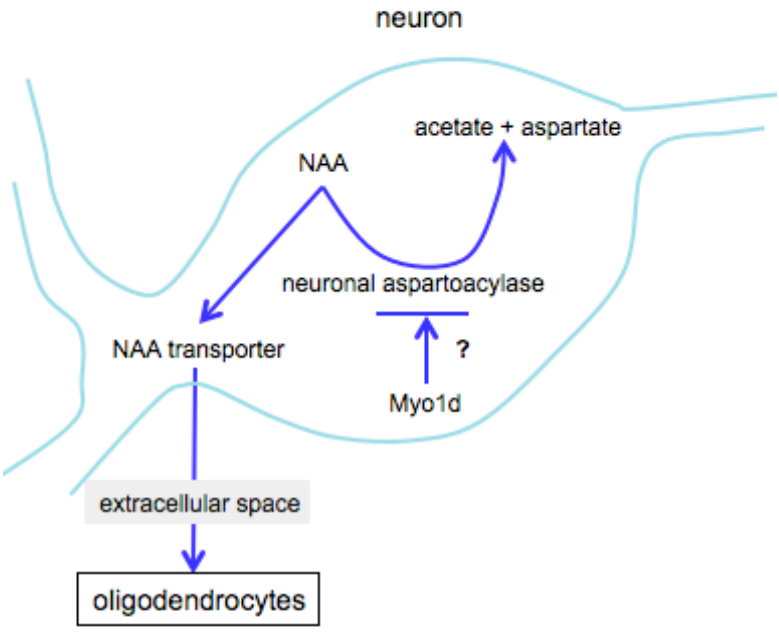

Figure 26 A model for the Myo1d-aspartoacylase interaction in neurons.

Myo1d may interact with aspartoacylase to buffer NAA concentrations in neurons. Increasing Myo1d levels hypothetically would increase NAA levels if the myosin tail inhibits aspartoacylase catabolic activity.

These studies demonstrate that Myo1d exhibits cell dependent subcellular localization. In enterocytes, Myo1d has a small cytosolic pool and is enriched at the lateral membranes. However, in neurons Myo1d has a large cytosolic pool. This may be a reflection in differences of membrane composition between enterocytes and neurons. For example, we postulate that a particular membrane binding structure in enterocytes is absent in neurons, resulting in the inability for the myosin to target to the plasma membrane. Taken together, these studies illustrate disparate roles for different class-I myosins in the intestine, but have the propensity for overlap and further suggest that Myo1d itself has tissue-specific identity. Thus, these studies provide evidence that class I myosin motors are adaptable, and will perform the function required for the tissue in which they are expressed.

Future directions

This dissertation lays the groundwork for studies that aim to explore the role of Myo1d in polarized cells of the small intestine and nervous system. In particular, work will address whether Myo1d function is conserved across these cell types, and if the motor has multiple roles within the cell. Our knowledge regarding Myo1d function will facilitate our understanding of how MYO1D mutations contribute to epithelial biology, development and autism (Stone et al., 2007).

Investigating a role for Myo1d at adherens junctions

Interestingly, we found that Myo1d localizes to the enterocyte lateral membrane, in addition to the microvillar tips and terminal web. Targeting to the lateral membrane potentially allows the molecule to participate in several cellular activities ranging from trafficking to signaling. Indeed, other studies demonstrate that Myo1d interacts with β-catenin (Speder et al., 2006), which targets to adherens junctions at the lateral membranes. Adherens junctions facilitate cell-cell communication and regulate cell geometry through the dimerization of E-cadherins on neighboring cells (Vasioukhin et al., 2000; Gumbiner, 2005; Harris and Tepass, 2010). β-catenin connects E-cadherin to the actin cytoskeleton through α-catenin (Hulsken et al., 1994; Rimm et al., 1995). Adherens junctions overexpressing E-cadherin do not complete polarization (Hermiston et al., 1996) and require β-catenin for proper actin organization (Tanentzapf et al., 2000), which ultimately 'secures' a single cell into an epithelial sheet and regulates cell shape (Gumbiner, 2005).

To determine if a Myo1d - β-catenin interaction is conserved in vertebrates, we stained confluent pig kidney cells (LLC-PK1-cells) overexpressing EGFP-Myo1d with an antibody specific to β-catenin. Strikingly, high-resolution confocal imaging revealed that EGFP-Myo1d and β-catenin colocalize at the lateral membrane (Figure 27) as seen in *Drosophila* embryos (Speder et al., 2006).

The significance of the interaction between Myo1d and β-catenin is unknown in the contexts of *Drosophila* embryo development and vertebrate cells.

Since β-catenin mediates the cadherin-cytokeletal scaffold at the adherens junction, Myo1d is ideally situated to contribute to this interaction. One hypothesis is that the Myo1d tail binds β-catenin and the motor associates with actin filaments. In this model, Myo1d may stabilize the cadherin complex either by targeting β-catenin to the junction or acting as a link between the cadherin complex and the actin cytoskeleton. For the latter role, the motor may generate forces or modulate tension that underlies cell geometry, polarization, or movement through an interaction with the actin cytoskeleton.

To understand the function of this interaction in vertebrate cells, we will first map the binding site between Myo1d and β-catenin. Since the myosin tail interacts with cargo we hypothesize that the Myo1d TH1 binds β-catenin. Thus, to identify the Myo1d residues, we will first narrow our possibilities by testing three truncation mutants (a.a. 743-828, 829-906, 907-1006); where each structure presents a unique electronegativity surface plot profile that can be further dissected to identify specific residues. The β-catenin structure is defined by 12 armadillo repeats, an N- and C- terminus (Huber et al., 1997), which can be separately generated to identify the site for reciprocal binding.

To test the hypothesis that an interaction between Myo1d and β-catenin stabilizes the adherens junction, we will take advantage of our Myo1d dominant negative construct (Myo1d IQ TH1) described in Chapter II. Confluent CL4 cells will be transfected with EGFP-Myo1d-IQ-TH1 and allowed to grow for a couple of days. After fixation, antibodies targeting β-catenin, E-cadherin, α-catenin will be applied to the cells and, Alexa-conjugated phalloidin will label F-actin.

Fluorescent intensities for the different markers will be compared between the control and experimental cells. A decrease in fluorescent intensities would suggest that Myo1d is needed for stabilizing the cadherin complex, while enrichment in marker intensities would signify a role for Myo1d to target molecules to the junction.

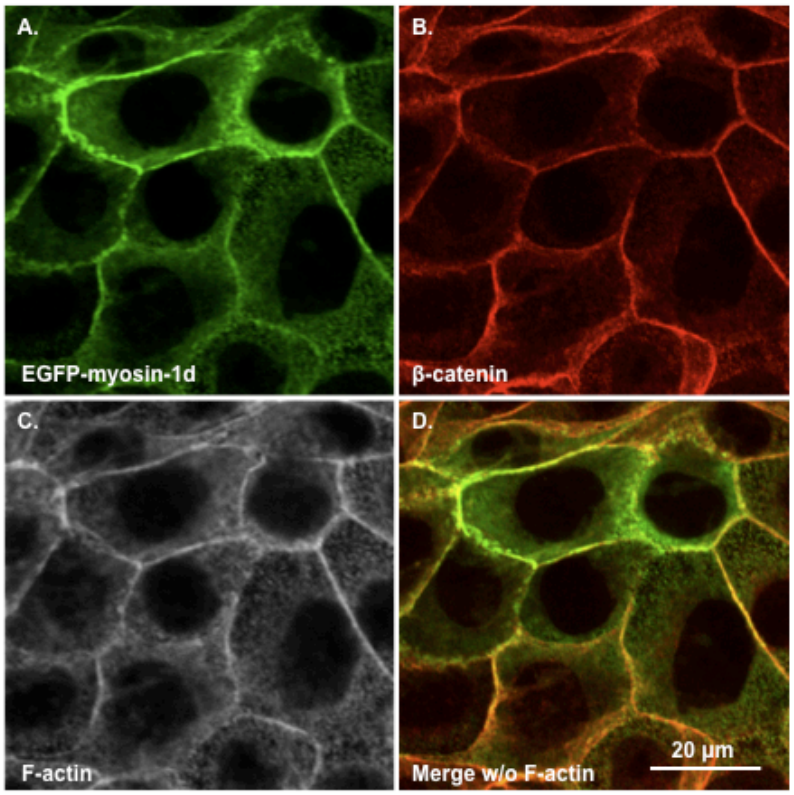

Figure 27 EGFP-Myo1d and β-catenin colocalize at adherens junctions in CL4 cells.

A) EGFP-Myo1d expressing CL4 cells were stained with anti-body targeting B) β-catenin. C) F-actin was labeled with phalloidin, and D) is a merge of (A& B).

If Myo1d modulates tension at the adherens junction, we can measure cell parameters including cell shape and the ability to polarize. These studies would involve comparing control and experimental cells prior to and after confluency. If Myo1d does contribute to the tension at the adherens junction, we would expect to see a failure for dominant negative expressing cells to fully polarize (Miyake et al., 2006). As suggested for *Drosophila* embryo development, this interaction may have significant implications for vertebrate organ morphogenesis and represents a novel role for class I motors that needs to be further explored.

In addition to maintaining the adherens junction, β-catenin is a crucial component of the Wnt signaling pathway, which is a key regulator of development (Willert and Nusse, 1998). Failure to modulate this pathway often leads to developmental defects and disease including cancer (Clevers, 2006). In the absence of Wnt ligand β-catenin is polyubiquitinated for degradation (Willert and Nusse, 1998). However, when Wnt binds the Frizzled receptor, cytoplasmic β-catenin translocates to the nucleus to activate target downstream genes (Willert and Nusse, 1998). Since β-catenin in this signaling pathway is largely found in the cytoplasm and is not membrane associated how an interaction with Myo1d contributes to Wnt signaling through β-catenin is less obvious. One possible explanation though, is that Myo1d sequesters a population of β-catenin to the lateral membrane, acting to buffer the cytoplasmic pool or to limit the available β-catenin for degradation. Hypothetically, a disruption to the Myo1d - β-catenin interaction would shift the β-catenin population from the lateral membrane to the cytoplasm and then into the nucleus. This can be tested by

fractionating cells overexpressing dominant negative EGFP-Myo1d-IQ-TH1 and measuring by Western blot cytoplasmic:nuclear levels. Increases in nuclear β-catenin would suggest that Myo1d stabilizes the cytoplasmic catenin population.

Investigating a role for Myo1d at microvillar tips and terminal web

Intriguingly, Myo1d also localizes to the microvilli tips of the brush border, while Myo1a is found along the microvillar axis. Myo1a powers the apical translation of plasma membrane along the microvillar actin bundles, but the exact mechanism of vesicle shedding is unknown (McConnell and Tyska, 2007). Since Myo1d is located apical to the actin bundles, the motor may contribute to vesicle release, actin nucleation, or additionally anchor proteins important in these processes. To explore a possible role for Myo1d at microvilli tips we attempted to generate a cell culture model system. First, we labeled CL4 cells with antibodies targeting Myo1d, but failed to observe discrete motor populations along the microvillar axis. Similarly, we did not observe tip labeling in EGFP-Myo1d overexpression studies. We were interested if we could reconstitute tip localization by co-overexpressing both Myo1d and Myo1a in CL4 cells. We hypothesized that Myo1a is able to force redistribution of Myo1d to the tips, however we observed colocalization between the two motors (Figure 28). We next hypothesized that the shorter microvilli present in the cell culture model failed to allow us to discern Myo1d populations along the microvillus. We then questioned if we could favor microvillar tip targeting by elongating actin bundles in cell culture. To accomplish this, we co-overexpressed the actin

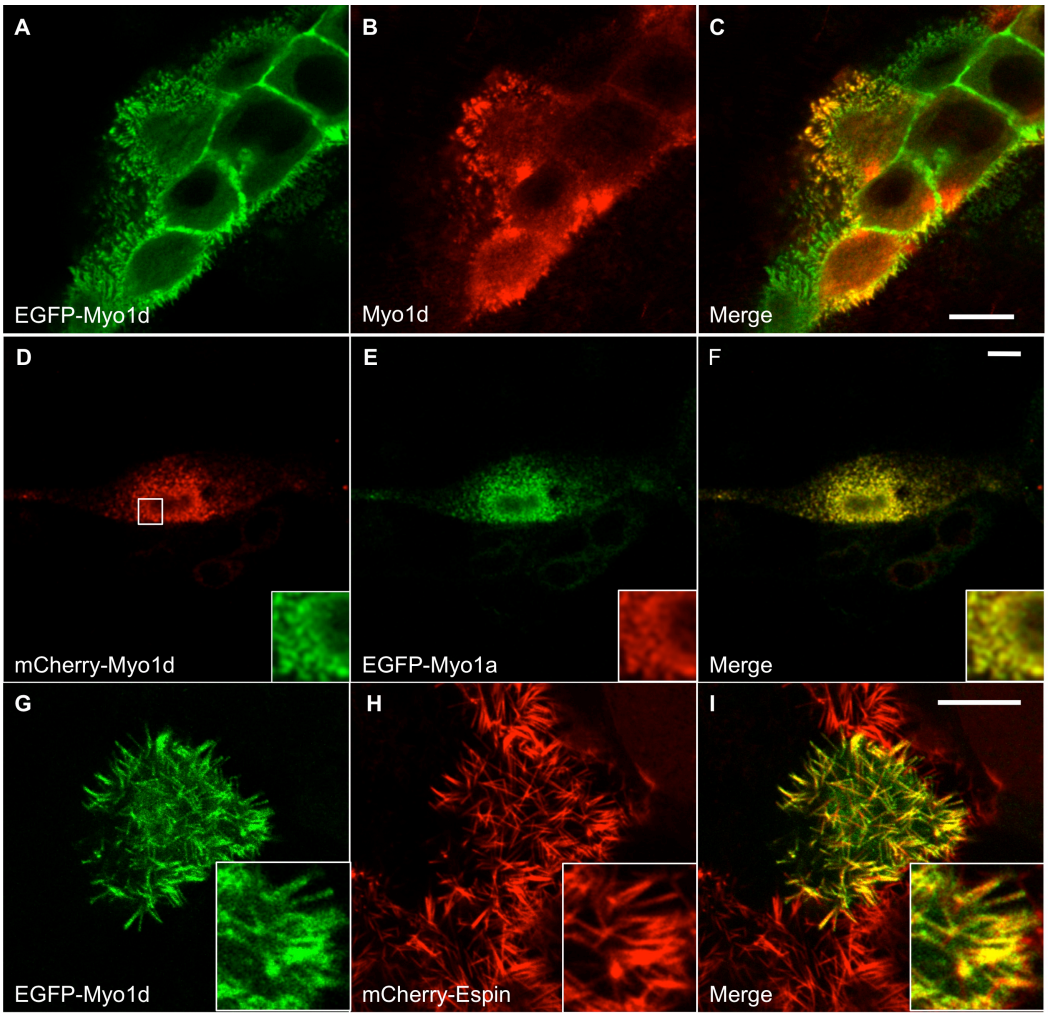

Figure 28 EGFP-Myo1d targets to microvllar tips in CL4 cells overexpressing mCherry-Espin

A-C) The H60 antibody targeting Myo1d (red) labels EGFP-Myo1d (green). (D) mCherry-Myo1d (red) and (E) EGFP-Myo1a (green) colocalize in CL4 cells. G-I) EGFP-Myo1d (green) appears as puncta along microvilli and is also present at tips in CL4 cells overexpressing mCherry-Espin (red). (A-C, G-I) Bar is 5 μm. (D-F) Bar is 10 μm.

bundler mCherry-Espin and EGFP-Myo1d in CL4 cells. Interestingly, we were able to observe punctate EGFP-Myo1d along the actin bundle, and also accumulations at the microvillar tips. This could prove to be a convenient model for exploring a role for the motor at microvillar tips. Live cell imaging could capture the motility of the motor along the actin bundle and allow us to probe what governs Myo1d localization.

Inconsistent Myo1d localization between polarized cell model systems may reflect differences in the affinity for and distribution of binding partners along the membrane. To assess the distribution of lipid species Jessica Mazerik (graduate student, Tyska laboratory) has demonstrated with phospholipid-labeling experiments in the rat brush border that PIP_2 is found at microvillar tips, which is reminiscent of Myo1d localization. Interestingly, recent work has identified a conserved PH motif in class I myosins that bind specific anionic phospholipids including PIP_2 and phosphatidylserine (PS) (Hokanson et al., 2006; Feeser et al., 2010; Patino-Lopez et al., 2010). Indeed, WT brush border lysates incubated with PIP strips revealed that Myo1d has a strong preference for PS and PIP_2, which is consistent with Myo1d and PIP_2 tip labeling (Figure 29). Myo1d association with PS was undetectable on the PIP strip incubated with Myo1a KO brush border lysates suggesting the recruitment of another factor with a tighter affinity.

The role for Myo1d at microvillar tips is unknown but we hypothesize that the motor is involved in sorting cargo for vesicle shedding or regulating release.

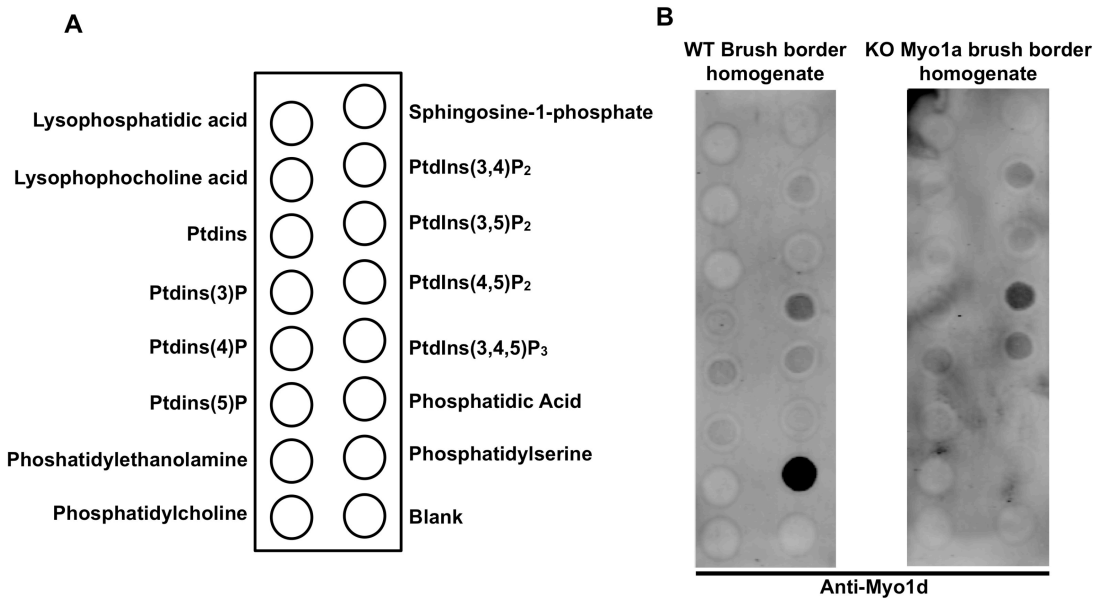

Figure 29 Myo1d binds phosphatidylserine in WT BBs.

A) Cartoon of PIP strip spots and associated phosphoinositide. B) WT and Myo1a KO BB lysates were applied to PIP strips. Membranes were blotted for the presence of Myo1d.

Our data demonstrates that Myo1d colocalizes with IAP at microvillar tips, but the motor is absent from vesicles suggesting a role for the molecule in sorting components. We will employ KD approaches to determine if Myo1d is involved in the sorting of components such as IAP or regulates vesicle shedding. Caco-2_{BBE} cells knocked down for Myo1d expression will be measured for vesicle composition and shedding rates. If Myo1d were needed for proper sorting of IAP onto vesicles, then we would expect less IAP cargo and a buildup of the phosphatase on the membrane. Vesicle protein levels compared to cell IAP

levels could be measured by Western blot or enzymatic activity could be assayed. However, if the motor were involved in the release of vesicles from the brush border, in knock down (KD) experiments we would expect to observe a decrease in vesicle number or changes to vesicle size.

Myo1d additionally targets to the terminal web, which has an active role in cell contractility (Burgess, 1982; Keller and Mooseker, 1982) and shape (Zarnescu and Thomas, 1999), and is the site of exo- and endocytic trafficking (Valentijn et al., 1997; Hansen et al., 2009). We hypothesize that if Myo1d participates in terminal web contractility, the motor population acts as an ensemble to affect cell geometry. We will KD Myo1d in fully differentiated Caco-2_{BBE} cells, and analyze terminal web composition and cell shape. To inhibit the role of myosin-2 in cell contractility we will apply blebbistatin, while simultaneously adding ATP to initiate Myo1d activity. If Myo1d does affect terminal web constriction, then decreasing motor activity will cause a relaxed cell cortex and larger cell circumference.

Coincidentally, different studies suggest Myo1d associates with trafficking vesicles and the early endocytic pathway (Bahler et al., 1994; Huber et al., 2000). While we did not explore Myo1d function in trafficking, our other yeast 2-hybrid hit (besides aspartoacylase) was the SNARE (Soluble N-ethylmaleimide Sensitive Factor Attachment Protein Receptor)-associated protein, Snapin. Preliminary biochemical results demonstrate that His-tagged Snapin pulls-down EGFP-Myo1d (Figure 30). This 18-kDa protein interacts with SNARE machinery and is ubiquitously expressed across tissues (Buxton et al., 2003).

We hypothesize that Myo1d acts as an anchor for SNARE components at the terminal web membrane. We will employ KD approaches to target Myo1d transcripts and screen for trafficking defects such as altered trafficking machinery or cargo levels. To determine protein levels in different cellular

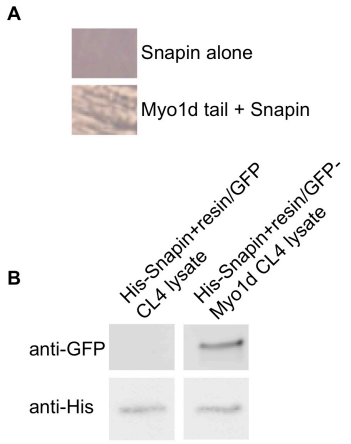

Figure 30 Myo1d tail binds Snapin.

A) We identified a Snapin as a putative Myo1d binding partner in a yeast 2-hybrid screen. B) His-Snapin associates with EGFP-Myo1d from CL4 lysates in pull-down.

compartments, we can fractionate whole cells and then immunoblot for Snapin. Likewise, to analyze cargo transport between cellular compartments we can perform immunofluorescence on Caco-2_{BBE} cells to visualize protein distribution in Myo1d KD cells. If Myo1d functions to anchor SNARE machinery to the cell periphery, we would expect decreased Snapin at the plasma membrane. Another possibility is the motor participates in in docking events and a decrease in Myo1d levels would cause a buildup of cargo at the membrane.

Myo1d may be involved in trafficking in other cellular pathways besides the enterocyte terminal web. Specifically, Paneth cells at the base of intestinal crypts have enlarged secretory vesicles that are positive for Myo1d (Figure 31). This is an interesting observation considering that Myo1d does not exhibit a similar distribution in other secretory cells such as Goblet cells. This suggests that there are differences underlying the mechanism of secretory transport among intestinal cells. One hypothesis is that the tail domain associates with these vesicles to facilitate transport in particular Paneth cells. These Paneth cells can be isolated for biochemical analysis to identify interacting partners and better understand the role of the motor in secretory trafficking.

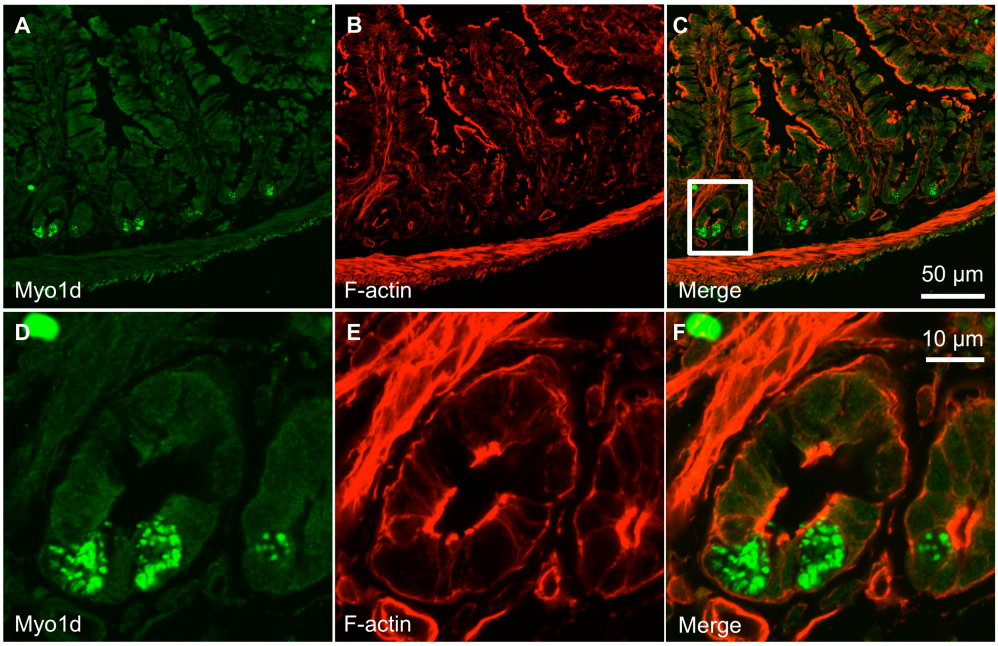

Figure 31 Myo1d is expressed in Paneth cells.

A-C) Myo1d (green) expression is detectable in *Rattus norvegicus* crypts. The BB is labeled with phalloidin (red). D-F) Magnification of crypt from (A-C). Myo1d is present in Paneth cells.

Characterizing Myo1d Function in Neurons

Future work exploring Myo1d neuronal function will focus on two findings: the interaction with aspartoacylase, and association with vesicles to assess if the motor is connected to Canavan disease or autism etiology. Eventually, these studies will lead into determining if the Myo1d-aspartoacylase interaction is conserved across cell types. For example, Myo1d and aspartoacylase are also expressed in the kidney and small intestine. Given that MYO1D is associated with autism (Stone et al., 2007), and autistic individuals exhibit neurological and gastrointestinal abnormalities do mutations in MYO1D contribute to both phenotypes? Or is expression of the protein in only one of these tissues relevant to the disease etiology? These studies will further our understanding of Myo1d in epithelial and neuronal biology, and may provide insight into mechanisms underlying autism or Canavan disease.

While most aspartoacylase studies have focused on Canavan disease and myelination (Namboodiri et al., 2006; Moffett et al., 2007), a neuronal role for the carboxypeptidase is not known. However, the interaction with Myo1d represents a promising avenue to further explore aspartoacylase function. Listed in the table are the multiple pull-down approaches we have attempted to validate the interaction between Myo1d and aspartoacylase, but this interaction appears to be transient and difficult to detect. While we present yeast 2-hybrid and biochemical data supporting binding between the two proteins, functional data would strengthen our understanding of this interaction. Thus, several questions

Table 3 Multiple approaches were taken to detect the Myo1d-asparotacylase interaction.

Method	Result	Explanation
His-tagged Aspa bound to Ni-NTA incubated with eGFP-Myo1d from cell lysate	Data confirms yeast-2-hybrid	A sizable portion of the His-tagged Aspa population interacts with eGFP-Myo1d
Native IP from myelin or whole brain	Technical Difficulties	We could not IP Myo1d from myelin nor whole brain in either low or high salt homogenization buffers
Mammalian Cos-7 cells expressing Flag-tagged Myo1d and eGFP-Aspa	No Detectable Interaction	Flag-tagged Myo1d did not pull-down eGFP-Aspa nor eGFP suggesting if there is an interaction, a miniscule portion of the Myo1d population is involved
SF9 expressed Flag-tagged Myo1d incubated with His-tagged Aspa	Technical Difficulties	His-tagged Aspa is insoluble

regarding the interaction between Myo1d and aspartoacylase must be investigated in neurons. Does the motor modulate aspartoacylase activity? And how does the interaction contribute to cellular physiology?

To address how Myo1d regulates aspartoacylase activity, we can perform enzymatic assays that take advantage of constructs generated in Chapter III. From our yeast 2-hybrid studies we identified that the Myo1d tail domain binds to the aspartoacylase carboxyl-terminus, which is predicted to sterically hinder catabolism (Bitto et al., 2007). We hypothesize that the Myo1d tail would strengthen this inhibition. To measure enzyme activity, we would measure the production of acetic acid by spectrometry. Purified aspartoacylase would be incubated with Myo1d-IQ-TH1 or Myo1a-TH1 to determine if Myo1d specifically inhibits or activates aspartoacylase activity. Since aspartoacylase catabolizes NAA into acetic and aspartic acid, we would expect to see a decrease in acetic acid concentration if Myo1d inhibits catabolic activity. If Myo1d modulates aspartoacylase activity, we could utilize a cell culture model system and either overexpress or KD Myo1d expression. When Myo1d is overexpressed, we would expect to see a similar decrease in acetic acid production, whereas in KD cells, we would hypothesize no change in aspartoacylase activity.

If Myo1d does modulate aspartoacylase catabolism, how does this affect neuronal health? These studies would benefit greatly from the generation of a MYO1D KO animal. If Myo1d and aspartoacylase do interact, we would expect to observe similar phenotypes in the MYO1D and ASPA KO models. For example, aspartoacylase deficient mice exhibit stalled neuronal maturation

(Kumar et al., 2009), and we then predict that MYO1D KO animals would also display neuronal developmental defects. Importantly, generation of a MYO1D KO model will allow us to determine to what extent the motor contributes to Canavan disease or autism pathogenesis. These mice will be analyzed for viability since Canavan disease is lethal at a young age. Mouse behavior will be observed because autistic people display repetitive behavior and exhibit stunted social development (Geschwind and Levitt, 2007). Motor coordination will be scored given that Canavan disease patients suffer from ataxia (Namboodiri et al., 2006). We will assess if neural connectivity is altered in mice similarly to autistic individuals (Geschwind and Levitt, 2007). Cell morphology is important to consider given that oligodendrocytes contain large vacuoles and neurons do not mature in Canavan disease (Surendran et al., 2005). NAA concentration across brain regions will be measured because in both autism and Canavan disease, NAA concentrations increase and distribution is shifted across the brain (Kleinhans et al., 2007; Moffett et al., 2007).

Another valuable approach for manipulating this interaction is performing KD experiments in cell culture. These studies will allow us to analyze parameters that have been implicated in aspartoacylase function including cell metabolism, membrane composition (Chakraborty et al., 2001), and maturation (Kumar et al., 2009). We hypothesize that disturbing Myo1d expression will result in cell metabolism deficiencies, membrane composition alterations, and retard cell maturation. To measure cell metabolism, we can measure acetic acid production as described in the prior paragraph. To examine membrane

composition, we will determine fatty acid content by chromatography. Cell maturation will be measured by immunoblotting for cell cycle progression markers such as cyclin A (S-phase) or cyclin B (M-phase).

Our studies and a previous report have demonstrated that Myo1d appears in a punctate localization pattern in neurons (Bahler et al., 1994). This suggests that the molecule associates with vesicles, but fractionation and immunoblotting will be needed to identify the trafficking pathway. Similar to experiments proposed in enterocytes, we can test if an interaction with snapin is conserved in neurons. Prior work has shown that the SNARE protein is a crucial component for exocytosis in neurons (Ilardi et al., 1999) and impaired snapin function leads to decreased dendrite patterning (Chen et al., 2005). By overexpressing Myo1d in a cell culture system, we hypothesize docking events would be altered with consequences for endo- or exocytosis rates. In fact, Myo1d overexpression may lead to changes in dendrite density. Supposing Myo1d coordinates snapin association with the membrane, which may be required to bring the proper factors to the membrane for dendrite patterning, overexpressing Myo1d could lead to increased dendrite patterning. Failure to specify appropriate dendrite patterning leads to neural connectivity issues as seen in autistic individuals. If Myo1d interacts with snapin, this would support a role for the motor in neuro-development and physiology.

These experiments represent a path forward to further delineate a role for the motor in neurons. Myo1d function may be conserved across cell types and have implications in Canavan disease and autism.

Exploring a role for Myo1d in glia

Our studies reveal that Myo1d expression is detectable by confocal immunofluorescence in Schwann cells, but not oligodendrocytes prior to P14. However, no published data currently exists that characterizes Myo1d expression in peripheral glia, and previous analysis of the adult mouse and human myelin proteome suggests Myo1d is present in oligodendrocytes (Yamaguchi et al., 2008; Ishii et al., 2009; Jahn et al., 2009). Moreover, in primary culture the Myo1d transcripts are reported to be greatly upregulated during oligodendrocyte maturation (Cahoy et al., 2008). Despite these published results, our study is the first attempt to validate Myo1d glial expression in the CNS and PNS with immunofluorescence microscopy. Our data does not refute the published data, but in combination with those previous studies supports the notion that Myo1d glial expression is developmentally regulated. Further immunofluorescence microscopy will be needed to detail Myo1d expression at similar developmental stages as the animals in the proteomic screens. We hypothesize that if Myo1d is important in oligodendrocyte biology, then motor expression may be more evident at maturity based on our data and the mass spectrometry data. In fact, Western blot analysis of adult mouse brain homogenate suggests that the motor is enriched in a myelin fraction (Figure 32).

After establishing a developmental profile for Myo1d in glial cells, we would like to perform functional assays to ascertain a role for the motor during myelination. In particular, we will utilize a primary co-culture system to study

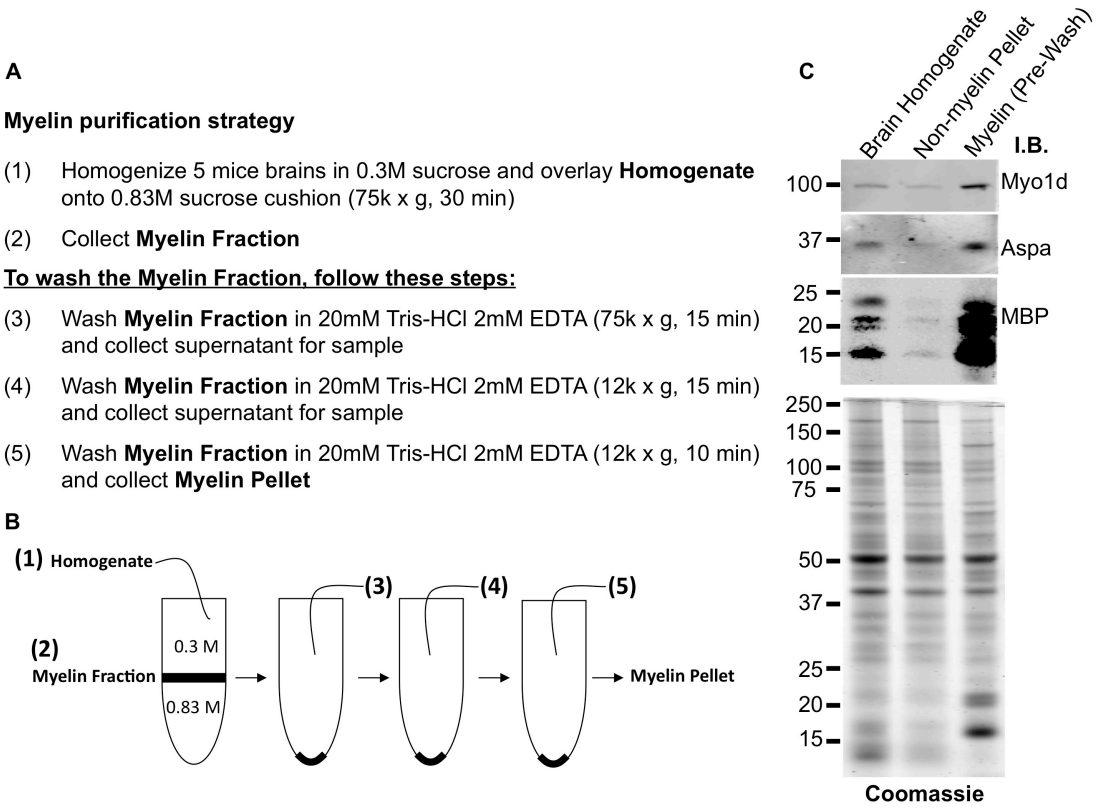

Figure 32 Myo1d is enriched in myelin fraction from adult mouse.

A) Steps for isolating myelin from the mouse brain. B) Cartoon representing our myelin purification strategy. C) Western blot and coomassie of a myelin isolation prep. Myo1d is enriched in myelin fraction harvested from an adult mouse.

either oligodendrocytes or Schwann cell biology in the presence of neurons. In these experiments, a Myo1d siRNA vector under the control of the Oct6 promoter will be transfected into co-cultures, and then myelination success will be measured (Schreiber et al., 1997; Svaren and Meijer, 2008). The goal of these KD experiments would be to assess any differences that may exist for Myo1d function in glial cells of the CNS compared to the PNS. There are two steps in myelination that are experimentally assessable: myelin wrapping and sheath maintenance.

If Myo1d is important in myelination initiation, then we would expect to observe delayed or decreased myelination progression. In this scenario, Myo1d could contribute to myelination by providing mechanical forces for pushing or pulling membrane from the actin cytoskeleton as described in other cell contexts (Nambiar et al., 2009, 2010). We can assay the primary cultures for MBP to determine the degree of myelination or even perform transmission electron microscopy (TEM) to visualize myelin.

However, if the motor is important in maintaining a myelin sheath, we hypothesize that disrupting Myo1d expression after initiation would result in less compact wrapping. We propose that Myo1d similarly acts as a cytoskeleton-membrane linker to maintain tension across the myelin sheath. To discern that Myo1d is important for maintenance rather than myelination, we will KD Myo1d expression in mature oligodendrocytes. As above, we will analyze myelin sheath thickness in cross-section by TEM comparing WT versus KD co-cultures.

In conjunction with these KD co-culture experiments, we will also study myelination in the Myo1d KO mouse. If we generate an oligodendrocyte and Schwann cell specific inducible KO model, we will be able to separate a role for the myosin in myelinating cells from neurons. The KO model will allow us to survey myelin pattern formation in the maturing mouse and assess if wrapping is delayed. We expect from our data that the Schwann cell myelin sheath would be disrupted, and if we can detect Myo1d in oligodendrocytes at later time points, we would likewise hypothesize to observe myelin malformations.

Final Thoughts

By further exploring how Myo1d contributes to trafficking in enterocytes or elaborating on the interaction with aspartoacylase, this work will have ramifications for our understanding of how class I myosins contribute to development and cell biology. Given Myo1d expression is present in a variety of tissues and exhibits subcellular localization to multiple sites, the motor possibly is involved in several functions. In particular, these studies will provide insight into how mutant Myo1d contributes to disease states such as autism spectrum disorders and other development defects.

REFERENCES

Abercrombie M (1980) The Croonian Lecture, 1978: The Crawling Movement of Metazoan Cells. Proceedings of the Royal Society of London Series B Biological Sciences 207:129-147.

Adams RJ, Pollard TD (1989) Binding of myosin I to membrane lipids. Nature 340:565-568.

Akhmanova A, Hammer JA, 3rd (2010) Linking molecular motors to membrane cargo. Current opinion in cell biology 22:479-487.

Alberts B, Johnson A, Lewis J, Raff M, Roberts K, Walter P (2002) Molecular Biology of the Cell, 4th edition.

Arif E, Wagner MC, Johnstone DB, Wong HN, George B, Pruthi PA, Lazzara MJ, Nihalani D (2011) Motor protein Myo1c is a podocyte protein that facilitates the transport of slit diaphragm protein Neph1 to the podocyte membrane. Mol Cell Biol 31:2134-2150.

Baas PW, Black MM (1990) Individual microtubules in the axon consist of domains that differ in both composition and stability. The Journal of cell biology 111:495-509.

Baas PW, Deitch JS, Black MM, Banker GA (1988) Polarity orientation of microtubules in hippocampal neurons: uniformity in the axon and nonuniformity in the dendrite. Proceedings of the National Academy of Sciences of the United States of America 85:8335-8339.

Bacon C, Lakics V, Machesky L, Rumsby M (2007) N-WASP regulates extension of filopodia and processes by oligodendrocyte progenitors, oligodendrocytes, and Schwann cells-implications for axon ensheathment at myelination. Glia 55:844-858.

Bahler M, Rhoads A (2002) Calmodulin signaling via the IQ motif. FEBS letters 513:107-113.

Bahler M, Kroschewski R, Stoffler HE, Behrmann T (1994) Rat myr 4 defines a novel subclass of myosin I: identification, distribution, localization, and mapping of calmodulin-binding sites with differential calcium sensitivity. J Cell Biol 126:375-389.

Baimbridge KG, Miller JJ (1982) Immunohistochemical localization of calcium-binding protein in the cerebellum, hippocampal formation and olfactory bulb of the rat. Brain Res 245:223-229.

Balda MS, Matter K (2008) Tight junctions at a glance. Journal of cell science 121:3677-3682.

Bamji SX, Shimazu K, Kimes N, Huelsken J, Birchmeier W, Lu B, Reichardt LF (2003) Role of beta-catenin in synaptic vesicle localization and presynaptic assembly. Neuron 40:719-731.

Barres BA, Raff MC (1999) Axonal control of oligodendrocyte development. The Journal of cell biology 147:1123-1128.

Baslow MH (1998) Function of the N-acetyl-L-histidine system in the vertebrate eye. Evidence in support of a role as a molecular water pump. J Mol Neurosci 10:193-208.

Baslow MH (2000) Functions of N-acetyl-L-aspartate and N-acetyl-L-aspartylglutamate in the vertebrate brain: role in glial cell-specific signaling. J Neurochem 75:453-459.

Baslow MH, Yamada S (1997) Identification of N-acetylaspartate in the lens of the vertebrate eye: a new model for the investigation of the function of N-acetylated amino acids in vertebrates. Exp Eye Res 64:283-286.

Baslow MH, Suckow RF, Sapirstein V, Hungund BL (1999) Expression of aspartoacylase activity in cultured rat macroglial cells is limited to oligodendrocytes. J Mol Neurosci 13:47-53.

Bauer NG, Richter-Landsberg C, Ffrench-Constant C (2009) Role of the oligodendroglial cytoskeleton in differentiation and myelination. Glia 57:1691-1705.

Baum B, Georgiou M (2011) Dynamics of adherens junctions in epithelial establishment, maintenance, and remodeling. The Journal of cell biology 192:907-917.

Belyantseva IA, Boger ET, Friedman TB (2003) Myosin XVa localizes to the tips of inner ear sensory cell stereocilia and is essential for staircase formation of the hair bundle. Proc Natl Acad Sci U S A 100:13958-13963.

Belyantseva IA, Boger ET, Naz S, Frolenkov GI, Sellers JR, Ahmed ZM, Griffith AJ, Friedman TB (2005) Myosin-XVa is required for tip localization of whirlin and differential elongation of hair-cell stereocilia. Nat Cell Biol 7:148-156.

Benesh AE, Nambiar R, McConnell RE, Mao S, Tabb DL, Tyska MJ (2010) Differential Localization and Dynamics of Class I Myosins in the Enterocyte Microvillus. Mol Biol Cell.

Berg JS, Cheney RE (2002) Myosin-X is an unconventional myosin that undergoes intrafilopodial motility. Nat Cell Biol 4:246-250.

Bhakoo KK, Craig TJ, Styles P (2001) Developmental and regional distribution of aspartoacylase in rat brain tissue. J Neurochem 79:211-220.

Bitto E, Bingman CA, Wesenberg GE, McCoy JG, Phillips GN, Jr. (2007) Structure of aspartoacylase, the brain enzyme impaired in Canavan disease. Proc Natl Acad Sci U S A 104:456-461.

Bose A, Guilherme A, Robida SI, Nicoloro SM, Zhou QL, Jiang ZY, Pomerleau DP, Czech MP (2002) Glucose transporter recycling in response to insulin is facilitated by myosin Myo1c. Nature 420:821-824.

Bretscher A (1981) Fimbrin is a cytoskeletal protein that crosslinks F-actin in vitro. Proceedings of the National Academy of Sciences of the United States of America 78:6849-6853.

Bryant DM, Mostov KE (2008) From cells to organs: building polarized tissue. Nat Rev Mol Cell Biol 9:887-901.

Burgess DR (1982) Reactivation of intestinal epithelial cell brush border motility: ATP-dependent contraction via a terminal web contractile ring. J Cell Biol 95:853-863.

Buxton P, Zhang XM, Walsh B, Sriratana A, Schenberg I, Manickam E, Rowe T (2003) Identification and characterization of Snapin as a ubiquitously expressed SNARE-binding protein that interacts with SNAP23 in non-neuronal cells. Biochem J 375:433-440.

Cahoy JD, Emery B, Kaushal A, Foo LC, Zamanian JL, Christopherson KS, Xing Y, Lubischer JL, Krieg PA, Krupenko SA, Thompson WJ, Barres BA (2008) A Transcriptome Database for Astrocytes, Neurons, and Oligodendrocytes: A New Resource for Understanding Brain Development and Function. J Neurosci 28:264-278.

Cao Z, Li C, Higginbotham JN, Franklin JL, Tabb DL, Graves-Deal R, Hill S, Cheek K, Jerome WG, Lapierre LA, Goldenring JR, Ham AJ, Coffey RJ (2008) Use of fluorescence-activated vesicle sorting for isolation of Naked2-associated, basolaterally targeted exocytic vesicles for proteomics analysis. Mol Cell Proteomics 7:1651-1667.

Catalioto RM, Maggi CA, Giuliani S (2011) Intestinal epithelial barrier dysfunction in disease and possible therapeutical interventions. Curr Med Chem 18:398-426.

Chakraborty G, Mekala P, Yahya D, Wu G, Ledeen RW (2001) Intraneuronal N-acetylaspartate supplies acetyl groups for myelin lipid synthesis: evidence for myelin-associated aspartoacylase. J Neurochem 78:736-745.

Chen M, Lucas KG, Akum BF, Balasingam G, Stawicki TM, Provost JM, Riefler GM, Jornsten RJ, Firestein BL (2005) A novel role for snapin in dendrite patterning: interaction with cypin. Mol Biol Cell 16:5103-5114.

Chen XW, Leto D, Chiang SH, Wang Q, Saltiel AR (2007) Activation of RalA is required for insulin-stimulated Glut4 trafficking to the plasma membrane via the exocyst and the motor protein Myo1c. Dev Cell 13:391-404.

Chen YT, Stewart DB, Nelson WJ (1999) Coupling assembly of the E-cadherin/beta-catenin complex to efficient endoplasmic reticulum exit and

basal-lateral membrane targeting of E-cadherin in polarized MDCK cells. The Journal of cell biology 144:687-699.

Chen ZY, Hasson T, Zhang DS, Schwender BJ, Derfler BH, Mooseker MS, Corey DP (2001) Myosin-VIIb, a novel unconventional myosin, is a constituent of microvilli in transporting epithelia. Genomics 72:285-296.

Cheney RE, Mooseker MS (1992) Unconventional myosins. Current opinion in cell biology 4:27-35.

Christiansen K, Carlsen J (1981) Microvillus membrane vesicles from pig small intestine. Purity and lipid composition. Biochim Biophys Acta 647:188-195.

Clevers H (2006) Wnt/beta-catenin signaling in development and disease. Cell 127:469-480.

Collins JH, Borysenko CW (1984) The 110,000-dalton actin- and calmodulin-binding protein from intestinal brush border is a myosin-like ATPase. J Biol Chem 259:14128-14135.

Coluccio LM (1997) Myosin I. Am J Physiol 273:C347-359.

Conde C, Caceres A (2009) Microtubule assembly, organization and dynamics in axons and dendrites. Nature reviews Neuroscience 10:319-332.

Cooper JA, Schafer DA (2000) Control of actin assembly and disassembly at filament ends. Current opinion in cell biology 12:97-103.

Croce A, Cassata G, Disanza A, Gagliani MC, Tacchetti C, Malabarba MG, Carlier MF, Scita G, Baumeister R, Di Fiore PP (2004) A novel actin barbed-end-capping activity in EPS-8 regulates apical morphogenesis in intestinal cells of Caenorhabditis elegans. Nat Cell Biol 6:1173-1179.

de Hoop MJ, Dotti CG (1993) Membrane traffic in polarized neurons in culture. J Cell Sci Suppl 17:85-92.

de Vries H, Hoekstra D (2000) On the biogenesis of the myelin sheath: cognate polarized trafficking pathways in oligodendrocytes. Glycoconjugate journal 17:181-190.

de Vries H, Schrage C, Hoekstra D (1998) An apical-type trafficking pathway is present in cultured oligodendrocytes but the sphingolipid-enriched myelin membrane is the target of a basolateral-type pathway. Mol Biol Cell 9:599-609.

Debanne D, Campanac E, Bialowas A, Carlier E, Alcaraz G (2011) Axon physiology. Physiol Rev 91:555-602.

Dent EW, Kalil K (2001) Axon branching requires interactions between dynamic microtubules and actin filaments. The Journal of neuroscience : the official journal of the Society for Neuroscience 21:9757-9769.

Dent EW, Gertler FB (2003) Cytoskeletal dynamics and transport in growth cone motility and axon guidance. Neuron 40:209-227.

Dent EW, Gupton SL, Gertler FB (2011a) The growth cone cytoskeleton in axon outgrowth and guidance. Cold Spring Harb Perspect Biol 3.

Dent EW, Merriam EB, Hu X (2011b) The dynamic cytoskeleton: backbone of dendritic spine plasticity. Current opinion in neurobiology 21:175-181.

Diefenbach TJ, Latham VM, Yimlamai D, Liu CA, Herman IM, Jay DG (2002) Myosin 1c and myosin IIB serve opposing roles in lamellipodial dynamics of the neuronal growth cone. The Journal of cell biology 158:1207-1217.

Dillon C, Goda Y (2005) The actin cytoskeleton: integrating form and function at the synapse. Annu Rev Neurosci 28:25-55.

Drubin DG, Nelson WJ (1996) Origins of cell polarity. Cell 84:335-344.

Drubin DG, Mulholland J, Zhu ZM, Botstein D (1990) Homology of a yeast actin-binding protein to signal transduction proteins and myosin-I. Nature 343:288-290.

DSM-IV APATFo (2000) Diagnostic and statistical manual of mental disorders DSM-IV-TR. In, 4th Edition. Washington, DC: American Psychiatric Association.

Edds KT (1977) Dynamic aspects of filopodial formation by reorganization of microfilaments. The Journal of cell biology 73:479-491.

Eroglu C, Barres BA (2010) Regulation of synaptic connectivity by glia. Nature 468:223-231.

Etournay R, El-Amraoui A, Bahloul A, Blanchard S, Roux I, Pezeron G, Michalski N, Daviet L, Hardelin JP, Legrain P, Petit C (2005) PHR1, an integral membrane protein of the inner ear sensory cells, directly interacts with myosin 1c and myosin VIIa. Journal of cell science 118:2891-2899.

Fabrizi C, Kelly BM, Gillespie CS, Schlaepfer WW, Scherer SS, Brophy PJ (1997) Transient expression of the neurofilament proteins NF-L and NF-M by Schwann cells is regulated by axonal contact. J Neurosci Res 50:291-299.

Faix J, Breitsprecher D, Stradal TE, Rottner K (2009) Filopodia: Complex models for simple rods. Int J Biochem Cell Biol 41:1656-1664.

Fath KR, Burgess DR (1993) Golgi-derived vesicles from developing epithelial cells bind actin filaments and possess myosin-I as a cytoplasmically oriented peripheral membrane protein. J Cell Biol 120:117-127.

Feeser EA, Ignacio CM, Krendel M, Ostap EM (2010) Myo1e binds anionic phospholipids with high affinity. Biochemistry 49:9353-9360.

Fifkova E, Delay RJ (1982) Cytoplasmic actin in neuronal processes as a possible mediator of synaptic plasticity. The Journal of cell biology 95:345-350.

Flock A, Cheung HC (1977) Actin filaments in sensory hairs of inner ear receptor cells. The Journal of cell biology 75:339-343.

Foth BJ, Goedecke MC, Soldati D (2006) New insights into myosin evolution and classification. Proceedings of the National Academy of Sciences of the United States of America 103:3681-3686.

Friedman SD, Shaw DW, Artru AA, Richards TL, Gardner J, Dawson G, Posse S, Dager SR (2003) Regional brain chemical alterations in young children with autism spectrum disorder. Neurology 60:100-107.

Gardel ML, Schneider IC, Aratyn-Schaus Y, Waterman CM (2010) Mechanical integration of actin and adhesion dynamics in cell migration. Annu Rev Cell Dev Biol 26:315-333.

Gardiner J, Overall R, Marc J (2011) The microtubule cytoskeleton acts as a key downstream effector of neurotransmitter signaling. Synapse 65:249-256.

Gassama-Diagne A, Yu W, ter Beest M, Martin-Belmonte F, Kierbel A, Engel J, Mostov K (2006) Phosphatidylinositol-3,4,5-trisphosphate regulates the formation of the basolateral plasma membrane in epithelial cells. Nat Cell Biol 8:963-970.

Geeves MA (1991) The dynamics of actin and myosin association and the crossbridge model of muscle contraction. Biochem J 274 (Pt 1):1-14.

Geli MI, Lombardi R, Schmelzl B, Riezman H (2000) An intact SH3 domain is required for myosin I-induced actin polymerization. Embo J 19:4281-4291.

Geschwind DH, Levitt P (2007) Autism spectrum disorders: developmental disconnection syndromes. Curr Opin Neurobiol 17:103-111.

Goldblum SE, Rai U, Tripathi A, Thakar M, De Leo L, Di Toro N, Not T, Ramachandran R, Puche AC, Hollenberg MD, Fasano A (2011) The active Zot domain (aa 288-293) increases ZO-1 and myosin 1C serine/threonine phosphorylation, alters interaction between ZO-1 and its binding partners, and induces tight junction disassembly through proteinase activated receptor 2 activation. The FASEB journal : official publication of the Federation of American Societies for Experimental Biology 25:144-158.

Gumbiner BM (2005) Regulation of cadherin-mediated adhesion in morphogenesis. Nat Rev Mol Cell Biol 6:622-634.

Hackney DD (1996) Myosin and kinesin: mother and child reunited. Chem Biol 3:525-528.

Hansen GH, Rasmussen K, Niels-Christiansen LL, Danielsen EM (2009) Endocytic trafficking from the small intestinal brush border probed with FM dye. Am J Physiol Gastrointest Liver Physiol 297:G708-715.

Harris TJ, Tepass U (2010) Adherens junctions: from molecules to morphogenesis. Nat Rev Mol Cell Biol 11:502-514.

Hartman MA, Finan D, Sivaramakrishnan S, Spudich JA (2011) Principles of Unconventional Myosin Function and Targeting. Annu Rev Cell Dev Biol.

Hasson T, Mooseker MS (1995) Molecular motors, membrane movements and physiology: emerging roles for myosins. Current opinion in cell biology 7:587-594.

Hasson T, Gillespie PG, Garcia JA, MacDonald RB, Zhao Y, Yee AG, Mooseker MS, Corey DP (1997) Unconventional myosins in inner-ear sensory epithelia. J Cell Biol 137:1287-1307.

Hayden SM, Wolenski JS, Mooseker MS (1990) Binding of brush border myosin I to phospholipid vesicles. The Journal of cell biology 111:443-451.

Heidemann SR, Landers JM, Hamborg MA (1981) Polarity orientation of axonal microtubules. The Journal of cell biology 91:661-665.

Heintzelman MB, Hasson T, Mooseker MS (1994) Multiple unconventional myosin domains of the intestinal brush border cytoskeleton. J Cell Sci 107 (Pt 12):3535-3543.

Hermiston ML, Wong MH, Gordon JI (1996) Forced expression of E-cadherin in the mouse intestinal epithelium slows cell migration and provides evidence for nonautonomous regulation of cell fate in a self-renewing system. Genes & development 10:985-996.

Hershfield JR, Madhavarao CN, Moffett JR, Benjamins JA, Garbern JY, Namboodiri A (2006) Aspartoacylase is a regulated nuclear-cytoplasmic enzyme. The FASEB journal : official publication of the Federation of American Societies for Experimental Biology 20:2139-2141.

Hirokawa N, Niwa S, Tanaka Y (2010) Molecular motors in neurons: transport mechanisms and roles in brain function, development, and disease. Neuron 68:610-638.

Hirokawa N, Sobue K, Kanda K, Harada A, Yorifuji H (1989) The cytoskeletal architecture of the presynaptic terminal and molecular structure of synapsin 1. The Journal of cell biology 108:111-126.

Hokanson DE, Ostap EM (2006) Myo1c binds tightly and specifically to phosphatidylinositol 4,5-bisphosphate and inositol 1,4,5-trisphosphate. Proceedings of the National Academy of Sciences of the United States of America 103:3118-3123.

Hokanson DE, Laakso JM, Lin T, Sept D, Ostap EM (2006) Myo1c binds phosphoinositides through a putative pleckstrin homology domain. Molecular biology of the cell 17:4856-4865.

Holmes R, Lobley RW (1989) Intestinal brush border revisited. Gut 30:1667-1678.

Hotulainen P, Hoogenraad CC (2010) Actin in dendritic spines: connecting dynamics to function. The Journal of cell biology 189:619-629.

Howe CL, Mooseker MS (1983) Characterization of the 110-kdalton actin-calmodulin-, and membrane-binding protein from microvilli of intestinal epithelial cells. J Cell Biol 97:974-985.

Hozumi S, Maeda R, Taniguchi K, Kanai M, Shirakabe S, Sasamura T, Speder P, Noselli S, Aigaki T, Murakami R, Matsuno K (2006) An unconventional myosin in Drosophila reverses the default handedness in visceral organs. Nature 440:798-802.

Huber AH, Nelson WJ, Weis WI (1997) Three-dimensional structure of the armadillo repeat region of beta-catenin. Cell 90:871-882.

Huber LA, Fialka I, Paiha K, Hunziker W, Sacks DB, Bahler M, Way M, Gagescu R, Gruenberg J (2000) Both calmodulin and the unconventional myosin Myr4 regulate membrane trafficking along the recycling pathway of MDCK cells. Traffic 1:494-503.

Hudson LD (2001) Oligodendrocytes. In: eLS: John Wiley & Sons, Ltd.

Hulsken J, Birchmeier W, Behrens J (1994) E-cadherin and APC compete for the interaction with beta-catenin and the cytoskeleton. J Cell Biol 127:2061-2069.

Ilardi JM, Mochida S, Sheng ZH (1999) Snapin: a SNARE-associated protein implicated in synaptic transmission. Nat Neurosci 2:119-124.

Insall RH, Machesky LM (2009) Actin dynamics at the leading edge: from simple machinery to complex networks. Dev Cell 17:310-322.

Ishii A, Dutta R, Wark GM, Hwang SI, Han DK, Trapp BD, Pfeiffer SE, Bansal R (2009) Human myelin proteome and comparative analysis with mouse myelin. Proc Natl Acad Sci U S A 106:14605-14610.

Ivanov AI (2008) Actin motors that drive formation and disassembly of epithelial apical junctions. Front Biosci 13:6662-6681.

Jahn O, Tenzer S, Werner HB (2009) Myelin proteomics: molecular anatomy of an insulating sheath. Mol Neurobiol 40:55-72.

Jande SS, Tolnai S, Lawson DE (1981) Immunohistochemical localization of vitamin D-dependent calcium-binding protein in duodenum, kidney, uterus and cerebellum of chickens. Histochemistry 71:99-116.

Jontes JD, Wilson-Kubalek EM, Milligan RA (1995) A 32 degree tail swing in brush border myosin I on ADP release. Nature 378:751-753.

Jontes JD, Emond MR, Smith SJ (2004) In vivo trafficking and targeting of N-cadherin to nascent presynaptic terminals. The Journal of neuroscience : the official journal of the Society for Neuroscience 24:9027-9034.

Jung G, Hammer JA, 3rd (1994) The actin binding site in the tail domain of Dictyostelium myosin IC (myoC) resides within the glycine- and proline-rich sequence (tail homology region 2). FEBS letters 342:197-202.

Kaul R, Gao GP, Balamurugan K, Matalon R (1993) Cloning of the human aspartoacylase cDNA and a common missense mutation in Canavan disease. Nat Genet 5:118-123.

Kawai K, Fujita M, Nakao M (1974) Lipid components of two different regions of an intestinal epithelial cell membrane of mouse. Biochim Biophys Acta 369:222-233.

Keller TC, 3rd, Mooseker MS (1982) Ca++-calmodulin-dependent phosphorylation of myosin, and its role in brush border contraction in vitro. J Cell Biol 95:943-959.

Khubchandani SR, Vohra P, Chitale AR, Sidana P (2011) Microvillous inclusion disease--an ultrastructural diagnosis: with a review of the literature. Ultrastruct Pathol 35:87-91.

Kleinhans NM, Schweinsburg BC, Cohen DN, Muller RA, Courchesne E (2007) N-acetyl aspartate in autism spectrum disorders: regional effects and relationship to fMRI activation. Brain Res 1162:85-97.

Klunder B, Baron W, Schrage C, de Jonge J, de Vries H, Hoekstra D (2008) Sorting signals and regulation of cognate basolateral trafficking in myelin biogenesis. J Neurosci Res 86:1007-1016.

Kohler D, Ruff C, Meyhofer E, Bahler M (2003) Different degrees of lever arm rotation control myosin step size. The Journal of cell biology 161:237-241.

Komaba S, Coluccio LM (2010) Localization of myosin 1b to actin protrusions requires phosphoinositide binding. The Journal of biological chemistry 285:27686-27693.

Kornguth SE, Anderson JW (1965) Localization of a basic protein in the myelin of various species with the aid of fluorescence and electron microscopy. J Cell Biol 26:157-166.

Krendel M, Osterweil EK, Mooseker MS (2007) Myosin 1E interacts with synaptojanin-1 and dynamin and is involved in endocytosis. FEBS letters 581:644-650.

Kumar S, Biancotti JC, Matalon R, de Vellis J (2009) Lack of aspartoacylase activity disrupts survival and differentiation of neural progenitors and oligodendrocytes in a mouse model of Canavan disease. J Neurosci Res 87:3415-3427.

Kureishy N, Sapountzi V, Prag S, Anilkumar N, Adams JC (2002) Fascins, and their roles in cell structure and function. Bioessays 24:350-361.

Kwiatkowski AV, Weis WI, Nelson WJ (2007) Catenins: playing both sides of the synapse. Current opinion in cell biology 19:551-556.

Laakso JM, Lewis JH, Shuman H, Ostap EM (2008) Myosin I can act as a molecular force sensor. Science 321:133-136.

Landis DM, Hall AK, Weinstein LA, Reese TS (1988) The organization of cytoplasm at the presynaptic active zone of a central nervous system synapse. Neuron 1:201-209.

Lauffenburger DA, Horwitz AF (1996) Cell migration: a physically integrated molecular process. Cell 84:359-369.

Les Erickson F, Corsa AC, Dose AC, Burnside B (2003) Localization of a class III myosin to filopodia tips in transfected HeLa cells requires an actin-binding site in its tail domain. Mol Biol Cell 14:4173-4180.

Levental I, Grzybek M, Simons K (2010) Greasing their way: lipid modifications determine protein association with membrane rafts. Biochemistry 49:6305-6316.

Levitt JG, O'Neill J, Blanton RE, Smalley S, Fadale D, McCracken JT, Guthrie D, Toga AW, Alger JR (2003) Proton magnetic resonance spectroscopic imaging of the brain in childhood autism. Biological psychiatry 54:1355-1366.

Lewallen KA, Shen YA, De la Torre AR, Ng BK, Meijer D, Chan JR (2011) Assessing the role of the cadherin/catenin complex at the Schwann cell-axon interface and in the initiation of myelination. The Journal of neuroscience 31:3032-3043.

Lewis AK, Bridgman PC (1996) Mammalian myosin I alpha is concentrated near the plasma membrane in nerve growth cones. Cell Motil Cytoskeleton 33:130-150.

Lewis JH, Lin T, Hokanson DE, Ostap EM (2006) Temperature dependence of nucleotide association and kinetic characterization of myo1b. Biochemistry 45:11589-11597.

Li Z, Sheng M (2003) Some assembly required: the development of neuronal synapses. Nat Rev Mol Cell Biol 4:833-841.

Lin CH, Espreafico EM, Mooseker MS, Forscher P (1996) Myosin drives retrograde F-actin flow in neuronal growth cones. Neuron 16:769-782.

Lin YC, Koleske AJ (2010) Mechanisms of synapse and dendrite maintenance and their disruption in psychiatric and neurodegenerative disorders. Annu Rev Neurosci 33:349-378.

Lund LM, Machado VM, McQuarrie IG (2005) Axonal isoforms of myosin-I. Biochem Biophys Res Commun 330:857-864.

Lynch TJ, Albanesi JP, Korn ED, Robinson EA, Bowers B, Fujisaki H (1986) ATPase activities and actin-binding properties of subfragments of Acanthamoeba myosin IA. The Journal of biological chemistry 261:17156-17162.

Madhavarao CN, Moffett JR, Moore RA, Viola RE, Namboodiri MA, Jacobowitz DM (2004) Immunohistochemical localization of aspartoacylase in the rat central nervous system. J Comp Neurol 472:318-329.

Madhavarao CN, Arun P, Moffett JR, Szucs S, Surendran S, Matalon R, Garbern J, Hristova D, Johnson A, Jiang W, Namboodiri MA (2005) Defective N-acetylaspartate catabolism reduces brain acetate levels and myelin lipid synthesis in Canavan's disease. Proc Natl Acad Sci U S A 102:5221-5226.

Marsh L, Letourneau PC (1984) Growth of neurites without filopodial or lamellipodial activity in the presence of cytochalasin B. The Journal of cell biology 99:2041-2047.

Martin-Belmonte F, Yu W, Rodriguez-Fraticelli AE, Ewald AJ, Werb Z, Alonso MA, Mostov K (2008) Cell-polarity dynamics controls the mechanism of lumen formation in epithelial morphogenesis. Curr Biol 18:507-513.

Maruthamuthu V, Aratyn-Schaus Y, Gardel ML (2010) Conserved F-actin dynamics and force transmission at cell adhesions. Current opinion in cell biology 22:583-588.

Matsudaira PT, Burgess DR (1979) Identification and organization of the components in the isolated microvillus cytoskeleton. J Cell Biol 83:667-673.

Mattila PK, Lappalainen P (2008) Filopodia: molecular architecture and cellular functions. Nat Rev Mol Cell Biol 9:446-454.

McConnell RE, Tyska MJ (2007) Myosin-1a powers the sliding of apical membrane along microvillar actin bundles. J Cell Biol 177:671-681.

McConnell RE, Tyska MJ (2010) Leveraging the membrane - cytoskeleton interface with myosin-1. Trends Cell Biol 20:418-426.

McConnell RE, Benesh AE, Mao S, Tabb DL, Tyska MJ (2011) Proteomic analysis of the enterocyte brush border. Am J Physiol Gastrointest Liver Physiol 300:G914-926.

McConnell RE, Higginbotham JN, Shifrin DA, Jr., Tabb DL, Coffey RJ, Tyska MJ (2009) The enterocyte microvillus is a vesicle-generating organelle. J Cell Biol 185:1285-1298.

McQuarrie IG, Lund LM (2009) Intra-axonal myosin and actin in nerve regeneration. Neurosurgery 65:A93-96.

Mellor H (2010) The role of formins in filopodia formation. Biochim Biophys Acta 1803:191-200.

Miettinen A, Virtanen I, Linder E (1978) Cellular actin and junction formation during reaggregation of adult rat hepatocytes into epithelial cell sheets. Journal of cell science 31:341-353.

Miller SL, Daikhin Y, Yudkoff M (1996) Metabolism of N-acetyl-L-aspartate in rat brain. Neurochem Res 21:615-618.

Mirsky R, Winter J, Abney ER, Pruss RM, Gavrilovic J, Raff MC (1980) Myelin-specific proteins and glycolipids in rat Schwann cells and oligodendrocytes in culture. J Cell Biol 84:483-494.

Miyake Y, Inoue N, Nishimura K, Kinoshita N, Hosoya H, Yonemura S (2006) Actomyosin tension is required for correct recruitment of adherens junction components and zonula occludens formation. Experimental cell research 312:1637-1650.

Miyoshi J, Takai Y (2008) Structural and functional associations of apical junctions with cytoskeleton. Biochim Biophys Acta 1778:670-691.

Moffett JR, Ross B, Arun P, Madhavarao CN, Namboodiri AM (2007) N-Acetylaspartate in the CNS: from neurodiagnostics to neurobiology. Prog Neurobiol 81:89-131.

Moffett JR, Arun P, Ariyannur PS, Garbern JY, Jacobowitz DM, Namboodiri AM (2011) Extensive aspartoacylase expression in the rat central nervous system. Glia.

Mogilner A, Keren K (2009) The shape of motile cells. Curr Biol 19:R762-771.

Mooseker MS (1985) Organization, chemistry, and assembly of the cytoskeletal apparatus of the intestinal brush border. Annu Rev Cell Biol 1:209-241.

Mooseker MS, Tilney LG (1975a) Organization of an actin filament-membrane complex. Filament polarity and membrane attachment in the microvilli of intestinal epithelial cells. J Cell Biol 67:725-743.

Mooseker MS, Tilney LG (1975b) Organization of an actin filament-membrane complex. Filament polarity and membrane attachment in the microvilli of intestinal epithelial cells. The Journal of cell biology 67:725-743.

Mooseker MS, Cheney RE (1995) Unconventional myosins. Annu Rev Cell Dev Biol 11:633-675.

Mooseker MS, Graves TA, Wharton KA, Falco N, Howe CL (1980) Regulation of microvillus structure: calcium-dependent solation and cross-linking of actin filaments in the microvilli of intestinal epithelial cells. The Journal of cell biology 87:809-822.

Morales M, Colicos MA, Goda Y (2000) Actin-dependent regulation of neurotransmitter release at central synapses. Neuron 27:539-550.

Murase S, Mosser E, Schuman EM (2002) Depolarization drives beta-Catenin into neuronal spines promoting changes in synaptic structure and function. Neuron 35:91-105.

Nakamori Y, Emoto M, Fukuda N, Taguchi A, Okuya S, Tajiri M, Miyagishi M, Taira K, Wada Y, Tanizawa Y (2006) Myosin motor Myo1c and its receptor NEMO/IKK-gamma promote TNF-alpha-induced serine307 phosphorylation of IRS-1. The Journal of cell biology 173:665-671.

Nambiar R, McConnell RE, Tyska MJ (2009) Control of cell membrane tension by myosin-I. Proc Natl Acad Sci U S A 106:11972-11977.

Nambiar R, McConnell RE, Tyska MJ (2010) Myosin motor function: the ins and outs of actin-based membrane protrusions. Cell Mol Life Sci 67:1239-1254.

Namboodiri AM, Peethambaran A, Mathew R, Sambhu PA, Hershfield J, Moffett JR, Madhavarao CN (2006) Canavan disease and the role of N-acetylaspartate in myelin synthesis. Mol Cell Endocrinol 252:216-223.

Nayak GD, Ratnayaka HS, Goodyear RJ, Richardson GP (2007) Development of the hair bundle and mechanotransduction. Int J Dev Biol 51:597-608.

Nielsen JA, Maric D, Lau P, Barker JL, Hudson LD (2006) Identification of a novel oligodendrocyte cell adhesion protein using gene expression profiling. J Neurosci 26:9881-9891.

Nobes CD, Hall A (1995) Rho, rac, and cdc42 GTPases regulate the assembly of multimolecular focal complexes associated with actin stress fibers, lamellipodia, and filopodia. Cell 81:53-62.

Odronitz F, Kollmar M (2007) Drawing the tree of eukaryotic life based on the analysis of 2,269 manually annotated myosins from 328 species. Genome Biol 8:R196.

Owaribe K, Kodama R, Eguchi G (1981) Demonstration of contractility of circumferential actin bundles and its morphogenetic significance in pigmented epithelium in vitro and in vivo. The Journal of cell biology 90:507-514.

Patino-Lopez G, Aravind L, Dong X, Kruhlak MJ, Ostap EM, Shaw S (2010) Myosin 1G is an abundant class I myosin in lymphocytes whose localization at the plasma membrane depends on its ancient divergent pleckstrin homology (PH) domain (Myo1PH). J Biol Chem 285:8675-8686.

Purcell TJ, Morris C, Spudich JA, Sweeney HL (2002) Role of the lever arm in the processive stepping of myosin V. Proceedings of the National Academy of Sciences of the United States of America 99:14159-14164.

Rimm DL, Koslov ER, Kebriaei P, Cianci CD, Morrow JS (1995) Alpha 1(E)-catenin is an actin-binding and -bundling protein mediating the attachment of F-actin to the membrane adhesion complex. Proc Natl Acad Sci U S A 92:8813-8817.

Rizo J, Rosenmund C (2008) Synaptic vesicle fusion. Nat Struct Mol Biol 15:665-674.

Roth J, Baetens D, Norman AW, Garcia-Segura LM (1981) Specific neurons in chick central nervous system stain with an antibody against chick intestinal vitamin D-dependent calcium-binding protein. Brain Res 222:452-457.

Salles FT, Merritt RC, Jr., Manor U, Dougherty GW, Sousa AD, Moore JE, Yengo CM, Dose AC, Kachar B (2009) Myosin IIIa boosts elongation of stereocilia by transporting espin 1 to the plus ends of actin filaments. Nat Cell Biol 11:443-450.

Sanger JW, Sanger JM, Jockusch BM (1983) Differences in the stress fibers between fibroblasts and epithelial cells. The Journal of cell biology 96:961-969.

Sartorius CA, Lu BD, Acakpo-Satchivi L, Jacobsen RP, Byrnes WC, Leinwand LA (1998) Myosin heavy chains IIa and IId are functionally distinct in the mouse. The Journal of cell biology 141:943-953.

Schachner M, Kim SK, Zehnle R (1981) Developmental expression in central and peripheral nervous system of oligodendrocyte cell surface antigens (O antigens) recognized by monoclonal antibodies. Dev Biol 83:328-338.

Schliwa M, Woehlke G (2003) Molecular motors. Nature 422:759-765.

Schnadelbach O, Ozen I, Blaschuk OW, Meyer RL, Fawcett JW (2001) N-cadherin is involved in axon-oligodendrocyte contact and myelination. Mol Cell Neurosci 17:1084-1093.

Schneider ME, Dose AC, Salles FT, Chang W, Erickson FL, Burnside B, Kachar B (2006) A new compartment at stereocilia tips defined by spatial and temporal patterns of myosin IIIa expression. J Neurosci 26:10243-10252.

Schreiber J, Enderich J, Sock E, Schmidt C, Richter-Landsberg C, Wegner M (1997) Redundancy of class III POU proteins in the oligodendrocyte lineage. J Biol Chem 272:32286-32293.

Siemens J, Lillo C, Dumont RA, Reynolds A, Williams DS, Gillespie PG, Muller U (2004) Cadherin 23 is a component of the tip link in hair-cell stereocilia. Nature 428:950-955.

Simons M, Trajkovic K (2006) Neuron-glia communication in the control of oligodendrocyte function and myelin biogenesis. Journal of cell science 119:4381-4389.

Simons M, Trotter J (2007) Wrapping it up: the cell biology of myelination. Current opinion in neurobiology 17:533-540.

Simpson PB, Armstrong RC (1999) Intracellular signals and cytoskeletal elements involved in oligodendrocyte progenitor migration. Glia 26:22-35.

Skoff RP, Price DL, Stocks A (1976) Electron microscopic autoradiographic studies of gliogenesis in rat optic nerve. II. Time of origin. J Comp Neurol 169:313-334.

Skowron JF, Mooseker MS (1999) Cloning and characterization of mouse brush border myosin-I in adult and embryonic intestine. J Exp Zool 283:242-257.

Skowron JF, Bement WM, Mooseker MS (1998) Human brush border myosin-I and myosin-Ic expression in human intestine and Caco-2BBe cells. Cell Motil Cytoskeleton 41:308-324.

Sloane JA, Vartanian TK (2007) Myosin Va controls oligodendrocyte morphogenesis and myelination. J Neurosci 27:11366-11375.

Sokac AM, Schietroma C, Gundersen CB, Bement WM (2006) Myosin-1c couples assembling actin to membranes to drive compensatory endocytosis. Dev Cell 11:629-640.

Soldati T (2003) Unconventional myosins, actin dynamics and endocytosis: a menage a trois? Traffic 4:358-366.

Sommer I, Schachner M (1981) Monoclonal antibodies (O1 to O4) to oligodendrocyte cell surfaces: an immunocytological study in the central nervous system. Dev Biol 83:311-327.

Sotelo-Silveira JR, Calliari A, Kun A, Benech JC, Sanguinetti C, Chalar C, Sotelo JR (2000) Neurofilament mRNAs are present and translated in the normal and severed sciatic nerve. J Neurosci Res 62:65-74.

Speder P, Noselli S (2007) Left-right asymmetry: class I myosins show the direction. Curr Opin Cell Biol 19:82-87.

Speder P, Adam G, Noselli S (2006) Type ID unconventional myosin controls left-right asymmetry in Drosophila. Nature 440:803-807.

Spiegel I, Adamsky K, Eshed Y, Milo R, Sabanay H, Sarig-Nadir O, Horresh I, Scherer SS, Rasband MN, Peles E (2007) A central role for Necl4 (SynCAM4) in Schwann cell-axon interaction and myelination. Nature neuroscience 10:861-869.

Spiller RC (1994) Intestinal absorptive function. Gut 35:S5-9.

Spudich JA (1994) How molecular motors work. Nature 372:515-518.

Steed E, Balda MS, Matter K (2010) Dynamics and functions of tight junctions. Trends Cell Biol 20:142-149.

Stone JL, Merriman B, Cantor RM, Geschwind DH, Nelson SF (2007) High density SNP association study of a major autism linkage region on chromosome 17. Hum Mol Genet 16:704-715.

Surendran S, Matalon R, Tyring SK (2006) Upregulation of aspartoacylase activity in the duodenum of obesity induced diabetes mouse: implications on diabetic neuropathy. Biochemical and biophysical research communications 345:973-975.

Surendran S, Campbell GA, Tyring SK, Matalon R (2005) Aspartoacylase gene knockout results in severe vacuolation in the white matter and gray matter of the spinal cord in the mouse. Neurobiology of disease 18:385-389.

Svaren J, Meijer D (2008) The molecular machinery of myelin gene transcription in Schwann cells. Glia 56:1541-1551.

Swanljung-Collins H, Collins JH (1991) Ca2+ stimulates the Mg2(+)-ATPase activity of brush border myosin I with three or four calmodulin light chains but inhibits with less than two bound. The Journal of biological chemistry 266:1312-1319.

Tabb DL, Fernando CG, Chambers MC (2007) MyriMatch: highly accurate tandem mass spectral peptide identification by multivariate hypergeometric analysis. J Proteome Res 6:654-661.

Tanentzapf G, Smith C, McGlade J, Tepass U (2000) Apical, lateral, and basal polarization cues contribute to the development of the follicular epithelium during Drosophila oogenesis. J Cell Biol 151:891-904.

Taylor KA (2007) Regulation and recycling of myosin V. Current opinion in cell biology 19:67-74.

Tilney LG, Mooseker M (1971) Actin in the brush-border of epithelial cells of the chicken intestine. Proceedings of the National Academy of Sciences of the United States of America 68:2611-2615.

Togashi H, Abe K, Mizoguchi A, Takaoka K, Chisaka O, Takeichi M (2002) Cadherin regulates dendritic spine morphogenesis. Neuron 35:77-89.

Tyska MJ, Mooseker MS (2002) MYO1A (brush border myosin I) dynamics in the brush border of LLC-PK1-CL4 cells. Biophys J 82:1869-1883.

Tyska MJ, Mooseker MS (2004) A role for myosin-1A in the localization of a brush border disaccharidase. J Cell Biol 165:395-405.

Tyska MJ, Mackey AT, Huang JD, Copeland NG, Jenkins NA, Mooseker MS (2005) Myosin-1a is critical for normal brush border structure and composition. Mol Biol Cell 16:2443-2457.

Valentijn JA, LaCivita DQ, Gumkowski FD, Jamieson JD (1997) Rab4 associates with the actin terminal web in developing rat pancreatic acinar cells. European journal of cell biology 72:1-8.

Vasioukhin V, Bauer C, Yin M, Fuchs E (2000) Directed actin polymerization is the driving force for epithelial cell-cell adhesion. Cell 100:209-219.

Veigel C, Coluccio LM, Jontes JD, Sparrow JC, Milligan RA, Molloy JE (1999) The motor protein myosin-I produces its working stroke in two steps. Nature 398:530-533.

Voogd J, Glickstein M (1998) The anatomy of the cerebellum. Trends Neurosci 21:370-375.

Walsh TP, Weber A, Davis K, Bonder E, Mooseker M (1984) Calcium dependence of villin-induced actin depolymerization. Biochemistry 23:6099-6102.

Wang FS, Liu CW, Diefenbach TJ, Jay DG (2003) Modeling the role of myosin 1c in neuronal growth cone turning. Biophysical journal 85:3319-3328.

Wang H, Tewari A, Einheber S, Salzer JL, Melendez-Vasquez CV (2008) Myosin II has distinct functions in PNS and CNS myelin sheath formation. J Cell Biol 182:1171-1184.

Weisz OA, Rodriguez-Boulan E (2009) Apical trafficking in epithelial cells: signals, clusters and motors. Journal of cell science 122:4253-4266.

Willert K, Nusse R (1998) Beta-catenin: a key mediator of Wnt signaling. Current opinion in genetics & development 8:95-102.

Witte H, Neukirchen D, Bradke F (2008) Microtubule stabilization specifies initial neuronal polarization. The Journal of cell biology 180:619-632.

Yamaguchi Y, Miyagi Y, Baba H (2008) Two-dimensional electrophoresis with cationic detergents: a powerful tool for the proteomic analysis of myelin proteins. Part 2: analytical aspects. J Neurosci Res 86:766-775.

Yoshihara Y, De Roo M, Muller D (2009) Dendritic spine formation and stabilization. Current opinion in neurobiology 19:146-153.

Zanazzi G, Matthews G (2009) The molecular architecture of ribbon presynaptic terminals. Molecular neurobiology 39:130-148.

Zarnescu DC, Thomas GH (1999) Apical spectrin is essential for epithelial morphogenesis but not apicobasal polarity in Drosophila. J Cell Biol 146:1075-1086.

Zhang B, Chambers MC, Tabb DL (2007) Proteomic parsimony through bipartite graph analysis improves accuracy and transparency. J Proteome Res 6:3549-3557.

Zhang J, Betson M, Erasmus J, Zeikos K, Bailly M, Cramer LP, Braga VM (2005) Actin at cell-cell junctions is composed of two dynamic and functional populations. Journal of cell science 118:5549-5562.

Zhang X, Baader SL, Bian F, Muller W, Oberdick J (2001) High level Purkinje cell specific expression of green fluorescent protein in transgenic mice. Histochem Cell Biol 115:455-464.